

5-1981

A Critical Study of Nonlinear Echo Phenomena

Monish Ranjan Chatterjee

University of Dayton, mchatterjee1@udayton.edu

Follow this and additional works at: http://ecommons.udayton.edu/ece_fac_pub

 Part of the [Computer Engineering Commons](#), [Electrical and Electronics Commons](#), [Electromagnetics and Photonics Commons](#), [Optics Commons](#), [Other Electrical and Computer Engineering Commons](#), and the [Systems and Communications Commons](#)

eCommons Citation

Chatterjee, Monish Ranjan, "A Critical Study of Nonlinear Echo Phenomena" (1981). *Electrical and Computer Engineering Faculty Publications*. Paper 295.

http://ecommons.udayton.edu/ece_fac_pub/295

This Dissertation is brought to you for free and open access by the Department of Electrical and Computer Engineering at eCommons. It has been accepted for inclusion in Electrical and Computer Engineering Faculty Publications by an authorized administrator of eCommons. For more information, please contact frice1@udayton.edu, mschlangen1@udayton.edu.

A CRITICAL STUDY OF NONLINEAR ECHO PHENOMENA

by

Monish Ranjan Chatterjee

A thesis submitted in partial fulfillment
of the requirements for the degree of
Master of Science in Electrical and Computer Engineering
in the Graduate College of
The University of Iowa

May 1981

Thesis supervisor: Professor Adrianus Korpel

ENGIN
T1981
C495

Graduate College
The University of Iowa
Iowa City, Iowa

CERTIFICATE OF APPROVAL

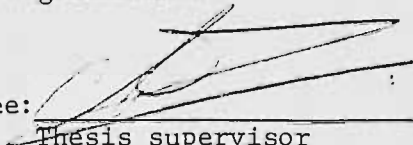
MASTER'S THESIS

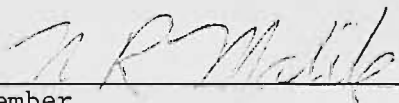
This is to certify that the Master's Thesis of

Monish Ranjan Chatterjee

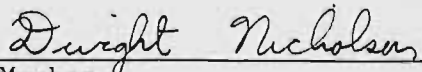
has been approved by the Examining Committee
for the thesis requirement for the Master of
Science degree in Electrical and Computer
Engineering at the May 1981 graduation.

Thesis committee:


Thesis supervisor


Member


Member


Member

ACKNOWLEDGMENTS

I take this opportunity to express my sincere gratitude and appreciation to Dr. Adrianus Korpel for his kind and invaluable advice, persistent encouragement, and close, personal involvement during the course of this study. Stimulating discussions between us are also gratefully acknowledged.

Special thanks are also due to Carma Grout for her patient, competent, and efficient typing of the manuscript.

Last, but not the least, I would like to thank the staff of the Physics and Main Libraries for the excellent cooperation and help extended to me at various stages of this study.

The research reported in this thesis was supported by the National Science Foundation under Grant No. ENG-7902889.

TABLE OF CONTENTS

	Page
LIST OF TABLES	ii
LIST OF FIGURES	iii
INTRODUCTION	1
CHAPTER	
I. SPIN ECHOES AND PHASE CONJUGATION	5
II. PHOTON ECHOES	17
III. FERRIMAGNETIC ECHOES	24
IV. CYCLOTRON ECHOES	29
V. PLASMA ECHOES	35
VI. PHONON (ELECTROACOUSTIC) ECHOES IN PIEZOELECTRIC CRYSTALS	40
VII. PHONON (ELECTROACOUSTIC) ECHOES IN POWDERS	45
VIII. ELECTRONIC HOLOGRAPHY	55
CONCLUSION	63
APPENDIX A MATHEMATICAL ANALYSIS OF SPIN-ECHO FORMATION	96
APPENDIX B OPTICAL PHASE CONJUGATION BY DEGENERATE FOUR WAVE MIXING [DFWM]	109
APPENDIX C GENERATION OF MULTIPLE TWO-PULSE ECHOES IN THE PRESENCE OF ANHARMONIC NONLINEARITY	113
REFERENCES	120

LIST OF TABLES

Table	Page
I. Types of echoes (after Gould (26), with additions).	65

LIST OF FIGURES

Figure	Page
1.1 Schematic arrangement for obtaining spin echoes (note that only pulse envelopes are shown). (After Hahn (1))	66
1.2 Response of a linear system to two r.f. pulses	67
1.3 Response of a nonlinear system to two r.f. pulses	67
1.4 Illustration of phase conjugation concept	68
1.5 Vector representation of spin-echo formation	69
1.6 Vector representation of echo-formation under weaker nonlinearities	71
2.1 Experimental setup for obtaining photon echoes. (After Kurnit et al. (10))	72
3.1 Echo gain as a function of sample irregularity. (After Kaplan et al. (22))	73
3.2 Two-pulse echo as a function of pulse separation τ , for (a) anharmonic nonlinearity, (b) nonlinear excitation	73
3.3 Pulse compression by two-pulse echo method (note that the figure shows overlap of two frequencies only; a pulse is obtained upon adding many frequencies)	74
4.1 Experimental arrangement for obtaining cyclotron echoes (E and B are the dominant TE and TM microwave fields; B_0 is the static magnetic field). (After Gould (26))	75
4.2 Phasor representation of oscillators in the complex plane	76
5.1 Schematic arrangement for obtaining plasma-wave echoes. (After Baker et al. (31))	78

Figure	Page
5.2 Electron trajectories and number density illustrating the formation of plasma-wave echoes	79
5.3 Typical pulse-sequence for a three-pulse echo	80
7.1 Variation of the transverse relaxation time with temperature. (After Rubinstein et al. (47)) . . .	81
7.2 Echo amplitude as a function of average particle diameter. (After Melcher et al. (51))	82
7.3 Echo amplitude as a function of two-pulse separation (solid curve is experimental; dashed curve is from theory). (After Kajimura et al. (54))	82
7.4 Stimulated echo amplitude versus recall time (T) at constant two-pulse separation (τ). (After Popov et al. (61))	83
7.5 Spatial orientation of electric field (\bar{E}) and dipole moment (\bar{p})	83
7.6 Particle orientation and energy versus frequency (a) just after the first pulse, (b) after the second pulse, (c) after the third pulse. (After Wilms et al. (63))	84
7.7 The time development of $\Sigma q_i \cos \alpha_i$ after the second pulse. (After Wilms et al. (63))	85
8.1 Time-inverted signal recalled by delta function as a short range echo. (After Korpel (5))	86
8.2 One of 20 LC circuits modeling a general ensemble of nonlinear oscillators. (After Korpel (5))	87
8.3 Double pulse excitation demonstrating the short range echo effect. Lower and upper traces show input and output pulses. (After Korpel (5))	88

Figure	Page
8.4 Long range echo experiment. Lower and upper traces show input and output pulses. (After Korpel (5))	90
8.5 Long range echo amplitude versus recall time. (After Korpel (5)).	92
8.6 Excitation with extended rectangular pulse. (After Korpel (5))	93
B.1 Optical phase conjugation (a) schematic arrangement, (b) vector representation	95

INTRODUCTION

Over the past two or three decades, the subject of radio frequency echo phenomena has been studied, extensively at times, by a variety of investigators. Echo effects occur in nonlinear systems that are characterized by a multiplicity of oscillating states or eigenmodes. When such systems are excited by a sequence of high energy r.f. pulses, they subsequently re-radiate, through nonlinear processes, r.f. power in the form of echo pulses that bear observable relationships to the exciting pulses. Such echo pulses are a specific instance of more general signal storage and recall, but in spite of this implication the subject has remained, by and large, confined to physicists and material scientists, and its potential for engineering applications is yet to be realized.

The present thesis attempts to give a concise and critical account of the evolution of the echo phenomena over the last thirty years. Starting with spin and photon echoes, which were among the earliest to be observed and studied, the thesis explores the experimental findings and the models proposed in connection with the more contemporary echo experiments, viz. those involving electroacoustic or polarization echoes in single and polycrystalline piezoelectric materials and in powders. Although the investigations regarding the various mechanisms of short and long term echo formation are by

no means complete, a coherent picture is beginning to emerge as will be shown in this study.

From the point of view of engineering concepts it is intriguing that the description of the echo phenomenon is most simply stated in terms dual to those used in describing more conventional effects. Thus, replacing time by frequency, nonlinear effects are seen to cause not frequency mixing, i.e. spurious frequencies, but rather time mixing, i.e. spurious pulses or echoes.

This duality reflects the underlying fact that configurations exhibiting the echo effect possess a physical frequency space. They are able to store individual frequencies in their corresponding oscillators or eigenmodes. Sometimes the storage is dynamic only; it disappears as soon as the oscillations decay. In other cases the storage is long term, as when some parameter of the oscillator or mode (resonant frequency, coupling factor, etc.) is changed permanently in the process. The latter effect is quite analogous to holography with the spatial frequencies (fringes) replaced by temporal frequencies and the fringe contrast by the coupling factor.

A key concept in the formation of echoes, or storage in general, is the notion of phase conjugation. Through the Fourier transform, phase conjugation in the frequency domain is connected with time reversal in the time domain. Here one begins to get a first inkling of how echoes could come about: If, through phase conjugation, time is reversed τ seconds after an event, it will occur again after a second interval of τ seconds!

As will be shown, nonlinearity is required to cause phase conjugation. The corresponding time reversal is usually not connected with the physical motion of a particle; more often it resides in the mathematics. An important exception is the precessional motion of the magnetic spins of certain atomic nuclei. Such a precession can actually be effectively reversed by strong nonlinear effects and spin echoes are consequently usually discussed in terms of time reversal rather than phase conjugation. In other instances of more direct relevance to engineering, weak nonlinear effects are involved and echo formation can best be seen as a nonlinear perturbation that induces phase conjugation. It would thus seem logical to delay the discussion of phase conjugation, until the appropriate (weakly nonlinear) phenomena are discussed. Yet the concept of phase conjugation is so powerful in teaching intuitive insight into nonlinear echo systems in general, that it was deemed appropriate to discuss it in connection with the first example, that of spin echoes.

Starting from a description of a classical spin echo experiment, it will be shown how nonlinearity has to be introduced in order to explain the observed effects. Then, using the simplest and most general nonlinear model of system response, it will be seen that this not only qualitatively describes the echo, but also predicts the multiple echoes which are, in fact, observed. Only then shall physical mechanism be discussed to eventually describe the magnetic spin echo effect in some detail.

In subsequent examples the same approach will be followed, i.e. describing the experiment, extending the heuristic theory where necessary and identifying the nonlinear mechanism responsible. By thus gradually building up the complete picture of present day research, in chronological order, the abundance of mathematics, that unified descriptions often invite, will be avoided.

Whether nonlinear signal storage ever becomes engineering practice remains to be seen. It is hoped that this thesis will contribute to that possibility.

In the pages that follow, the major known nonlinear echo phenomena are discussed in a chronological sequence wherever feasible. While each chapter is devoted to a distinct class of nonlinear echoes, an attempt has been made to maintain a continuity of the concepts, reinforcing earlier ones wherever similarities in the physical processes are observed; discarding or modifying them wherever experiments are in conflict with theory. Furthermore, guided by the experience that mathematical details tend to obscure the understanding of the material in simple, logical terms, the mathematical derivations have been relegated, wherever appropriate, to the appendices that follow the main text. The reader may refer to these for a more quantitative understanding of the associated phenomena.

CHAPTER I

SPIN ECHOES AND PHASE CONJUGATION

Spin echoes were first reported by Hahn [1,2] in 1949. These echoes are associated with the phenomena of nuclear and ferromagnetic resonance. A typical experimental arrangement for obtaining spin echoes is shown in Fig. 1.1*. A large d.c. magnetic field \bar{H}_0 is applied to a sample containing nuclear spins. The sample is placed in a coil which forms the inductance of a tuned circuit. The d.c. magnetic field establishes a net spin population at thermal equilibrium, and the resulting macroscopic moment \bar{M}_0 is oriented parallel to \bar{H}_0 . As is well known, the nuclear spins, when perturbed, will precess about \bar{H}_0 with frequency γH_0 , where γ is the so called gyromagnetic ratio. The precession of any particular spin is eventually dephased by field perturbations due to neighboring spins in the lattice. The time during which the precession maintains phase memory is called the spin-spin or transverse relaxation time, denoted by T_2 . After a time T_1 , the spins also begin losing energy to the lattice. T_1 is called the spin-lattice or longitudinal relaxation time. In the experiment, the spin system is subjected to two intense radio frequency pulses applied via the coil at the precession frequency $\omega = \omega_0 = \gamma H_0$. The pulses are of duration t_ω and separation τ , where both t_ω and τ are small compared to T_2 and T_1 .

Since the relaxation times of nuclei in liquids are generally large enough to favor this condition, experiments with protons in glycerine, water, solutions of $\text{Fe}(\text{NO}_3)_3$ etc. yield satisfactory results.

When the above requirements are satisfied, the individual spins will start precessing upon the application of the first pulse, and will not yet have dephased or decayed by the time the second pulse is applied. Following the latter pulse, identical to the first, the precessing spins somehow interfere constructively at time $t = 2\tau$ to give rise to a spontaneous nuclear induction signal, which is referred to as the two-pulse spin echo.

Now, how does this come about? If we think of the individual spins as elementary oscillators at frequency ω_0 , their macroscopic effect decays at a rate $\exp(-t/T'_{\text{eff}})$ where $\frac{1}{T'_{\text{eff}}} = \frac{1}{T_1} + \frac{1}{T_2}$. If T_1, T_2 are both large compared to the observation time, we would expect results as shown in Figure 1.2. Here each pulse excites an oscillation whose envelope decays according to $\exp(-t/T'_{\text{eff}})$. Upon adding the two impulse responses at time $t = 2\tau$, we do not see any pulse echo; in fact, we do not see any pulses at all! They are completely smeared out by the narrow bandwidth ($\sim \frac{1}{T'_{\text{eff}}}$) of the oscillator ensemble.

In actual practice, however, the response is as shown in Fig. 1.3. Although some ringing is visible in the response, it is certainly much less than expected; also an echo is observed at $t = 2\tau$.

It turns out that the absence of ringing can be explained by the fact that, due to local inhomogeneities ΔH_0 in the magnetic

field, there is a distribution $\Delta f = \frac{\gamma \Delta H_0}{2\pi} = \frac{1}{T_3}$ of resonance frequencies among the spins such that $\frac{1}{T_3} \gg \frac{1}{T_2}, \frac{1}{T_1}$. Consequently the spin ensemble acts as a wideband filter with envelope response determined by $\frac{1}{T_{\text{eff}}} \approx \frac{1}{T_3} = \Delta f$; so the observed decay is of the form $\exp(-t\Delta f)$, where Δf is large enough to ensure a sharp reduction of ringing, although the latter is not completely eliminated. (Note that, although the macroscopic effect has decayed, the individual oscillators are still ringing and will continue to do so for a time $\sim T_1$).

As regards the echo, no explanation based on linear effects is adequate. It is immediately obvious that a linear system whose r.f. impulse response does not show an echo, cannot produce an echo by having two r.f. pulses applied in succession. Consequently the explanation must lie in the fact that the system is basically non-linear. This was first explicitly stated by Gould as a general principle for any system of gyrating charged particles [3,4] and was later used by Korpel as the basis of a phase conjugation formalism applying to any system of independent oscillators [5]. Although we will discuss phase conjugation later in more detail, it is helpful to introduce it, at this point, as a key concept in the description of echo phenomena.

The basic idea, illustrated in Fig. 1.4, is as follows. Let a delta function excite a system of independent oscillators at time $t = 0$. The oscillators, which for simplicity's sake are here

assumed to cover the entire frequency spectrum from 0 to ∞ , will start vibrating and hence preserve the information about the frequency spectrum of the delta function. Their individual response may be represented by $\exp(j\omega t)$. The phases of the individual oscillators at $t = \tau$ are given by ϕ_τ such that $\exp(j\omega t) = \exp[j\omega(t-\tau) + j\phi_\tau]$, hence $\phi_\tau = \omega\tau$. Assume now that, by some mechanism, we conjugate the phases at time $t = \tau$. Then, from $t = \tau$ onwards, the oscillators individually are described by $\exp[j\omega(t-\tau) - j\phi_\tau] = \exp[j\omega(t-2\tau)]$ and their macroscopic response by $\int_0^\infty \exp[j\omega(t-2\tau)] d\omega$. Such a response obviously represents a delta function at $t = 2\tau$, i.e. an echo of the original pulse. Thus phase conjugation naturally leads to the prediction of echoes. (It should be noted that recently, in optics, it has been proposed to use this time reversal aspect of phase conjugation for the purpose of restoring aberrated wavefronts [6]).

Now, how is phase conjugation brought about? The simplest mechanism is the existence of a cubic nonlinearity in the function that describes the excitation mechanism of the system. This can be seen as follows. If we apply delta functions to the system at $t = 0$ and $t = \tau$, then the response of the individual oscillators is described by $A_1 \exp(j\omega t) + A_2 \exp[j\omega(t-\tau)]$ where A_1 and A_2 are the amplitudes. The response of the system (ensemble of independent oscillators) is then given by $\int [A_1 \exp(j\omega t) + A_2 \exp[j\omega(t-\tau)]] d\omega = A_1 \delta(t) + A_2 \delta(t-\tau)$, where we have left out nonessential constants. In the presence of a cubic nonlinearity the additional response $R(t)$

of a particular oscillator may be described by (using real notation this time)

$$R(t) = [A_1 \cos \omega t + A_2 \cos \omega(t-\tau)]^3, \quad (1.1)$$

which, after some algebra, may be written as:

$$\begin{aligned} R(t) = & \frac{3}{4} A_1^2 A_2 \cos \omega(t+\tau) + \left(\frac{3}{4} A_1^3 + \frac{3}{2} A_1 A_2^2\right) \cos \omega t + \frac{1}{4} A_1^3 \cos 3\omega t \\ & + \left[\frac{3}{4} A_2^3 + \frac{3}{2} A_1^2 A_2\right] \cos \omega(t-\tau) + \frac{1}{4} A_2^3 \cos 3\omega(t-\tau) + \\ & \frac{3}{4} A_1^2 A_2 \cos 3\omega(t-\tau/3) + \frac{3}{4} A_1 A_2^2 \cos 3\omega(t-\frac{2\tau}{3}) + \\ & \frac{3}{4} A_1 A_2^2 \cos \omega(t-2\tau). \end{aligned} \quad (1.2)$$

We next assume that (a) the oscillators in the system have high Q and (b) the oscillators are restricted to a range ω_c , and we use "practical" delta functions of width $\approx 2\pi/\omega_c$. Under those conditions we can ignore the 3ω terms and the macroscopic response of the system for $t > \tau$ can be written as:

$$\begin{aligned} R(t) = & \int \left(\frac{3}{4} A_1^3 + \frac{3}{2} A_1 A_2^2\right) \cos \omega t \, d\omega + \int \left(\frac{3}{4} A_2^3 + \frac{3}{2} A_1^2 A_2\right) \cos \omega(t-\tau) \, d\omega \\ & + \int \frac{3}{4} A_1^2 A_2 \cos \omega(t+\tau) \, d\omega + \int \frac{3}{4} A_1 A_2^2 \cos \omega(t-2\tau) \, d\omega. \end{aligned} \quad (1.3)$$

Inspecting (1.3) term by term, we find that the term involving $\cos \omega(t+\tau)$ refers to a 'virtual' delta function at $t = -\tau$, which does not contribute to the physical response for times $t > \tau$. The same applies to the first two terms which represent virtual delta

functions at $t = 0$ and $t = \tau$. The only term of physical significance in the region $t > \tau$ is the one involving $\cos \omega(t-2\tau)$ and this represents a delta function at $t = 2\tau$, which, in fact, turns out to be the two pulse echo.

When deriving (1.2) from (1.1) it will be noted that the term in the expansion of (1.1), responsible for the echo, is of the form $A \cos^m[\omega(t-\tau)] \cos^{m-1}(\omega t)$, where $m + m - 1 = 2m - 1 = n$ is the order of the nonlinearity involved (e.g. $n = 3$ for cubic nonlinearity). It therefore becomes evident that for echoes to be predicted, the nonlinearity must be of an odd order. Hence it is also easy to conclude that the minimum order of nonlinearity is cubic, since for $n < 3$, i.e. $n = 1$, the system is linear.

A simple extension of the cubic nonlinearity discussed above leads to the prediction of multiple echoes, i.e. two pulse echoes at $t = n\tau$, where $n \geq 2$. This is shown as follows. Suppose the system under consideration has nonlinearity up to the fifth order. Then, as already shown, the cubic nonlinearity leads to an echo at $t = 2\tau$. Upon examining the echo-term corresponding to the fifth order, we find:

$R_5(t) = A \cos^3 \omega(t-\tau) \cos^2 \omega t$, where $R_5(t)$ is the part of the response for the echo-term of the fifth order. We then have,

$$R_5(t) = \frac{3}{8} A \cos \omega(t-\tau) + \frac{A}{8} \cos 3\omega(t-\tau) + \frac{3}{16} A \cos 3\omega(t-\tau/3) + \\ + \frac{3}{16} A \cos \omega(t+\tau) + \frac{A}{16} \cos 5\omega(t - \frac{3\tau}{5}) + \frac{A}{16} \cos \omega(t-3\tau). \quad (1.4)$$

Inspecting (1.4) term by term, we recognize the last term as an additional echo at $t = 3\tau$. Thus, a fifth order nonlinearity leads to an additional echo at $t = 3\tau$. More generally, it may be concluded that a p th order nonlinearity leads to an echo at $t = (\frac{p+1}{2})\tau$. Thus simple considerations of phase conjugation and nonlinearity leads to the prediction of multiple echoes, a phenomenon which has in fact been observed.

Returning to the echo-term associated with cubic linearity we find that the contribution to the ensemble response following the application of two pulses is given by:

$$R_3(t) \propto \int A \cos^2 \omega(t-\tau) \cos \omega t \, d\omega = \frac{A}{2} \int [1 + \cos 2\omega(t-\tau)] \cos \omega t \, d\omega.$$

We observe from the above that the mixing product actually responsible for the echo at $t = 2\tau$ is of the form $A \cos \omega t \cos 2\omega(t-\tau)$. We can interpret this, as the interaction of a parameter of the system, made to vary at 2ω by the second pulse, with the fundamental response at ω caused by the first pulse. Such a parametric interpretation of the echo process is quite equivalent to the one discussed before and, in some cases, more convenient.

In our heuristic analysis of echoes we have assumed ideal or practical delta functions limited in spectral width to a frequency ω_c . In experimental practice the ensemble of oscillators is more often characterized by a spread of frequencies $\Delta\omega$ around a center frequency ω_0 . The "practical" delta functions then become r.f.

pulses of envelope width $\sim \frac{2\pi}{\Delta\omega}$; however, all the arguments used in the pulse echo analysis remain the same.

In the case of spin echoes the oscillators are centered around the precession frequency ω_0 and the spread $\Delta\omega$ is determined by the inhomogeneity ΔH_0 in the magnetic field; hence $\Delta\omega = \gamma\Delta H_0$. In order to explain the spin echoes we must now, according to the preceding analysis, try to identify an appropriate nonlinearity in the response mechanism of magnetic spins. As it turns out, spin echoes are most easily explained in the case where the nonlinearities are large. The method described in the preceding pages then no longer applies. However, the principle that nonlinearity in some form is essential remains.

We proceed then to investigate the physical processes involved in the formation of echoes in a spin system. By applying angular momentum conservation to a local system of nuclear spins [7,8] subjected to a magnetic field \bar{H} , the following so called Bloch equation is derived for the local macroscopic magnetization \bar{M} :

$$\frac{d\bar{M}}{d\tau} = \gamma(\bar{M} \times \bar{H}), \quad (1.5)$$

where γ is the gyromagnetic ratio, i.e. the ratio of the magnetic moment of the spin to its angular momentum. Considering, for the moment, only a bias field \bar{H}_0 along the Z axis, the equilibrium situation will be given by $\bar{M} = M_0 \vec{a}_z$ where M_0 depends on \bar{H}_0 and the temperature. This is shown in Fig. 1.5a. A small deviation of \bar{M}

from this position will establish a precession of \bar{M} about the Z axis with frequency $\omega_0 = \gamma H_0$. This is shown in Fig. 1.5b. In a time of the order of T_2 this macroscopic precession will disappear because of irreversible loss of phase coherence due to interaction between individual spins. Individual precessions will also damp out in a time $\sim T_1$, because of loss of energy to the lattice. We assume, for simplicity, that both T_1 and T_2 are very long compared with our observation time.

Assume next that a radio frequency field, $H_1 \cos \omega_0 t$ is applied in the X direction. If we decompose this field into clockwise (H^+) and counterclockwise (H^-) circular polarization, as shown in Fig. 1.5c, it is intuitively obvious that, because of phase synchronism, only the clockwise component will interact with any precessing dipoles. What will actually happen is that the dipoles, initially at rest, are set precessing, the precession angle θ increasing with time as $\theta = \gamma H^+ t$. The rate of rotation, γH^+ , is called the Rabi or spin-flipping frequency. It is easiest to visualize this in a coordinate system that rotates with the precession and the applied field. This is shown in Fig. 1.5d where, in the rotating system, the increase of θ with time is depicted as a precession of \bar{M} about X.

We are now in a position to describe the actual process of echo formation. First an intense, short r.f. pulse is applied, at frequency ω_0 , duration t_0 , and effective amplitude H^+ such that $\gamma H^+ t_0 = \pi/2$. This " $\pi/2$ " pulse will move the magnetization \bar{M} towards

the Y axis as shown in Fig. 1.5e. Once arrived there, the dipoles continue their main precession about Z at frequency ω_0 , i.e. in the rotating frame the magnetization remains in the Y direction. Now, due to inhomogeneities in the bias field ω_0 , not all local dipole systems precess at the same frequency. Let the local ensembles -1, -2, 1 and 2 be characterized by precession frequencies $\omega_0 - 2\delta\omega_0$, $\omega_0 - \delta\omega_0$, $\omega_0 + \delta\omega_0$ and $\omega_0 + 2\delta\omega_0$. The magnetization of these groups, having arrived at Y in the rotating frame, will not stay there but rather precess about Z at (relative) rates $-2\delta\omega_0$, $-\delta\omega_0$, $+\delta\omega_0$, $+2\delta\omega_0$. Fig. 1.5f shows relative positions a time τ after application of the " $\pi/2$ " pulse. It is obvious that, for sufficiently large $\delta\omega_0\tau$ (i.e. for large enough homogeneity), the total macroscopic dipole moment will average out to zero and hence not be observable. Memory of the event is however still preserved in the precessing spins, as long as their phases are not randomized irreversibly or have decayed, i.e. as long as $\tau < T_2, T_1$.

The second step in the echo process is to apply a short intense " π " pulse at time τ . The effect of this is to precess the individual magnetization vectors 180° about X so that they end up as shown in Fig. 1.5g (it has been assumed that the duration of the " π " pulse is short compared to τ). It is readily seen that, from this "time reversal" situation, the spin magnetization vectors will keep on precessing about Z to, ultimately at $t = 2\tau$, add up in phase again (Fig. 1.5h) and cause an observable echo.

Although the above description is not exact, (spins at different $\delta\omega$ precess about slightly different axes) it nevertheless portrays the essence of the phenomenon. The nonlinearity of the process resides in the fact that the initially induced transverse magnetization is not proportional to H^+ but rather to $\sin\theta = \sin(\gamma H^+ t)$ which can be written as $\gamma H^+ t - \frac{1}{3} (\gamma H^+ t)^3 + \dots$ for weak nonlinearities where $\gamma H^+ t \ll 1$. In the case of " $\pi/2$ " and " π " pulses the nonlinearity is no longer weak and the process cannot be described by the above power series. Nevertheless, the underlying principle is the same, as can be seen from the fact that spin echoes appear, too, in experiments with other than exact $\pi/2$ and π pulses [1].

A graphical description of the echo formation for small nonlinearities has been given by White [9]. The effect of the first pulse, much smaller than $\pi/2$, is now to establish a spin population shown in Fig. 1.6a which replaces Fig. 1.5f. Immediately after the second pulse of equal amplitude to the first one, the plane of the circle has become tilted, all vectors having precessed a small amount about X. This is shown in Fig. 1.6b. The transverse momenta are now distributed along an ellipse rather than a circle in the xy plane. This leads to a bunching in the phase distribution and ultimately to an echo at $t = 2\tau$. We shall return to such a graphical representation later, when we discuss cyclotron echoes.

A somewhat detailed quantitative analysis of the spin echo, using the Bloch equations, appears in Appendix A. Some important

features of phase conjugation by degenerate four-wave mixing are discussed in Appendix B.

CHAPTER II

PHOTON ECHOES

In 1964, Kurnit and coworkers reported the observation of a photon echo from a ruby crystal [10]. In Fig. 2.1 is shown a schematic diagram of the experimental setup used to demonstrate its existence.

As shown in Fig. 2.1, a sample of ruby crystal (RS) is excited by two strong pulses of light obtained by passing part of the 6935 Å beam of a Q-switched ruby laser through a beam splitter (BS) and lens L1; the other part of the beam is delayed via an optical delay line (D) and made incident on the sample a time $t = \tau$ later. The value of τ is of the order of 100 ns. The direction of the delayed pulse makes an angle $\phi \approx 3^\circ$ with that of the undelayed one. These original pulses, emerging from the ruby sample, are blocked by a stop (S). It is now found that the ruby sample emits a strong pulse of light at $t = 2\tau$, which emerges at angle 2ϕ relative to the undelayed pulse. This echo pulse passes through an aperture in the stop and is gated by a Kerr cell shutter (KCS) which is used to reduce scattered light from the excitation pulses. The pulse is then detected electrically by a photomultiplier (PM). In order for the echo to occur, the following requirements must be satisfied:

- (i) The ruby sample must be cooled to liquid He temperature in order to obtain relaxation times long compared to the pulse interval τ .

(ii) A d.c. magnetic field must be applied to the sample, parallel to the optic axis of the crystal. The latter requirement is not fundamental. It appears to be necessary in order to inhibit a relaxation effect due to a complicated dynamic iteration involving the magnetic spins of the Al nuclei in the ruby [11]. We discuss this briefly later.

In the experiment described above no electric dipole moment is connected with either the ground state 1 or the excited state 2 of the atomic system [11,12,13]. Hence the convenient classical picture of precessing dipoles no longer applies. Instead we must now start thinking in terms of quantum mechanical transitions between the two levels 1 and 2, brought about by an applied electrical field $E_1(t)$. Feynman et al. [14,15] have shown how such a situation may be analyzed conveniently by the introduction of a pseudo polarization \bar{r} . The vector \bar{r} is defined as follows:

$$\begin{aligned} r_x &= \rho_{21} + \rho_{12}, \\ r_y &= i(\rho_{21} - \rho_{12}), \\ r_z &= \rho_{22} - \rho_{11}, \end{aligned} \tag{2.1}$$

where ρ_{ij} are matrix elements of the so-called density matrix [11,12]. In terms of the probability amplitudes a and b for the upper level and lower level respectively, we have [12]:

$$\rho_{21} = \overline{ab^*}, \quad \rho_{12} = \overline{a^*b}, \quad \rho_{22} = \overline{aa^*}, \quad \rho_{11} = \overline{bb^*}, \tag{2.2}$$

where the bars denote ensemble averages. Also, the ensemble average $\langle \mu \rangle$ of the physical dipole moment, induced by the perturbation $E_1(t)$, is given by:

$$\langle \mu \rangle = \mu_{12}(\rho_{12} + \rho_{21}) = \mu_{12} \bar{r}_x, \quad (2.3)$$

where $\rho_{12} = \rho_{21}$ denotes the off-diagonal matrix element for the component of the dipole moment along E.

Thus, the X component of the pseudo polarization \bar{r} is proportional to the real induced polarization, while the Z component $|a|^2 - |b|^2$, is proportional to the difference $\Delta N = N_2 - N_1$ between the populations of levels 2 and 1.

In addition to \bar{r} , we now define a vector $\bar{\omega}$, such that:

$$\begin{aligned} \omega_1 &= \frac{-2\mu_{12}}{\hbar} E_1(t), \\ \omega_2 &= 0, \\ \omega_3 &= \omega_0, \end{aligned} \quad (2.4)$$

where $\omega_0 = \Delta E/\hbar$ and ΔE is the energy difference between levels 1 and 2. It may now be shown [14] that the time dependent Schroedinger equation for this two level, $\Delta m = 0$, system may be written as:

$$\frac{d\bar{r}}{dt} = + \bar{\omega} \times \bar{r} = -\bar{r} \times \bar{\omega}. \quad (2.5)$$

It is seen that this is of the same form as the Bloch equation (1.5) with $\bar{r} \rightarrow \bar{M}$ and $-\bar{\omega} \rightarrow \gamma \bar{H}$. Therefore the same reasoning concerning

precession in stationary and rotating frames may be applied here, the only difference being that the space of operations is mathematical rather than physical. (Also, in the rotating frame, it is the r component in the XY plane, rather than along the X axis specifically, that determines the magnitude of the induced dipole moment [16].) Consequently, the same conclusions follow: upon application of a $\pi/2$ pulse followed a time τ later by a π pulse, an echo appears at time 2τ . The first pulse rotates the \vec{r} vector into the XY plane i.e it maximizes the induced dipole moment and equalizes the populations of levels 1 and 2. In this "superradiant" state the dipoles are all in phase and behave collectively as a macroscopic dipole which radiates strongly through spontaneous coherent emission [11]. The superradiant state consists of a linear combination of superradiant energy states of maximum "cooperation number" as defined by Dicke [17]. The radiation intensity from such a state is given by:

$$I_{SR} = \frac{1}{2} N \left(\frac{1}{2} N + \frac{1}{2} \right) I_0, \quad (2.6)$$

where I_0 is radiation intensity of a single isolated atom, and N is the number of atoms in the sample.

The above intensity is much larger than the incoherent radiation intensity, $I_{inco.} = \frac{1}{2} N I_0$.

Following the superradiant state, dipoles belonging to different $\delta\omega$'s (brought about by inhomogeneous crystal strains, for instance) gradually get out of phase. Finally, the second or " π " pulse moves the system through maximum inversion to equal level population again.

From this time reversal situation (Fig. 1.5e) the induced dipoles rephase again after a time 2τ . It should be remarked that the quantum mechanical formalism given above may, with appropriate redefinitions, also be applied to $\Delta m = 1$ spin transitions. In the case of magnetic spins it then becomes formally identical to the classical description of precessing dipoles in physical space.

The directional aspect of the photon echo experiment is, at least qualitatively, explainable in terms of phase conjugation. Let the direct pulse be incident along the Z axis: $\exp \{j(\omega t - kz)\}$, and the delayed pulse be incident at a small angle ϕ a time τ later: $\approx \exp \{j[\omega(t-\tau) - kz - k\phi y]\}$, where $k_y = k \sin \phi \approx k\phi$. A cubic nonlinearity will then give rise to a term $\exp 2j[\omega(t-\tau) - kz - k\phi y] * \exp \{-j(\omega t - kz)\} = \exp \{j[\omega(t-2\tau) - kz - k2\phi y]\}$ showing that the echo at 2τ propagates at an angle 2ϕ . Similarly, 5th order nonlinear terms should give rise to echoes at 3τ propagating at 3ϕ etc. Multiple echoes were, in fact, observed in the experiment but, for practical reasons, the angle between direct and delayed excitation pulses was chosen to be zero, hence the echoes propagated in the same direction.

Abella et al. [11] have analyzed the photon echo in terms of the quantum-mechanical transitions in a two-level system, as discussed above. To simplify the calculations, they assume the volume of the sample to be small compared to λ^3 , when $\lambda = \frac{2\pi c}{\Omega_0}$ is the transition wavelength, and Ω_0 is the transition frequency as given by $\hbar\Omega_0 = E_2 - E_1$, E_2 and E_1 being the excited and ground state energies, respectively. The above assumption ensures that the radiation field is

uniform in the sample. For such a sample, the echo is emitted by a single, phased oscillating dipole. In the case of a sample of larger volume, the echo is emitted by an array of phased oscillating dipoles, which form a large, directional antenna.

The requirement of a magnetic field in order to obtain a photon echo, as established in experiments, is not a fundamental one. Rowan et al. [18] and Abella et al. [11] have proposed a tentative model to explain the magnetic field requirement, which is based on the effect of an internally modulated magnetic field at the Cr^{3+} sites in ruby, on echo relaxation. According to this description, the electronic spin of the Cr^{3+} ion aligns midway between the optic axis and the applied magnetic field, under a $\pi/2$ pulse. This is due to the anisotropy of the electronic g factors in the ground and excited states of ruby. The direction of the Cr^{3+} spin is along the local magnetic field in the ground state and the optic axis in the excited state. The reorientation under a $\pi/2$ pulse occurs due to the superposition of the wavefunctions of the two levels. This reorientation changes the direction of the effective magnetic field at the Al sites. Consequently, the Al nuclei begin to precess around the resulting magnetic field. This precession, in turn, modulates the magnetic field at the Cr^{3+} sites, resulting in a modulation of the energy level separation, which degrades the amplitude of the photon echo. From this description, it is clear, that the echo-degradation can be minimized if the effective magnetic field at the Cr^{3+} site be aligned parallel to the optic axis, which prevents any pulse-induced reorientation. Since

the local magnetic fields in the ruby sample are random, only an externally applied magnetic field (stronger than the local fields), directed along the optic axis, can assure that the degradation of the echo due to reorientation is minimum.

The photon echo discussed above involved electronic transitions with the emitted light in the visible. Entirely analogous echoes have been observed in the IR due to molecular vibrations [19], and in the microwave region due to molecular rotations [20,21].

CHAPTER III

FERRIMAGNETIC ECHOES

Echoes in single crystals of Yttrium Iron Garnet were first observed in 1968 by Kaplan et al. [22]. Although precession of magnetic spins is involved here, as in paramagnetic echoes, a number of important differences exist. This is mainly due to the fact that neighboring spins are highly coupled so that a description in terms of collective spin modes rather than individual spins is necessary. From a conceptual point of view this makes, of course, no difference because modes are by definition linearly independent. However, this independence may be partly destroyed through nonlinear mode coupling which, if excessive, prevents the formation of nonlinear echoes. From an experimental point of view it is thus desirable that modes overlap spatially as little as possible. Such a spatial localization of modes may be brought about by the combination of the (conventional) inhomogeneous magnetic bias field and an irregularly shaped crystal. As pointed out by Kaplan and co-workers "the stationary waves then assume the form of very narrow wave packets about surfaces along which resonance conditions appropriate to the mode frequency hold" [23]. To verify this claim the Kaplan group devised an

ingenious experiment in which the crystal had the shape of a truncated sphere. As shown in Fig. 3.1, the more severe the truncation, the larger the echo amplitude.

Another difference with paramagnetic echoes is the dependence of the echo amplitude on the separation τ between pulses. As indicated in Fig. 3.2a the amplitude first increases with τ and reaches a maximum before decreasing due to the usual irreversible dephasing and damping effects. For comparison the echo behavior for paramagnetic spin echoes is shown in Fig. 3.2b; we see that here the initial growth with τ is lacking.

From these observations we may conclude that the nonlinear mechanism of echo formation is not the same for these two cases. Whereas paramagnetic echoes are generated because the coupling to the oscillators is nonlinear, ferrimagnetic echoes are brought about because the oscillators are anharmonic, i.e. their frequency depends on the square of the amplitude. That this gives rise to the behavior shown in Fig. 3.2a may be seen as follows. Assume that two pulses $\int A_1 \exp(j\omega t) d\omega$ and $\int A_2 \exp[j\omega(t-\tau)]$, where $A_2 \gg A_1$, are used to modulate a carrier ω_c and applied to the crystal, and that, for simplicity's sake, $\omega_c \tau = n \times 2\pi$, where n is an integer. At a time immediately following $t = \tau$, the amplitude squared of the oscillator (mode) at ω is then given by $a^2 = A_1^2 + A_2^2 + 2A_1A_2 \cos(\omega\tau)$. It will undergo a frequency shift of magnitude, say, αa^2 , where α is some appropriate constant. Neglecting the irrelevant constant terms in a^2 we can write

$\Delta\omega = 2\alpha A_1 A_2 \cos(\omega\tau)$. Then, from τ onwards, the macroscopic response of the oscillators (modes) is given by:

$$\int \exp[j\Delta\omega(t-\tau)] [A_1 \exp(j\omega\tau) + A_2 \exp j\omega(t-\tau)] d\omega. \quad (3.1)$$

Assuming, for simplicity, that $\Delta\omega(t-\tau) \ll 1$ we write:

$$\exp[j\Delta\omega(t-\tau)] \approx 1 + j\Delta\omega(t-\tau) = 1 + j(t-\tau)2\alpha A_1 A_2 \cos(\omega\tau). \quad (3.2)$$

Neglecting the constant term, which merely represents the linear contribution, we may write the macroscopic response as:

$$2j\alpha A_1 A_2 (t-\tau) \int \cos(\omega\tau) [A_1 \exp(j\omega\tau) + A_2 \exp j\omega(t-\tau)]. \quad (3.3)$$

Finally, using $\cos \omega\tau = \frac{1}{2} (\exp(j\omega\tau) + \exp(-j\omega\tau))$, we find that the response contains a term,

$$j\alpha A_1 A_2^2 (t-\tau) \int \exp j\omega(t-2\tau) d\omega. \quad (3.4)$$

As is readily seen, this represents a delta function at time $t = 2\tau$. The significance of the imaginary factor is that the phase of the echo carrier will be shifted by 90° .

Thus, at least for small τ , the echo amplitude should increase linearly with pulse separation, as is indeed the case.

The third difference between paramagnetic and ferrimagnetic echoes is that for the latter the echo is amplified i.e. its

magnitude is much larger than that of the signal (first) pulse. It is argued [23] that this is caused by nonlinear mode coupling. Such coupling, although destroying the echo effect when excessive, serves, when present to a moderate extent, to parametrically couple power into the echo.

The ferrimagnetic echo is a good illustration of the physical complexities involved in actual echo formation. It introduces a second kind of nonlinearity, i.e. anharmonicity and also the use of modes rather than particles as independent oscillators. Nevertheless, as was shown, with a slight modification of the phase conjugation formalism, the basic effect is readily explained, at least qualitatively. Detailed calculation of the echo amplification due to nonlinear mode coupling is more complicated. A simple model using gaussian mode frequency overlap [23] leads to very good qualitative agreement with experiments in the case of echo amplitude dependence on pulse separation.

The Kaplan group also did some interesting time compression signal processing using ferrimagnetic echoes. That this is possible was first demonstrated by Mims [24], using paramagnetic electron spin echoes. The principle of operation is readily explained by means of Fig. 3.3. Assume that the first pulse is replaced by a more complicated signal consisting of two short bursts of frequencies f_1 and f_2 occurring at $t = 0$ and $t = \Delta$. The second pulse is replaced by a similar sequence with the bursts occurring at $t = \tau$ and $t = \tau + \Delta/2$. It is readily seen that the f_2 and f_1 echoes will

overlap at $t = \tau$. More generally, this is true whenever the first signal is a slowly varying frequency and the second one is of the same form but varying at twice the rate. In the actual experiment, which operated at carrier frequencies near 10 GHz, a frequency sweep of 450 MHz was used with a duration (for the signal) of 1 μ sec. The observed echo lasted 5 nsec thereby demonstrating a time compression of 200:1.

We will return later to a more general description of signal processing [5], made possible by the use of parametric echoes.

A mathematical treatment of the generation of echoes due to anharmonic nonlinearity appears in Appendix C.

CHAPTER IV
CYCLOTRON ECHOES

Cyclotron echoes were first observed by Hill and Kaplan [25] in 1965. The independent oscillators in this case consist of electrons gyrating around the magnetic field lines with cyclotron frequencies $\frac{eB_0}{m}$ where e is the charge on the electron, m its mass and B_0 the (inhomogeneous) magnetic bias field. A typical arrangement for observing echoes, using microwave horns, is shown in Fig. 4.1. It is assumed that the dimension of the plasma in the direction of wave propagation is small compared to the wavelength, so that the electrons are excited in phase.

The cyclotron echo case is an interesting example of the search for a nonlinear mechanism to explain echo formation. Two candidates come to mind immediately [26]: a) nonlinear excitation because the electric field, which is a traveling wave, varies (very slightly) across the electron orbit [9] in the direction of propagation, b) anharmonicity because of relativistic effects. As it turns out, neither is the dominant mechanism. It has been shown convincingly by Kaplan and Hill [27] that a third mechanism must be invoked, that of energy dependent collisions. That this leads to echoes can be seen by again examining our model of two modulation pulses, $\int A_1 \exp(j\omega t) d\omega$ and $\int A_2 \exp[j\omega(t-\tau)]$. Let us use a simple

model of the loss mechanism: $\exp(-\beta a^2 t)$ where a represents the amplitude and β an appropriate constant. Then from τ on, the macroscopic response is given by:

$$\int \exp[-\beta a^2(t-\tau)] [A_1 \exp(j\omega t) + A_2 \exp(j\omega(t-\tau))] d\omega. \quad (4.1)$$

[Actually A_1 has decreased slightly prior to τ , but we shall neglect that as it only represents a scaling factor.] Now, as before, $a^2 = A_1^2 + A_2^2 + 2A_1A_2 \cos \omega\tau$. Neglecting constant terms, we now write, in analogy to (3.2):

$$\begin{aligned} \exp[-\beta a^2(t-\tau)] &\approx 1 - 2\beta A_1A_2(t-\tau) \cos \omega\tau = \\ &= 1 - \beta A_1A_2(t-\tau) \exp(j\omega\tau) - \beta A_1A_2(t-\tau) \exp(-j\omega\tau). \end{aligned} \quad (4.2)$$

If (4.2) is substituted into (4.1) we find, that there exists a term which, around $t = \tau$, is described by $-\beta A_1A_2^2 \tau \int \exp j\omega(t-2\tau) d\omega$. As in (3.4) this represents a delta function at $t = 2\tau$ modulated on a carrier which is shifted by 180° .

A more detailed calculation considering both anharmonicity and energy dependent loss has been given in [27].

Gould has given an interesting description of echo formation as a frustration of echo cancellation in linear systems [26]. We shall here apply his reasoning to a general system of oscillators rather than gyrating particles. Assume again that we apply at time $t = 0$ and $t = \tau$ the pulses,

$$V_1(t) = \operatorname{Re} \int_0^{\infty} \exp(j\omega t) d\omega, \quad V_2(t) = \operatorname{Re} \int_0^{\infty} \exp[j\omega(t-\tau)] d\omega. \quad (4.3)$$

Note that (4.3) represents the total physical signal, not just the modulation as in (3.1). Now the state of any oscillator may be visualized in the complex plane by the phasor $\exp[j\phi(t)]$, it being understood that the physical amplitude is represented by the real part. Thus, at a time immediately after the application of the first pulse, all oscillators are characterized by $\phi = 0$ and find themselves at 1 in the diagram of Fig. 4.2a. After a time τ , immediately preceding the second pulse, the oscillators have spread out along the unit circle as indicated for individual oscillators A \rightarrow H. Oscillators A_n \rightarrow H_n exhibit higher frequencies and have made n additional circuits of the unit circle so that $\phi(A_n) = \phi(A) + n2\pi$. Immediately after application of the second pulse, the value 1 has been added to all phasors and the situation is as shown in Fig. 4.2c. Following the second pulse the oscillator phasors continue turning around 0 and the groups $(A_1 A_n)$, $(B_1 B_n)$ etc. break up to distribute themselves along the circles marked A, B etc. in Fig. 4.2d. It is readily seen that at times $t = n\tau$ the groups coalesce again into discrete points on their respective circles. Fig. 4.2e and 4.2f show the situation for $t = 2\tau$ and $t = 3\tau$ respectively. Note that at these times there has occurred a bunching of oscillators (C-G) in the left half plane, all giving a negative real contribution. Hence it could be concluded that a macroscopic effect (echo) occurs at times $n\tau$.

We know that this conclusion is wrong because we are describing a linear system in which echoes are not possible. What really happens is that the summed projections of C-G on the real axis are exactly cancelled by those of the remaining oscillators (H,A,B), the latter, although fewer in number, having larger amplitudes. The point is now that this balance (echo cancellation) may be upset (frustration of echo cancellation) by a slight change in oscillator density along the unit circle. In turn, such a change may be brought about by the nonlinear effects described before. For instance, a nonlinear coupling changes the initial circle into an ellipse [16] as was earlier shown in Fig. 1.6. For the case of spins, anharmonicity changes the distribution along the circle by introducing perturbations in the phasor rotation rate, and nonlinear damping contracts the patterns non uniformly toward the origin. Thus Gould's description provides an elegant and convenient way to visualize the process of echo formation.

To account for the fact that the cyclotron echo associated with an r.f. electric field propagating perpendicular to the d.c. magnetic field is much stronger than that associated with an r.f. electric field which propagates parallel to the d.c. magnetic field, White [9] has proposed that for the perpendicular case (with the magnetic field along the Z-axis, and the r.f. field along Y), any drift in an electron's orbit in the z-direction does not affect the phase of the electron (since the electric field does not vary along Z). For the parallel case (with both

fields along Z), however, a drift in the orbit causes the phase of the electron to change irreversibly. Such an irreversible dephasing degrades the echo considerably.

From a quantum-mechanical viewpoint, White [9] has argued that a system of oscillators can rephase in time only if the non-linear mixing due to pulsed excitation is a periodic function of the perturbation. This, in turn, requires that the energy levels of the system be finite in number. To show that a cyclotron system indeed has a finite number of energy levels, White considered the Hamiltonian for an electron subjected to a d.c. magnetic field $H_0 \hat{a}_z$, constrained to move in the X-Y plane:

$$H_0 = \frac{p_x^2}{2m} + \frac{(p_y + m\omega_c x)^2}{2m} . \quad (4.4)$$

The above resembles the Hamiltonian of a displaced harmonic oscillator. Using the above for a spin-system, and evaluating the upward and downward transition probabilities, TP_{up} and TP_{down} , respectively, White obtained:

$$TP_{up} \propto (n+1)(1-n/2s), \text{ and,} \quad (4.5a)$$

$$TP_{down} \propto n[1-(n-1)/2s], \quad (4.5b)$$

where n is the level number and $s = \frac{m\omega_c}{\hbar k}$. For $n = 2s$, we see that $TP_{up} = 0$. Hence a spin system is clearly truncated (i.e. has only

a finite number of levels with non-zero upward transition probabilities) at $n = 2s$. The analysis for a cyclotron system is more involved, but yields similar results.

In order to demonstrate that velocity dependent collisions play the key role in cyclotron echo effects, Kaplan et al. [27] used a highly ionized cesium plasma (ensuring that collisions would be Coulombic only), with a relatively large electron density ($\sim 10^{12} \text{ cm}^{-3}$). By considering typical values for electron-ion collision time, electron drift time and electron temperature, the minimum electron density required for electron-ion collisions to dominate was found to be about 10^{11} cm^{-3} . In experiments, it was observed that no two-pulse echoes were generated when the electron density in the plasma was below the minimum value predicted. In afterglow plasmas, however, electron-neutral atom collisions generated two-pulse echoes for much lower electron densities ($\sim 10^7 \text{ cm}^{-3}$). The typical values of T_2 and T_1 were found to be 200 ns and 400 ns respectively. One notable exception was a three pulse echo that persisted upto 40 μs . Very large longitudinal lifetimes, however, have been observed and studied only since about 1973.

CHAPTER V
PLASMA ECHOES

In 1967 Gould et al predicted that "if a longitudinal wave is excited in a collision free plasma and Landau damps away, and a second wave is excited and also damps away, then a third (i.e., the echo) will spontaneously appear in the plasma" [28].

The phenomenon of Landau damping is essential to the echo formation. This kind of damping occurs through interaction of the wave fields with electrons which have thermal velocities near the wave phase velocity [29]. Electrons slower than the phase velocity will acquire energy from the field and be accelerated, electrons faster than the phase velocity will impart energy to the field and be decelerated. Since, for a Maxwellian distribution function $f(v) \propto \exp(-\frac{1}{2} m_e v^2 / kT)$, there are more slow electrons than fast ones, energy is, on the whole, removed from the wave and damping occurs, even in the absence of collisions. Landau damping can also be understood by considering the evolution of the electron distribution function $f(v)$ in time and space [30]. If an electric field $\cos(\omega t)$ excites the plasma it will modulate the distribution function [31] leaving a perturbation of the form $f(v)\cos\{\omega_1 t - \omega_1 x/v\}$. For large x , the macroscopic field associated with this perturbation (i.e. the integral over v) phase averages out to zero. Hence Landau

damping may be thought of as a dephasing of signals traveling on electron "beams" [29] with different velocities v and hence different phase velocities. The crucial feature which makes echo formation possible is the reversibility of the phase mixing, in contrast to collision processes which would cause irreversible dephasing.

Following Baker et al. [31], the generation of an echo is best explained by considering the experiment shown in Fig. 5.1. At point 1 a plasma wave is launched at frequency ω_1 . This causes a perturbation of the distribution function which may be written as:

$$f_1(v) \cos\{\omega_1 t - \omega_1 x/v\}. \quad (5.1)$$

A second wave, at frequency ω_2 , is launched at point 2, separated a distance ℓ from 1. This second wave will remodulate the perturbation caused by the first wave so that it will evolve in time and space as:

$$f_{12}(v) \cos\{\omega_1 t - \omega_1 x/v\} \cos\{\omega_2 t - \omega_2(x - \ell)/v\}. \quad (5.2)$$

The above second order perturbation in the velocity distribution contains a term proportional to:

$$\cos\{(\omega_1 - \omega_2)t + (\omega_2 - \omega_1)x/v - \omega_2 \ell/v\} \quad (5.3)$$

In general the macroscopic effect due to this term averages out to zero again. However, for $x = \frac{\omega_2}{\omega_2 - \omega_1} \ell$ the coefficient of v vanishes and an echo should be observable at frequency $\omega_2 - \omega_1$.

Baker et al have given an interesting picture of this process, using electron trajectories as shown in Fig. 5.2. They assume, for the sake of simplicity, that the first signal, at point 1 acts as a gate letting particles through at time $t = n \times 2\pi/\omega_1 = n\tau$. The fan of trajectories originating at each $n\tau$ represents the velocity distribution function $f(v)$. The diagram to the right of the main figure represents the temporal density of particles $n(t)$ at various distances. We see that, at $x = \ell$, all traces of the original modulation have disappeared. At point 2 a second gate operates at a frequency $\omega_2 = 2\omega_1$ i.e. opening every $\tau/2$. The result of this is that at $x = 2\ell$ a periodic modulation at ω_1 is restored, in accordance with the theory ($\omega_2 = 2\omega_1$, $x = \omega_2 \ell / (\omega_2 - \omega_1) = 2\ell$).

Both electron-and ion-wave echoes have been observed. In one ion wave experiment [32], $f_2 - f_1$ was kept fixed at 100 kHz, with exciting frequencies f_1 at 80, 120 and 140 kHz. In another experiment [31], the length ℓ was changed as well as the ratio $(\omega_2 - \omega_1)/\omega_1$. In both cases the measured position of the echo was in good agreement with theoretical prediction. Electron-wave experiments [33] have been performed at 140 MHz and have shown the existence of higher order echoes at appropriate frequencies. It is interesting to note that, in plasma echoes, the role of the ensemble of oscillators with frequency spread Δf is assumed by waves propagating on charged particle "beams" with velocity spread Δv . This is again an example of the general case where, instead of independent local oscillators, independent spatial modes are involved. The

nonlinearity of the process is due to the fact that the phase velocity of the waves (velocity of the beams) depends on the electric field.

Summary of pre 1970 results

We have seen that pulse echoes appear in many systems. All such systems are characterized by exhibiting a large number of independent oscillators or modes with a sufficiently large spread in fundamental parameters such as frequency or (phase) velocity. In addition, nonlinearities must be present to achieve the phase conjugation which leads to echoes. Gould [26] has divided the nonlinear mechanisms into three groups:

- a) nonlinear excitation;
- b) anharmonicity;
- c) nonlinear damping.

Table 1 shows Gould's assignment of nonlinearities to the phenomena we have discussed so far and some additional ones such as fluxoid echoes [34,35].

All the echoes reviewed up to this point are of a dynamic nature: The second pulse must be applied before the oscillations excited by the first one have died out or otherwise irreversibly dephased. We have also limited our description to two-pulse echoes, although three-pulse echoes have been observed. As shown in Fig. 5.3, in the latter case pulses are applied at times $t = 0$, τ and T , whereupon a third echo will appear at $t = T + \tau$ in addition to the usual one at $t = 2\tau$. The mechanism of echo formation

is basically the same, as can be demonstrated by considering the effect of a cubic nonlinearity on the three exciting pulses:

$$\{A_1 \cos(\omega t) + A_2 \cos(\omega t - \omega\tau) + A_3 \cos(\omega t - \omega\tau - \omega T)\}^3,$$

which contains a term $\propto A_1 A_2 A_3 \cos(\omega t - 2\omega\tau - \omega T)$. If all excitations die away with the same time constant T_d then it may be readily shown that the time dependence of the two pulse echo, $\exp(-2\tau/T_2)$, and that of the three pulse echo, $\exp(-2\tau/T_2 - (T-\tau)/T_1)$, should be approximately the same i.e. $T_1 \approx T_2 \approx T_d$. This has indeed found to be the case, with some exceptions.

We now come to a class of echoes (phonon echoes in crystals and powders) where this behaviour is no longer similar but may, in fact, be vastly different. Three pulse echo relaxation times have been observed that to all intents and purposes are infinite. Obviously, some quasi permanent storage must have been effected by the first two (write) pulses so that, as in a hologram, information may be read out much later by a third (read) pulse. In the remaining part of this review we shall discuss such phonon echoes, emphasizing the "static" echo effect, the search to find the correct mechanism and the possibilities for engineering applications.

CHAPTER VI

PHONON (ELECTROACOUSTIC) ECHOES IN PIEZOELECTRIC CRYSTALS

Between 1970 and 1973 several investigators reported the observation of radio frequency echoes in single crystal and polycrystalline piezoelectric or ferroelectric materials [36-40]. Joffrin and Levelut [39] used the term "boson echoes" for this phenomenon and attributed their existence to nonlinear phonon-phonon interactions. Other workers used the names "polarization echo", "electroacoustic echo" or "parametric echo". The new class of echoes differed from most previous ones mainly in the fact that no specific pulse carrier frequency was required and also that the three pulse echo decay time T_1 was many orders of magnitude larger than the two pulse echo decay time T_2 . Working at 9 GHz with CdS cooled to 4°K, Joffrin and Levelut reported T_2 to be about 10μsec and T_1 to be about 0.1 sec.

Shiren et al. [40] reported echoes in piezoelectric photoconductors such as CdS, ZnO etc. Crystal rods were placed in high electric field regions of reentrant or rectangular X band cavities (at ~ 9 GHz) or between the plates of a capacitor ($f < 500$ MHz). For frequencies below 500 MHz, echoes were reported between 1.4°K to 400°K, while for frequencies above 1 GHz, no echoes were reported

above 70°K. The following additional properties were observed during the experiment:

- (a) No echo was produced if the sample was not "charged" with visible light. Following "charging", the experiments could be conducted both in the dark or under illumination.
- (b) The echo amplitude was maximum when the wavelength of the light approached the band gap wavelength of the crystal. However, correspondingly, the ultrasonic attenuation was maximum near this wavelength, and T_2 was reduced considerably.
- (c) In general, the two pulse echo amplitude decayed as a simple exponential:

$A_{DE} \propto \exp(-2\tau/T_2)$, where the subscript DE refers to a dynamic echo. T_2 is of the order of 10 μ sec.

- (d) The three pulse echo amplitude also decayed as a simple exponential:

$A_{SE} \propto \exp\left(\frac{-2\tau}{T_2} - \frac{T-\tau}{T_1}\right)$, where the subscript SE refers to a stimulated, or, as discussed later, static echo. T_1 was found to be of the order of 20 hrs. at 4°K.

In order to explain the two-pulse echo phenomenon, Melcher and Shiren [41] proposed an electroacoustic interaction model.

According to this model, the first r.f. pulse generates a forward-traveling sound wave, by the direct piezoelectric effect, with parameters (ω_1, \vec{k}_1) , where ω_1 is the acoustic frequency (equal to the r.f. pulse carrier frequency) and \vec{k}_1 denotes the propagation

vector in the forward direction. The acoustic wave, traveling in the bulk of the sample, rapidly loses phase coherence due to the thinness, roughness and inhomogeneities of the sample. (In other words, the acoustic wave is carried by a variety of modes with a spread in \vec{k} vectors.) At time $t = \tau$, a second pulse is applied at frequency ω_2 . The crystal dimension is such that even at microwave frequencies the r.f. pulse generates only a static electric field in the sample with parameters $(\omega_2, 0)$, where the zero refers to its non-propagating character. According to the present model, harmonics $m\omega_2$ of this static field are generated through a non-linear effect that is associated with the ionization of shallow trap electrons into the conduction band. In turn these harmonics interact (through the same nonlinearity) with the piezoelectric field associated with the acoustic wave (ω_1, \vec{k}_1) , and produce a mixing term $(\omega_1, \vec{k}_1) * (m\omega_2, 0) = (m\omega_2 - \omega_1, -\vec{k}_1)$. Thus, a backward propagating acoustic wave at frequency ω_1 is generated whenever $m\omega_2 = 2\omega_1$. (This is, in fact, the selection rule that is actually observed [41].) As this phase conjugation process happens for each of the modes mentioned before, they will all get back in phase again after $t = 2\tau$ so that, at that time, the re-constructed wave is detected as an echo pulse in the receiver.

To account for the very slow decay of the three-pulse or stimulated echo, Shiren et al. [40] proposed and others [42,43] clarified a model based on an induced electronic space charge grating. On illumination, shallow electron traps ($\epsilon_T \sim 10^{-2}$ eV) in the crystal

near the conduction level are filled up. This requires a photon energy close to the band gap energy. At liquid helium temperature the traps have the lifetimes of the order of a few days. The forward propagating acoustic wave due to the first pulse, proportional to $\cos(\omega t - kx)$, interacts nonlinearly with the static electric field due to the second pulse, proportional to $\cos\{\omega(t-\tau)\}$, to yield a component of field proportional to $\cos(kx - \omega\tau)$. This represents an interference pattern stationary in time but periodic in space, with a spatial period corresponding to the acoustic wavelength. According to Shiren et al. [40] and Asadullin et al. [42], the above stationary field causes, through field-induced ionization into the conduction band, an inhomogeneous space charge distribution over the traps, which contains the information about the frequency ω as well as about the time interval τ of the two exciting pulses. This distribution forms an internal grating made of electrons. The electric field of the third pulse, whose piezoelectric coupling is spatially distorted in conformance with this grating, now generates a backward as well as a forward acoustic wave, which are detected piezoelectrically at the crystal surface in the form of the stimulated echo. (This situation is analogous to the excitation of acoustic surface waves by a grating of interdigital electrodes [43].) The decay time T_1 of these stimulated echoes is thus the same as that of the traps, which explains the very long persistence of the effect. It should be remarked, in passing, that the effect is entirely analogous

to that employed in the fabrication of semiconductor acoustic surface wave convolvers [44].

Another model has been proposed in the Soviet literature. According to Krainik et al. [45] the temporally invariant, spatially periodic wave, discussed above, produces a fixed elastic pattern in the crystal which comprises an acoustic hologram. This pattern may be produced by interaction of the acoustic wave with crystal defects. The third pulse, called the read pulse, acts on the acoustic hologram to produce an echo.

Two pulse phonon echoes have also been observed in polycrystalline magnetic ferrites [46]. In this case the echo is due to magnetostrictive excitation of elastic waves. The required non-linearity is believed to be related to defects.

CHAPTER VII

PHONON (ELECTROACOUSTIC) ECHOES IN POWDERS

The first (dynamic) echoes due to acoustic resonances of individual powder particles were observed and interpreted as such by Rubinstein and Stauss [47]. In their work on lithium ferrite powders they noticed that (magnetic) excitation of echoes was only observed when the dimensions of the particles were of the order of an acoustic wavelength. Furthermore, the echoes disappeared when the particles were suspended in a liquid, an effect that was correctly ascribed to acoustic damping. (In fact, a thorough cleaning and drying of the sample was required to restore the echo phenomenon). Also, the transverse relaxation time T_2 increased with decreasing temperature as shown in Fig. 7.1. The investigators proposed a magnetic nonlinear excitation mechanism that they believed to be due to the modulation of the magnetic anisotropy forces by lattice vibrations. Phenomena similar to those described above have also been observed in metals [35,48] and in commercial ferrites [45].

Since the early 1970's the emphasis in echo experiments has shifted to the area of r.f. echoes in piezoelectric powders. The fact that powder echoes can be obtained in an extremely wide range of powdered crystals, over a wide range of frequencies, and require

rather simple experimentation, has no doubt contributed to the enthusiastic investigations by many groups.

The piezoelectric powder echoes differ from the crystal echoes in the following ways:

- a) They can be obtained from the powdered form of some materials which, in the crystalline form, do not generate any echoes;
- b) They do not depend on illumination;
- c) They exhibit very large longitudinal relaxation times (T_1) of the stimulated echoes, even at elevated temperatures approaching 300°K;
- d) The decay curve for the three-pulse powder echoes generally shows evidence of several values of T_1 .

Melcher and Shiren [49] reported two-pulse and three-pulse echoes in powders of quartz, sand, LiNbO_3 , $\text{K}_x\text{Li}_{1-x}\text{NbO}_3$, BaTiO_3 , $\text{Gd}_2(\text{MoO}_4)_3$, Li_2GeO_3 , PLZT ceramic, Se, CdS, ZnO, ZnSe, CdTe and GaAs. Similar echoes were observed by Krainik et al. [50].

Fig. 7.2 shows a plot of the two-pulse echo amplitude against the average particle diameter in a powder sample of GaAs, using 30 MHz pulses at 300°K. The echo amplitude is observed to pass through a maximum for a particle diameter of about 67mm. This particle size corresponds to a half-wavelength of sound at 300 MHz, assuming a velocity of 4×10^5 cm per second, a fact which lends strong support to the claim that the two-pulse echo in powders corresponds to the acoustic resonance of the powder grains. Moreover, as in the case of ferrite powders, it has been observed that the surface condition of the particles strongly determines the

magnitude of the transverse relaxation time T_2 . In one case, careful etching of the particles after grinding resulted in an increase of T_2 by two orders of magnitude [51]. This points to some form of damping due to the interaction of the particles with the environment or with each other. Kuindersma et al. [52] diluted active particles of SiO_2 with a fine grained inert powder such as Al_2O_3 and found that T_2 was linearly proportional to the inverse concentration. This argues for a neighboring particle interaction as the mechanism of transverse relaxation.

Various theories were proposed to explain the short term echo. Kuindersma et al. derived pseudo Bloch equations, starting from a nonlinear Hamiltonian for each particle [52], whereas Kessel et al. used a nonlinear free energy formalism to calculate the effect [53]. Both theories predicted two pulse echoes with a simple τ dependence of the kind $\exp(-2\tau/T_2)$.

Kajimura et al. at IBM [54] pointed out that careful measurements of echo amplitudes did not confirm this simple decay but that instead a behavior was found in which the echo first increased from zero to a maximum and then decayed exponentially with T_2 . This behavior is shown in Fig. 7.3. As we have seen before (Ch. III) it is characteristic of anharmonicity. Starting from an anharmonic wave equation and using a slowly varying envelope approximation, the IBM group derived an expression for the two-pulse echo amplitude of the form $[1 - \exp(2\tau/T_2)] \exp(-2\tau/T_2)$. This is in good agreement with experiment as can be seen from the dashed curve in Fig. 7.3. Even

closer agreement can be achieved (solid curve) when it is assumed that there exists a distribution of damping rates in the sample. It should be noted, though, that at very high excitation levels, the decay behavior becomes power sensitive and quantitatively different from that shown in Fig. 7.3. This effect (and a corresponding variation in pulse shape) is greatly emphasized by lowering the temperature.

Following the above investigation, the IBM group greatly extended its experimental work on piezoelectric echoes and refined the theory. Full details can be found in an extensive article reviewing these investigations [55], and in an account of parallel efforts elsewhere [56].

As pointed out in Chapter III, echoes caused by anharmonicity not only should show the behavior of Fig. 7.3, but also their phase should be shifted by 90° relative to the phase of an echo caused by nonlinear excitation. Kunkel et al. [57] reported on such phase measurements using the spin echo from the nuclear resonance in water as a reference. They found a phase angle of 78° for (Lorentz force excited) Al powder and 93° for (magnetostrictively excited) Ni powder.

Some other observations concerning dynamic echoes are of interest here. Gurevich et al. [58] have observed echoes at double the frequency, located near $t = (3/2)\tau$. These echoes should be due to an $E_2^3 E_1$ term in the excitation. The time dependence of this for two pulses is $E_2^3 \cos^3(\omega t - \omega\tau) E_1 \cos \omega t$. It is readily seen

that this contains a term:

$$E_2^3 E_1 \cos(3\omega t - 3\omega\tau - \omega t) = E_2^3 E_1 \cos 2\omega(t - \frac{3}{2}\tau), \quad (7.1)$$

thus correctly predicting the observed echo. Kopvillem and Prants [59,60] have developed a quantum mechanical theory of coherent polarization effects that predicts echoes in all physically inhomogeneous non piezoelectric dielectrics.

Although the mechanism of the dynamic echo has been firmly established, that is not the case for the stimulated echo. The anomalous persistence of this echo in powders was first reported in 1975 by Popov et al. [61,62]. The discovery led to the possibility of obtaining very long and stable memories in powders. Relaxation times of weeks at room temperature were reported in powders of Rochelle salt and bismuth germanate. Such anomalous behaviour was later also found to exist in powders of KDP, ADP, LiNbO_3 , NH_4Cl , $\text{Bi}_{12}\text{SiO}_{20}$ etc. [42].

In a typical three-pulse experiment the powder sample is subjected to two intense r.f. pulses at times $t = 0$ and $t = \tau$, at a frequency corresponding to acoustic resonance of the average particle. Next, a third pulse is applied (at the same center frequency) at a time $t = T$. The value of T is varied from $T = \tau$ to very high values, keeping the two-pulse separation τ constant, and the amplitude of the echo at $T + \tau$ is plotted against T . Fig. 7.4 shows a typical plot. It will be seen that the echo amplitude

follows a decay pattern characterized by two relaxation times. For low values of T (close to τ) it decays roughly exponentially as $\exp[-(T-\tau)/T_2]$. This evidently represents the usual dynamic decay of the acoustic vibrations of the powder particles. However, for values of T approaching several days and even weeks, the echo is found to remain practically constant.

The non-dynamic part of the stimulated echo, also termed the static-, storage-, memory-, or stimulated echo, was found to disappear [61,62] when the ampoule containing the powder grains was rotated by 90° relative to its axis. The echo reappeared when the original orientation was restored. In testing the variation of the storage echo amplitude with pulse carrier frequency, the echo was found to have a sharp maximum when the frequency of all pulses coincided with the average resonant frequency of the powder grains.

The fact that the recall time for the third pulse is far longer than the lifetime of an acoustic phonon or an electron in a trap makes previous explanations inadmissible; hence a new storage mechanism had to be found.

Melcher and Shiren [49,51] proposed an orientation mechanism on rotation of powder particles due to the second applied pulse. In their model the first pulse develops a vibrating piezoelectric dipole $\bar{p} \cos(\omega t)$ where $p \propto E_1 \cos\theta_0$; θ_0 is the angle between the applied field and the piezoactive axis, ω is the resonant frequency of the particular particle and E_1 is the component at ω in the frequency spectrum of the exciting pulse. The relevant configuration

is shown in Fig. 7.5. The second pulse (also at frequency ω) will now cause a d.c. torque $(\bar{p} \times \bar{E}_2)_{\omega=0}$ which will cause the particle to rotate by an angle $\Delta\theta$. If viscous forces predominate, the rotation angle is given by:

$$\Delta\theta \propto E_1 E_2 \cos\theta_0 \sin\theta_0 \cos\phi, \quad (7.2)$$

where $\phi = \omega\tau$ denotes the phase difference between the components at ω of the first and second pulse. A third pulse at $t = T$ will now reexcite the particles and cause a macroscopic dipole moment along the piezoactive axis whose amplitude is:

$$E_3 \cos\theta'_0 = E_3 \cos(\theta_0 + \Delta\theta). \quad (7.3)$$

For small $\Delta\theta$ this contains a term:

$$E_3 \sin\theta_0 \Delta\theta = E_1 E_2 E_3 \cos\theta_0 \sin^2\theta_0 \cos(\omega\tau). \quad (7.4)$$

Finally, the macroscopic component along the field axis is given by (after multiplication by $\cos\theta_0$):

$$E_1 E_2 E_3 \sin^2 2\theta_0 \cos(\omega\tau). \quad (7.5)$$

Summing all macroscopic components over all oscillators we find:

$$E_1 E_2 E_3 \sin^2 2\theta_0 \int \cos(\omega t - \omega T) \cos(\omega\tau) d\omega, \quad (7.6)$$

which contains a term:

$$E_1 E_2 E_3 \sin^2 2\theta_0 \int \cos(\omega\tau - \omega T - \omega\tau) d\omega. \quad (7.7)$$

The last expression represents a delta function at $t = T + \tau$ i.e. the stimulated echo. In reality, of course, (7.7) should be averaged over the distribution of θ_0 's in the sample but that will not change the essential features of the explanation. Wilms and Vertogen [63] have performed numerical calculations in accordance with the above model, using the equations:

$$\ddot{q}_i = -\omega^2 q_i + E \cos\alpha_i, \quad (7.8)$$

$$\ddot{\alpha}_i = -k\dot{\alpha}_i - q_i E \sin\alpha_i, \quad (7.9)$$

where q_i is the dipole moment of the i^{th} particle and α_i is the angle discussed before. The calculation was performed for a system of between 100 and 400 particles with a random resonant frequency distribution $0.90 < \omega < 1.10$. The applied field was given a Lorentzian line shape in time: $\delta \text{sinc}/(1+0.01t^2)$ and allowed to act for a time $\Delta t = 20\pi$. The time between pulses was varied between $100 < \tau < 1000$. The initial orientation was taken to be $\theta_0 = \frac{\pi}{4}$ for all particles. Fig. 7.6 shows, as a function of ω , the energy of particle vibration and the particle orientation at $t = 0$, $t = \tau^+$ and $t = (T + \tau)^+$. Note that the strength of the stored information (i.e. α) has increased after application of the third or "read" pulse. This somewhat mysterious behavior has actually been observed in experiments [64,65]. Fig. 7.7 shows two echoes at times τ and 2τ

after the second pulse. Note the ringing due to the finite number of particles used in the calculation.

It is interesting to note that the memory mechanism outlined above could well be called "electronic holography". As in optical holography [66], both the phase and amplitude of a spectral component of the signal E_1 (plane wave spectrum in optics) are stored by recording the pattern of interference ($\cos \omega t$ in the electrical case) with a signal E_2 . The recording takes the form of a change in the coupling parameter: amplitude transmission in optics, angle between dipole and field in electronics. A third "read-out" signal acts via the coupling parameter to reconstruct the original signal. We will return to this description in Ch. VIII.

An apparent confirmation of the orientation model was given by the fact that mechanical shaking ("a sharp rap") [49] destroyed the static echo. However, Asadullin et al. [67] reported that the original echo could be restored partially by a light tapping during read-out or by a "rest" of several tens of minutes after shaking. Berezov and Romanov [68] reported even stranger behavior: after complete stirring (sifting) of the exposed sample, the echo signal still appeared at 1/7 of the original amplitude.

Other objections to the rotation model of echo storage follow from the observed dependence of echo amplitude on sample rotation before final read-out. According to the simple description given before, the echo should be proportional to $\cos 2\theta_0 \cos(2\gamma + 2\theta_0)$ where γ is the sample rotation. It had already been observed in

the earliest experiments [61,62] that the echo disappeared upon rotating the sample by 90° , in disagreement with this prediction. More detailed measurements confirmed this and showed an approximate $\cos^2 \gamma$ dependence [69-71].

It is clear from the above findings that the orientation model by itself is not sufficient to explain the memory echo and that other mechanisms must be active in addition. It has been proposed that a d.c. dipole may be established in the particles through charge transfer [72] or that the effect may be due to dislocation nonlinearities [68] or plastic deformations [73]. In connection with the latter it is claimed that both plastic deformations and memory echoes disappear upon heating to a few hundred degrees C.

Although the exact mechanism of memory echo formation has thus not yet been unambiguously established, it is nevertheless clear that there is a potential for more general signal storage. In this context it is of interest that the echo can be reinforced by repeated exposure of the sample to write-in pulse pairs [42]. It has also been shown that the echoes show frequency selectivity i.e. the frequency may be used as an address for information [74], again in analogy to multiple recording of holograms by spatial carriers [75].

Finally, from the few experiments that have been performed with signals other than short pulses, [5,76] it appears that interesting signal processing should indeed be possible. We shall discuss this next.

CHAPTER VIII
ELECTRONIC HOLOGRAPHY

Most of the phenomena discussed so far may be described by a formalism similar to that used in optical holography. To see why this is so, let us return to the case of two pulses applied at $t = 0$ and $t = \tau$. We have seen how, due to a cubic nonlinearity, the individual oscillators generate signals of the kind $A_2^2 A_1 \cos \omega t \cos^2 \omega(t-\tau)$ which contribute to the echo component $A_2^2 A_1 \cos \omega(t-2\tau)$. If we had used phasor notation the echo could be written as $A_2^2 A_1^*$ where $A_2 = |A_2| \exp(-j\omega\tau)$ and $A_1 = A_1^* = |A_1|$ in this case. It is easy to generalize this description by assuming that the first pulse is characterized by a frequency spectrum $\phi_1(\omega)$ and the second one by $\phi_2(\omega)$. The parametric signal generated by the individual oscillator at ω is then given by $\phi_2^2(\omega)\phi_1^*(\omega)$ and hence this expression also represents the spectrum of the macroscopic signal. This notion was first advanced by Fossheim et al [55] in the context of piezoelectric powders and later used independently by Korpel as the basis of a general formalism [5]. In this formalism it is assumed that the oscillator ensemble is excited by a general signal $e(t)$ (which may consist of the two pulses just discussed) of finite duration T . If $\phi(\omega)$ is the frequency spectrum of $e(t)$ it may be shown that, for cubic nonlinearities, the

parametrically generated signal $E'(t)$ has a frequency spectrum $\phi'(\omega)$ given by:

$$\phi'(\omega) \propto \phi^2(\omega)\phi^*(\omega). \quad (8.1)$$

Eq. (8.1) is valid only in the time domain $t > T$. Prior to that time the ordinary Fourier spectrum of $e(t)$ cannot be calculated as $e(t)$ is not yet over. For $t < T$ we must then use the instantaneous frequency spectrum as defined by Page [77]. We shall not, however, discuss such details here but restrict our attention to $t > T$.

In the case of two delta functions, at $t = 0$ and $t = \tau$, we find:

$$e(t) = \delta(t) + \delta(t-\tau), \quad (8.2)$$

$$\phi(\omega) \propto 1 + \exp(-j\omega\tau), \quad (8.3)$$

$$\begin{aligned} \phi'(\omega) &\propto |1 + \exp(-j\omega\tau)|^2 [1 + \exp(j\omega\tau)] \\ &= 3 + 3 \exp(-j\omega\tau) + \exp(j\omega\tau) + \exp(-2j\omega\tau). \end{aligned} \quad (8.4)$$

Of the four terms in this expression only the fourth has a physical significance for $t > T$ and represents the echo at 2τ . That the concept is more general may be seen by considering the case where

$$e(t) = e_1(t) + \delta(t-\tau), \quad (8.5)$$

as illustrated in Fig. 8.1. Here we find that (8.1) contains a term:

$$\phi'_t(\omega) = \phi_1^*(\omega) \exp(-2j\omega\tau) \quad (8.6)$$

which corresponds to a macroscopic signal

$$E'(t) = e_1(2\tau-t), \quad (8.7)$$

i.e. a time reversed delayed version of e_1 itself. More generally, the time domain equivalent of (8.1) may be written:

$$E'(t) \propto \int \phi^2(\omega) \phi^*(\omega) \exp(j\omega t) d\omega = e(t) * e(t) * e(t), \quad (8.8)$$

where $*$ denotes convolution and $*$ denotes correlation.

It is interesting to note that the formalism of Eq. 8.8 is analogous to the one used in Fourier holography if ϕ_t is taken to represent the sum of the reference wave and the signal wave. This may be seen as follows. Assume that, in the Fourier plane of a lens, there exists an interference pattern with amplitude distribution $\phi(u,v)$ brought about by the interference between a reference wave ϕ_r , and a signal wave ϕ_s . The pattern is recorded on photographic film. With the photographic processing used in holography, the amplitude transparency of the resulting negative is given by $\phi\phi^*$. Suppose now that, in the reconstruction process, the negative is illuminated with ϕ rather than, as is commonly done, with ϕ_r . In the Fourier plane there would then be created a field $\phi\phi\phi^* = \phi^2\phi^*$.

After an inverse Fourier transform this would in turn give rise to a field:

$$E'(x,y) \propto \iint \phi^2 \phi^* \exp[jc(xu + yv)] dudv, \quad (8.9)$$

where c is an appropriate constant. Taking into account that Eq. (8.9) represents a two-dimensional process, the resemblance with Eq. (8.8) is evident.

The long term or memory echo may also be analyzed by the same formalism. In that case it is assumed that the coupling factor K to the individual oscillators is modified by the first signal $e(t)$ as:

$$\Delta K \propto |\phi(\omega)|^2. \quad (8.10)$$

If the recall pulse $e_r(t)$ has a spectrum $\phi_r(\omega)$, the spectrum $\phi''(\omega)$ of recalled signal $E''(t)$ is then given by:

$$\phi''(\omega) \propto |\phi(\omega)|^2 \phi_r(\omega), \quad (8.11)$$

so that

$$\begin{aligned} E''(t) &\propto \int \phi(\omega) \phi^*(\omega) \phi_r(\omega) \exp(j\omega t) d\omega \\ &= e(t) * e(t) * e_r(t). \end{aligned} \quad (8.12)$$

As before, (8.11) and (8.12) are valid only for times subsequent to the end of the recall pulse. For the case of two delta functions, at $t = 0$ and $t = \tau$, followed by a recall delta function at $t = T$, we have:

$$\phi(\omega) = 1 + \exp(j\omega\tau), \quad (8.13)$$

$$\phi_r(\omega) = \exp(-j\omega T), \quad (8.14)$$

from which it follows readily, with (8.11),

$$\phi''(\omega) \propto 2 \exp(-j\omega T) + \exp[-j\omega(T-\tau)] + \exp[-j\omega(T+\tau)]. \quad (8.15)$$

Of the three terms in (50), only the third one has physical significance in the region $t > T$; it represents the memory echo.

That more general signal processing is possible can be seen by assuming that $e(t)$ consists of two well separated functions $e_1(t)$ and $e_2(t-\tau)$, and that the recall signal is again a delta function at $t = T$. In that case,

$$\phi(\omega) = \phi_1(\omega) + \phi_2(\omega)\exp(-j\omega\tau), \quad (8.16)$$

$$\phi_r(\omega) = \exp(-j\omega T), \quad (8.17)$$

from which, with (8.11),

$$\begin{aligned} \phi'' = & |\phi_1|^2 \exp(-j\omega T) + |\phi_2|^2 \exp(-j\omega T) + \phi_2^* \phi_1 \exp[-j\omega(T-\tau)] + \\ & + \phi_2 \phi_1^* \exp[-j\omega(T+\tau)]. \end{aligned} \quad (8.18)$$

The last term represents the potentially useful correlation signal $e_2 * e_1$ centered at $t = T + \tau$. If now e_1 is a delta function centered at $t = 0$, then this useful part of the recalled signal is the non time inverted replica of e_2 , centered at $t = T + \tau$. Hence it would appear that permanent storage of arbitrary signals should be possible.

It is of interest that the concept of signal storage in the above manner was first formulated by Longuet-Higgins [78] in 1968, independently of any of the echo work then in progress. Longuet-Higgins was interested in the behavioral problem of recall and recognition. He suggested a model consisting of a bank of resonators whose coupling constants were to be altered by an amount proportional to the energy in the spectral components to be stored. Gabor [79,80] suggested that the function of the resonators could also be performed in the time domain by a triple product involving correlation and convolution. This triple product is in essence identical to the one described by (8.12). As neither Longuet-Higgins nor Gabor seem to have been aware of investigators in the field of parametric echoes, (and vice versa), this development is a beautiful example of convergent scientific evolution!

An actual model experiment [5] using 20 nonlinear electronic resonators was performed by Korpel in 1977. As shown in Fig. 8.2, the resonators consisted of parallel LC circuits in which varactor diodes served as nonlinear capacitors. The circuits were tuned in steps of 25 kHz, from 1.750 MHz to 2.225 MHz. The Q of each circuit was of the order of 200, corresponding to an oscillator decay time of 20 μ sec. Fig. 8.3a shows the generation of a dynamic echo, Fig. 8.3b the results of the corresponding low level control experiment. The same experiment also showed multiple echoes but these are off the time axis in Fig. 8.3.

In order to generate a memory echo, the circuit of Fig. 8.2 was modified so as to make it possible for the voltage across the circuit to change the coupling coefficient in a quasipermanent fashion by self biasing of the varactor diode. The relevant time constant of the bias circuit was of the order of 1 msec, long compared to the decay time of the individual oscillators. Fig. 8.4a shows the result of a three pulse experiment, Fig. 8.4b is again the control. The amplitude of the memory echo was also measured, as a function of the delay T of the recall pulse. This is shown in Fig. 8.5. As expected the observed decay is exponential with a time constant approximately equal to that of the bias circuit. For small delays the echo amplitude appears to be saturated.

More general dynamic signal processing is shown in Fig. 8.6. The exponential tail to the rectangular pulse is in agreement with the theory and has also been seen by Smolyakov and Khaimovich [76].

The latter have, however, also observed a single sharp echo following the rectangular pulse, which is not seen here.

CONCLUSION

It has been seen how what seemed originally an isolated phenomenon - the spin echo - turned out to be a universal manifestation of nonlinear systems containing a large number of independent modes. The phenomena discussed make it clear that this insight only came about gradually. The role of nonlinearities was perceived first and nonlinearities were subsequently classified in various categories such as anharmonicity, nonlinear coupling and nonlinear loss. The nature of the individual modes was broadened in scope from individually resonating particles to dispersive eigenmodes. It was seen that phase conjugation and time reversal played important roles and that the whole process was, in a formal sense and sometimes even in a practical sense, very similar to holography. This in turn opened up the possibility of general signal processing, a possibility which, curiously enough, had been foreseen by researchers in an entirely different discipline.

The first stage of exploration has now come to an end, but further developments and, above all, applications appear to be strangely lacking. Yet the promise of fairly general utility seems to be clear. It may be that, as has happened with so many other intriguing techniques of analog signal storage and parallel processing, this one too will succumb to sequential processing using

digital large scale integration. On the other hand, it may be that this particular technique just is not very well known among engineers. Whatever the reason, it is hoped that this study may give some fresh impetus to developments in this intriguing area of "Fourier space engineering".

Table I. Types of echoes (after Gould (26), with additions).

Type	System	Probable Nonlinearity	Possible Nonlinear Effects
Spin echo	Precessing nuclear spins in a magnetic field; electron spins in ferromagnetic materials	(a)	(a) Nonlinear excitation (b) Anharmonicity
Photon echo	Oscillating electric dipoles of Cr^{3+} ions in ruby crystal and of SF_6	(a)	(c) Nonlinear damping (d) Permanent plastic deformations/change of coupling constants due to nonlinear stress and strain in oscillators
Ferrimagnetic echo	Precessing magnetic spins with moderately high coupling	(b)	
Cyclotron echo	Gyrating free electrons of a plasma in a magnetic field	(b),(c)	
Molecular echo	Rotating molecules in a gas; oscillating electric dipoles in NH_3	(a)	
Plasma wave echo	Streaming free electrons in a plasma	(a),(b)	
Fluxoid echo	Fluxoid excitations in type II superconductors	(b)	
Phonon echo in crystals	Electroacoustic interactions in bulk piezoelectric crystals	(a)	
Phonon echo in powders	Oscillating powder grains under intense r.f. electric fields	(b),(d)	

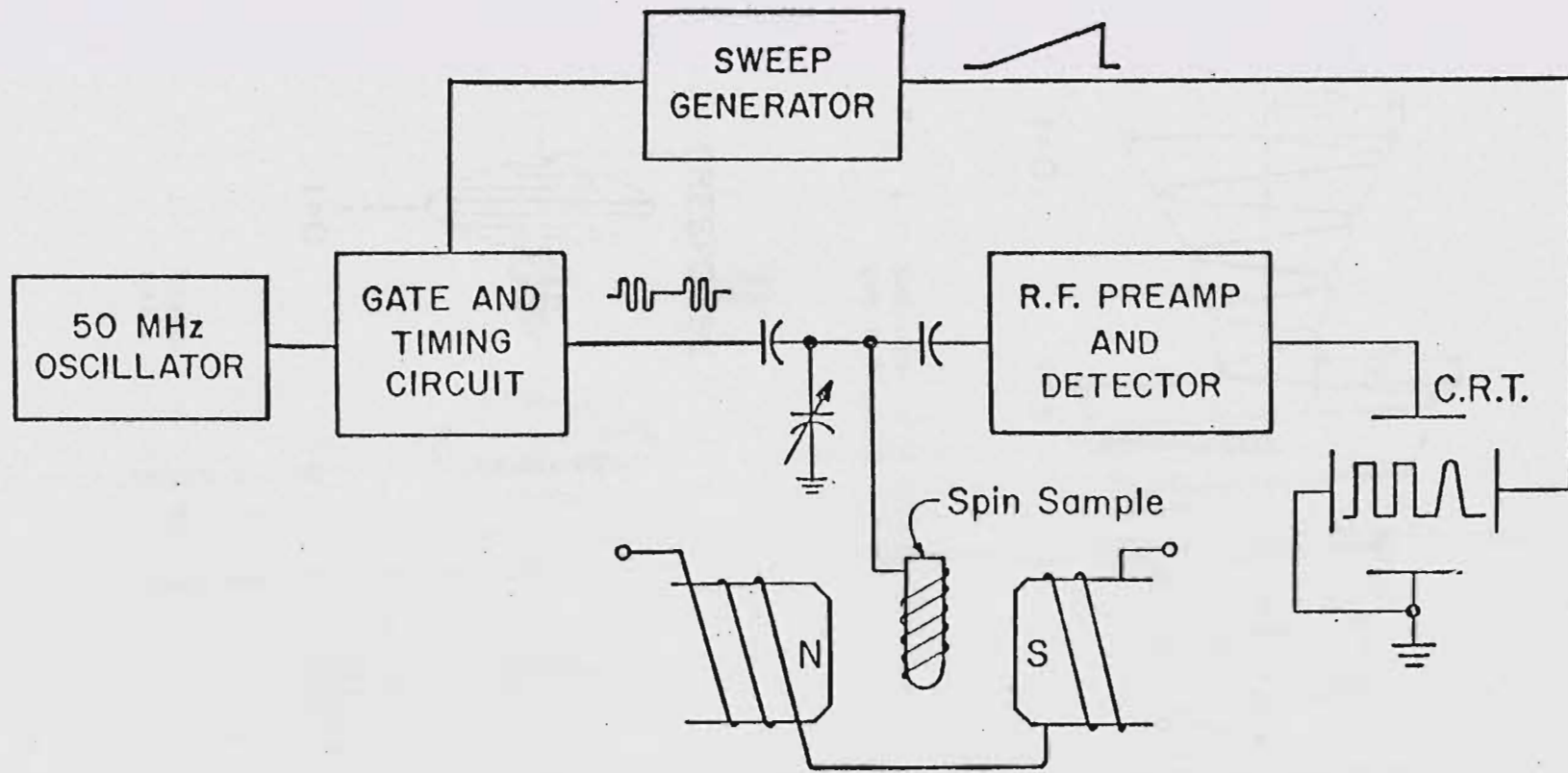


Fig. 1.1 Schematic arrangement for obtaining spin echoes (note that only pulse envelopes are shown). (After Hahn (1)).

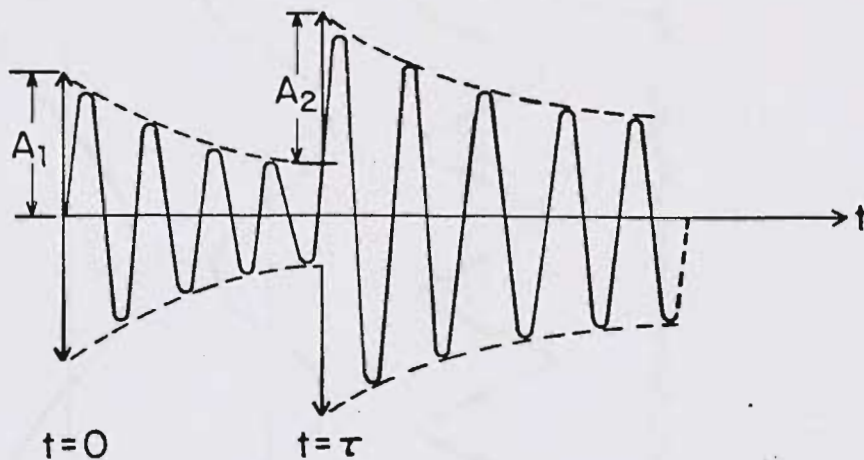


Fig. 1.2 Response of a linear system to two r.f. pulses.

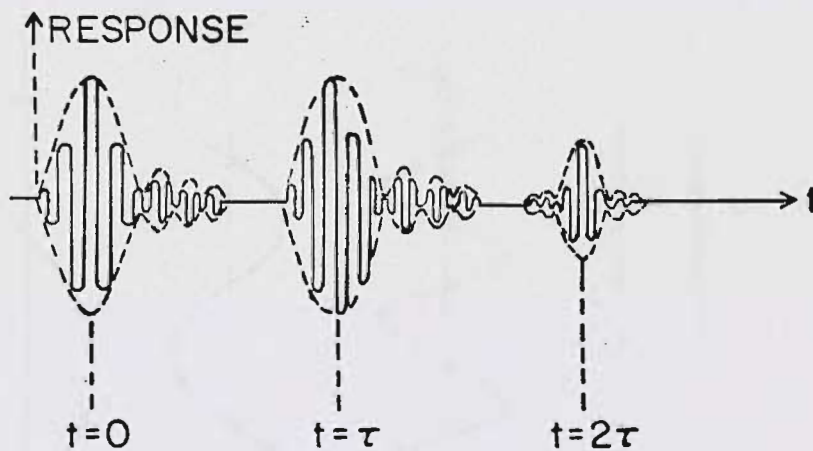


Fig. 1.3 Response of a nonlinear system to two r.f. pulses.

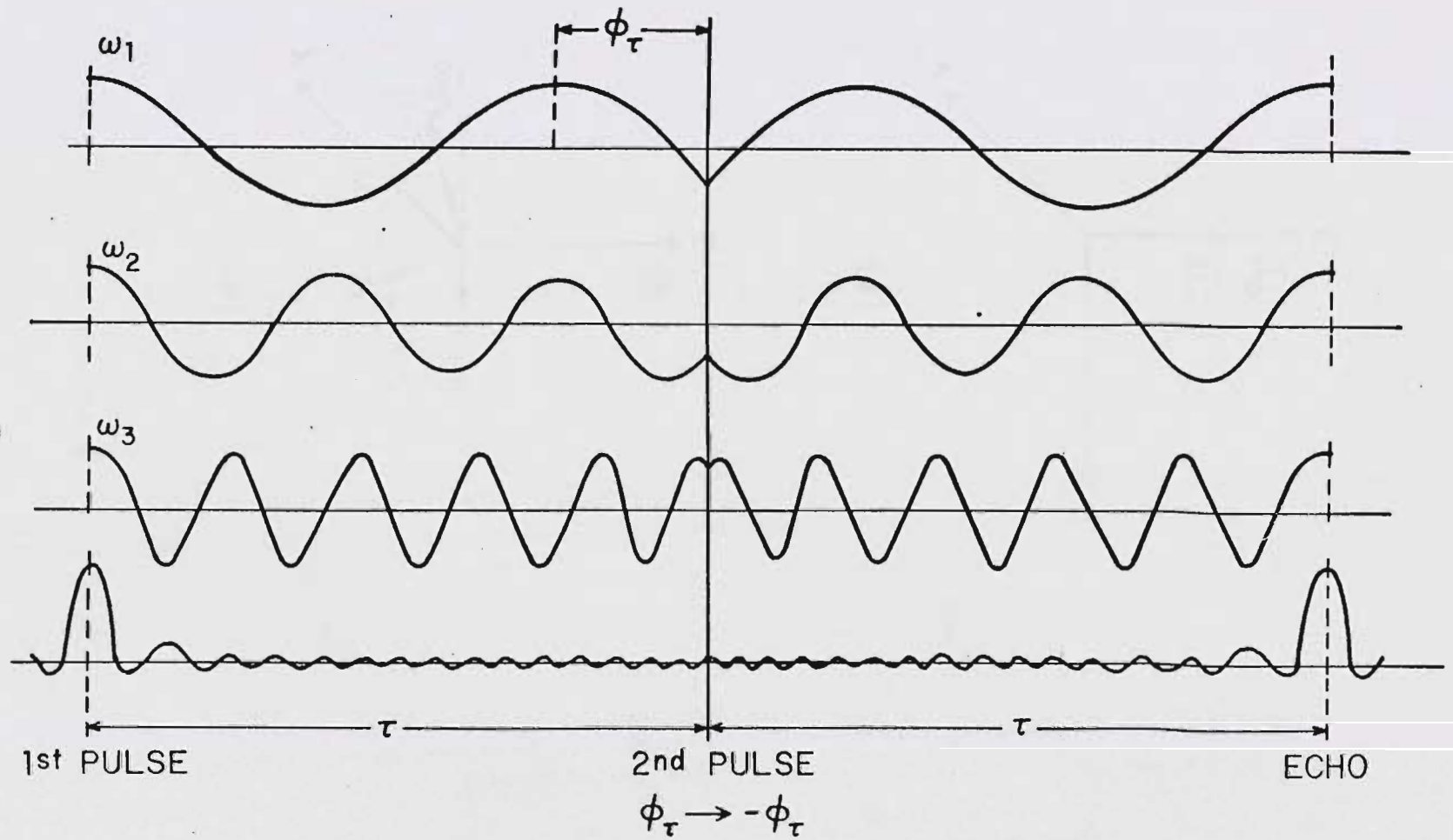


Fig. 1.4 Illustration of phase conjugation concept.

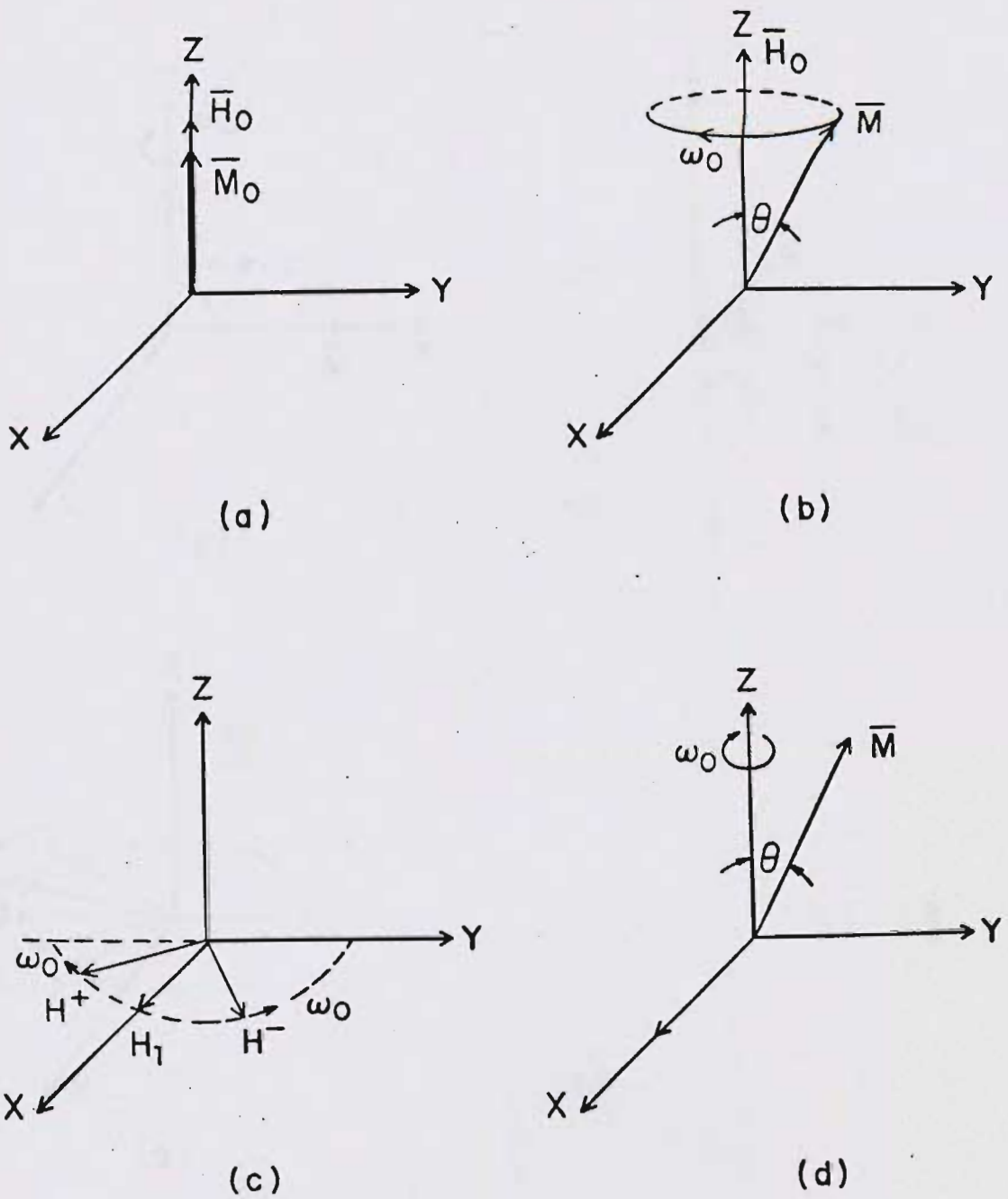


Fig. 1.5 Vector representation of spin-echo formation.

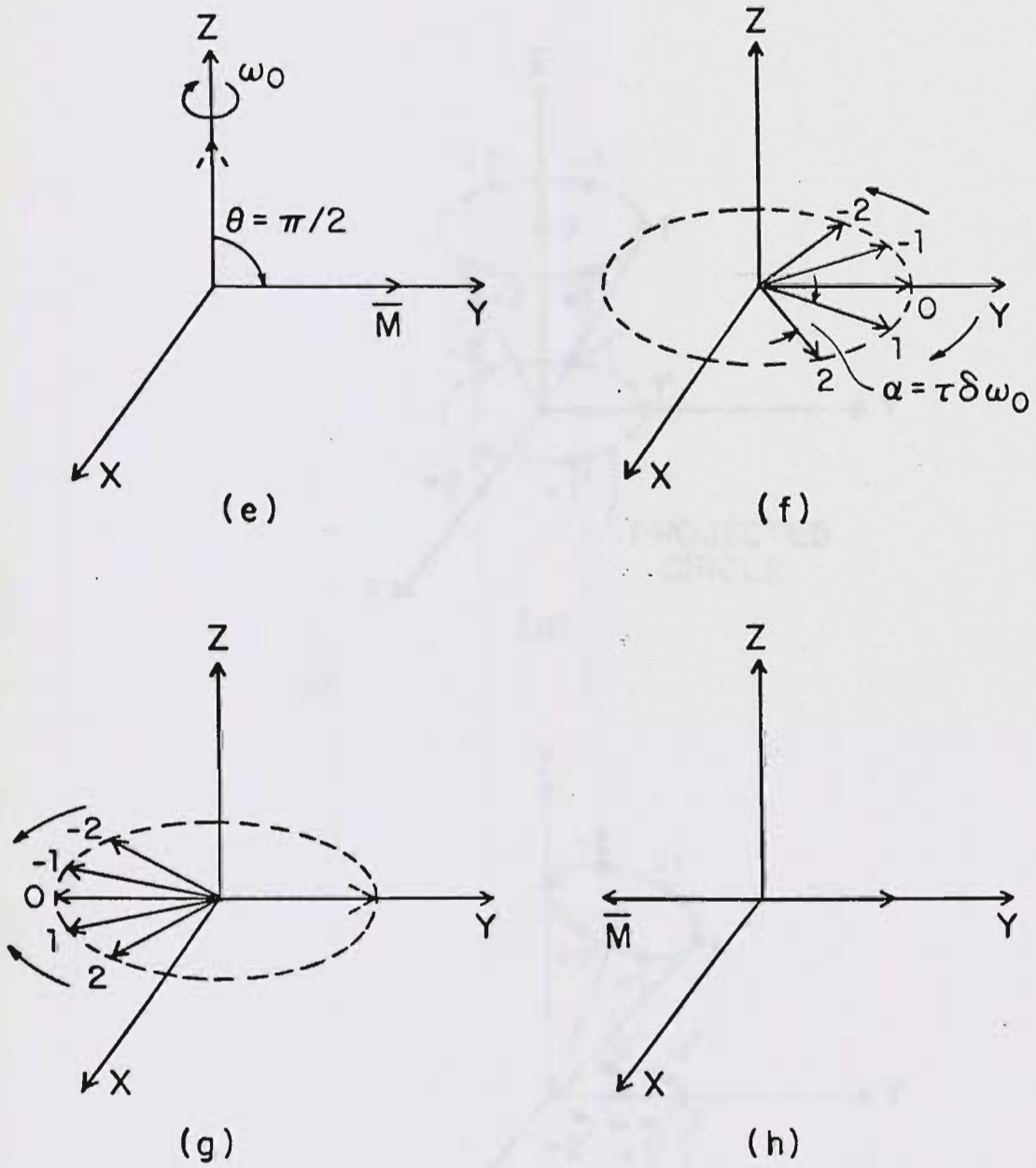


Fig. 1.5 cont'd.

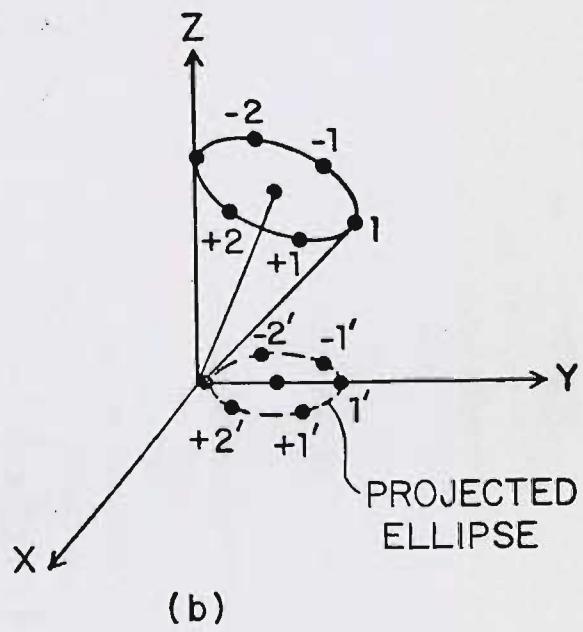
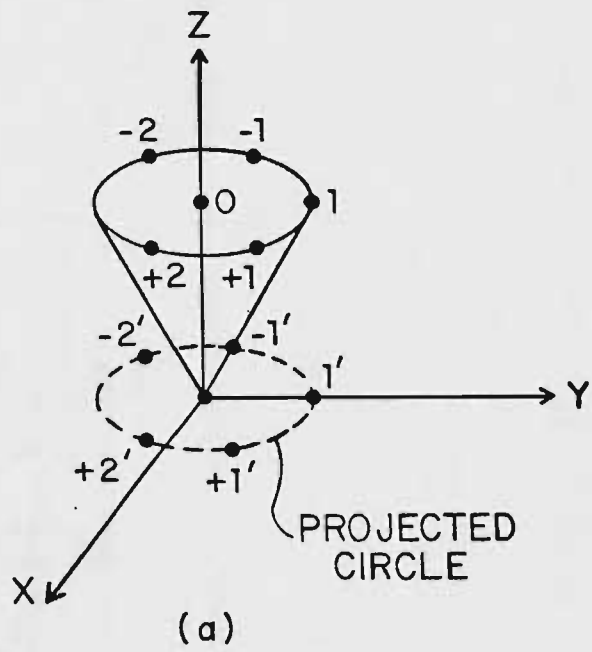


Fig. 1.6 Vector representation of echo-formation under weaker nonlinearities.

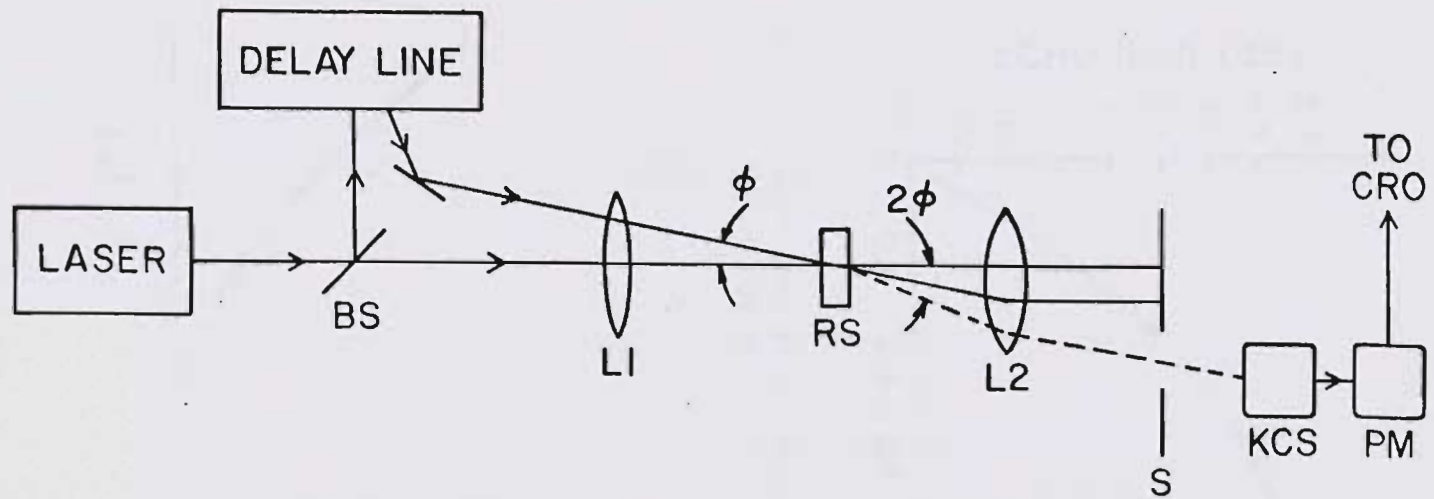


Fig. 2.1 Experimental setup for obtaining photon echoes. (After Kurnit et al. (10)).

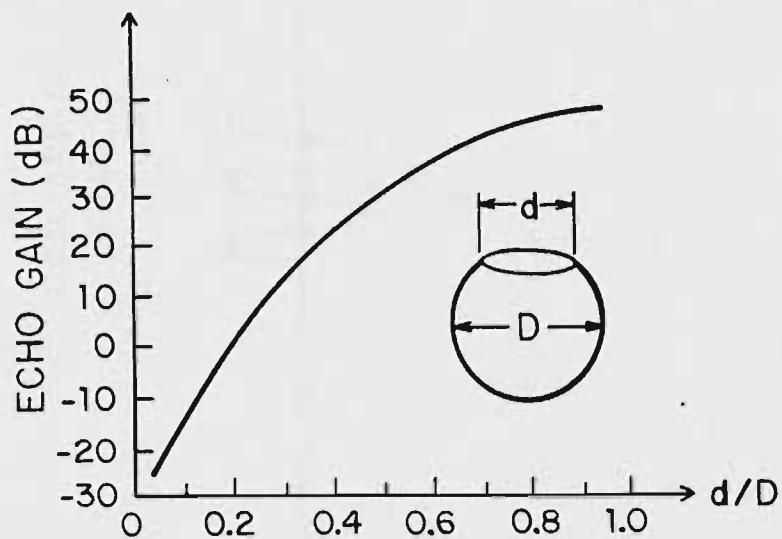


Fig. 3.1 Echo gain as a function of sample irregularity. (After Kaplan et al. (22)).

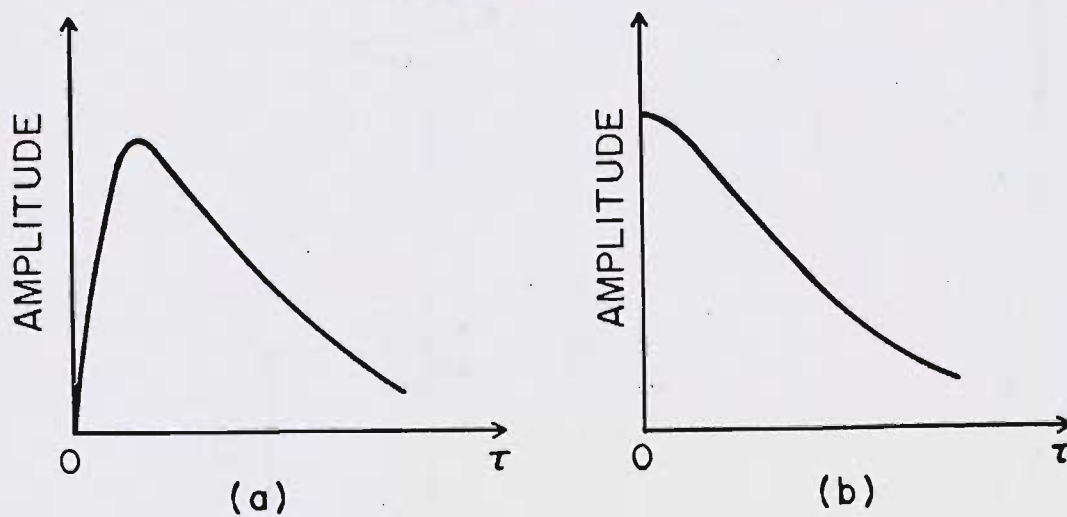


Fig. 3.2 Two-pulse echo as a function of pulse separation τ , for (a) anharmonic nonlinearity, (b) nonlinear excitation.

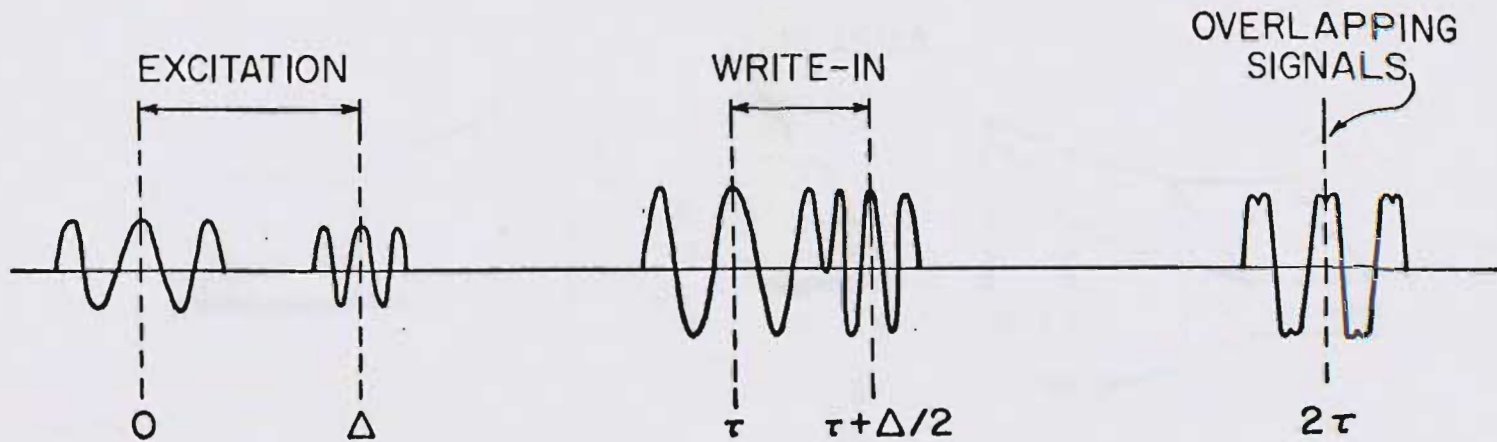


Fig. 3.3 Pulse compression by two-pulse echo method (note that the figure shows overlap of two frequencies only; a pulse is obtained upon adding many frequencies).

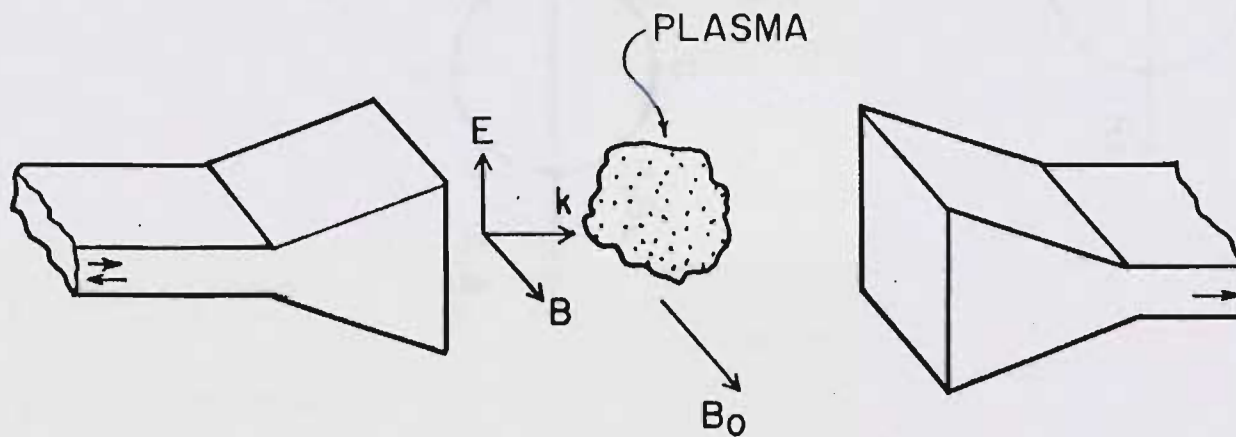


Fig. 4.1 Experimental arrangement for obtaining cyclotron echoes (E and B are the dominant TE and TM microwave fields; B_0 is the static magnetic field). (After Gould (26)).

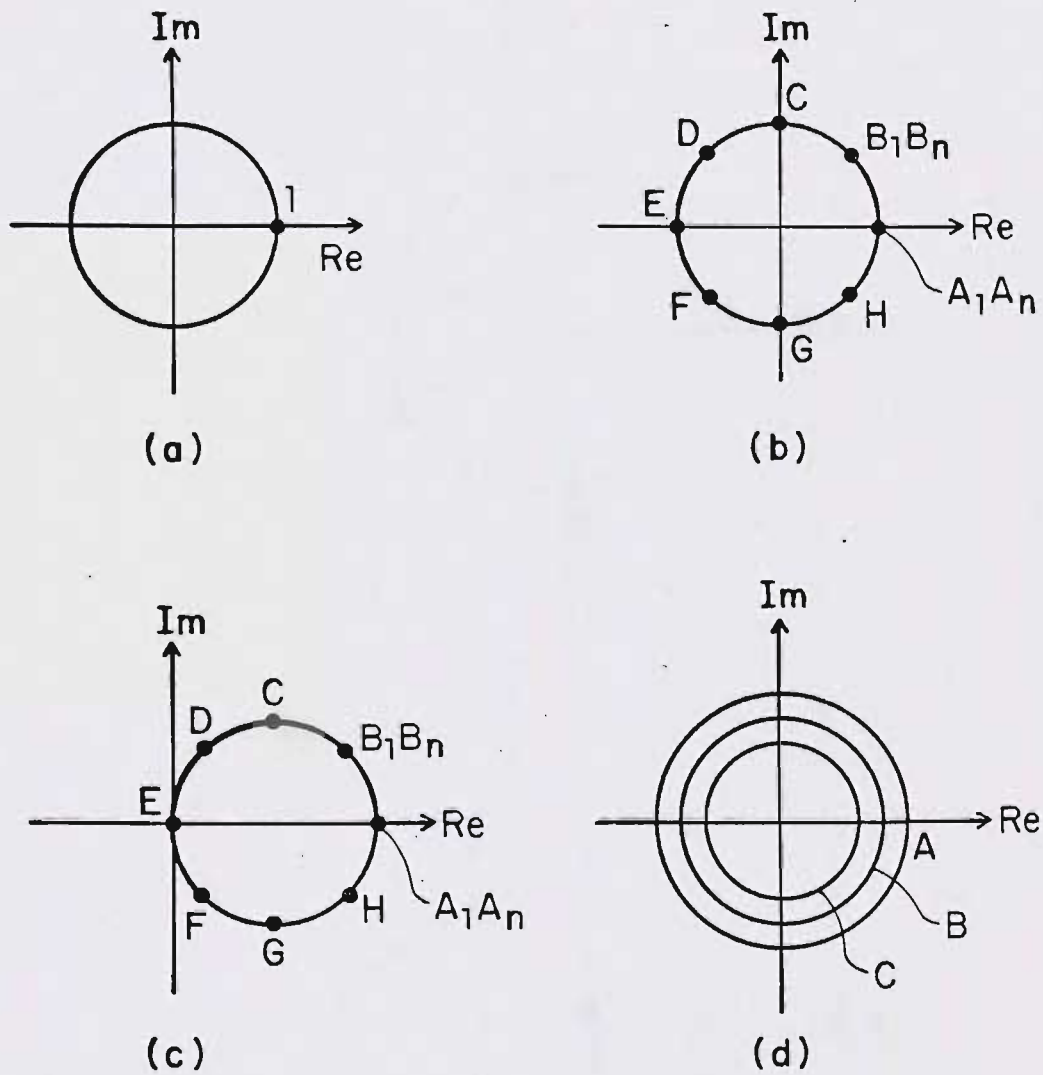


Fig. 4.2 Phasor representation of oscillators in the complex plane.

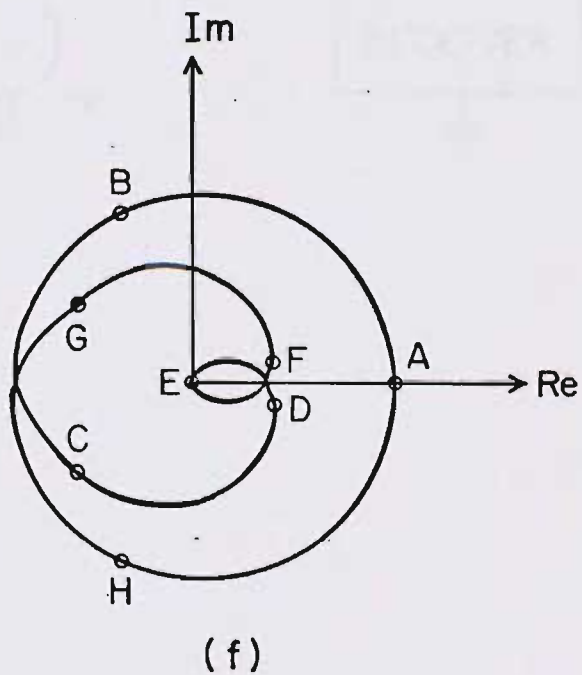
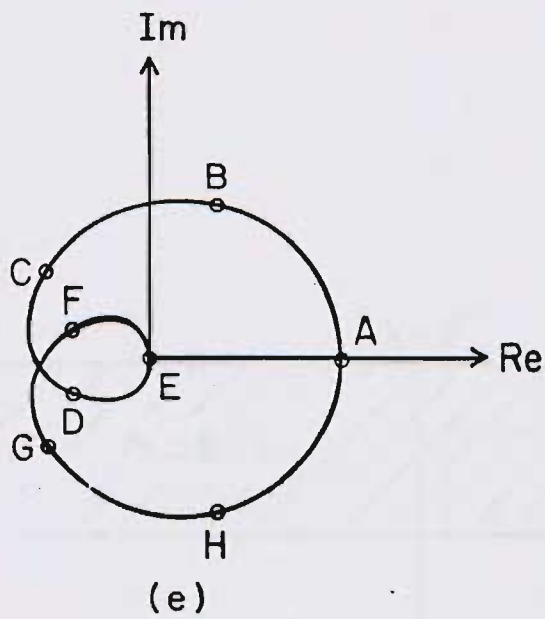


Fig. 4.2 cont'd.

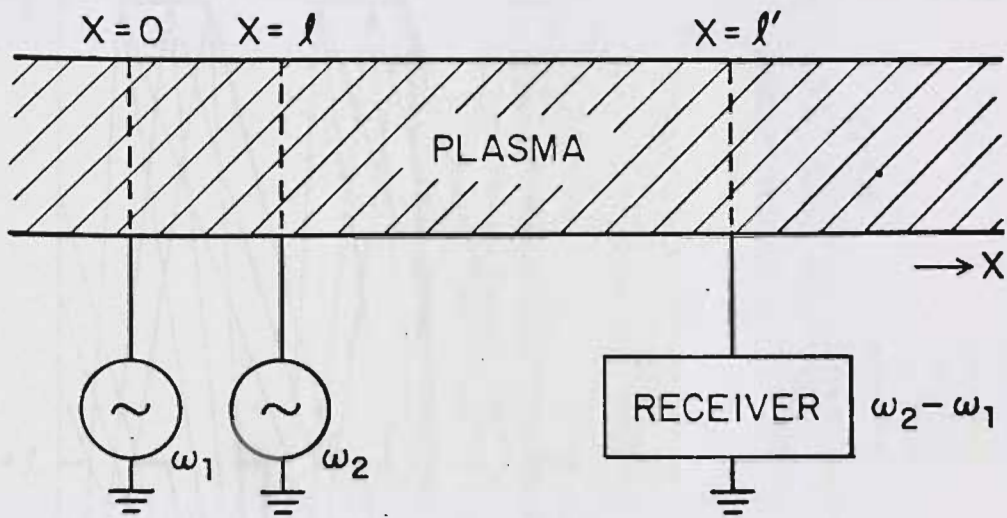


Fig. 5.1 Schematic arrangement for obtaining plasma-wave echoes. (After Baker et al. (31)).

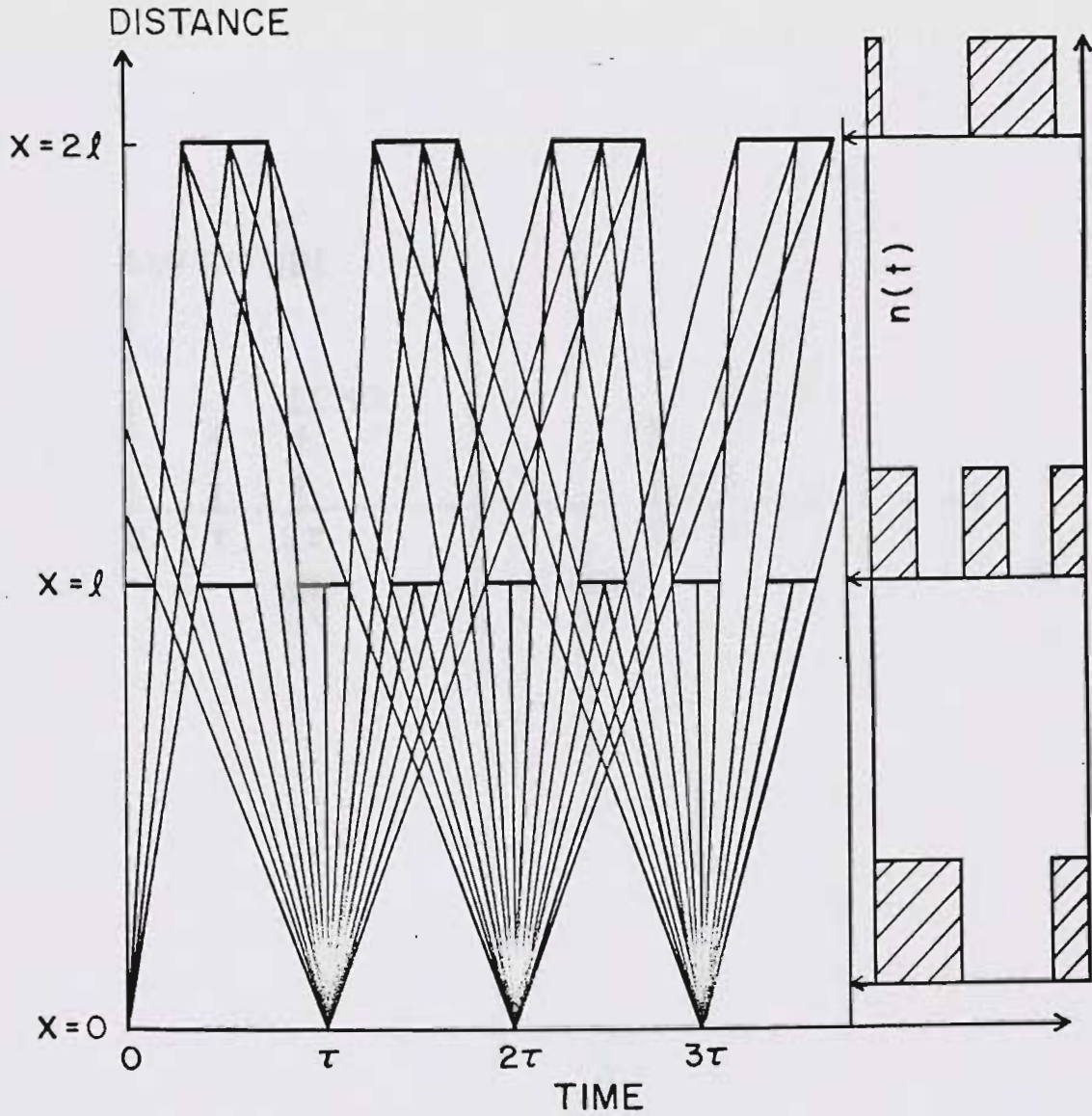


Fig. 5.2 Electron trajectories and number density illustrating the formation of plasma-wave echoes. (After Baker et al. (31)).

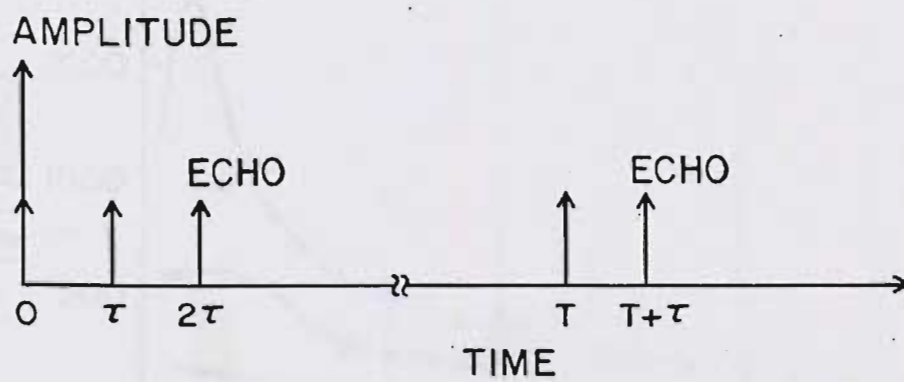


Fig. 5.3 Typical pulse-sequence for a three-pulse echo.

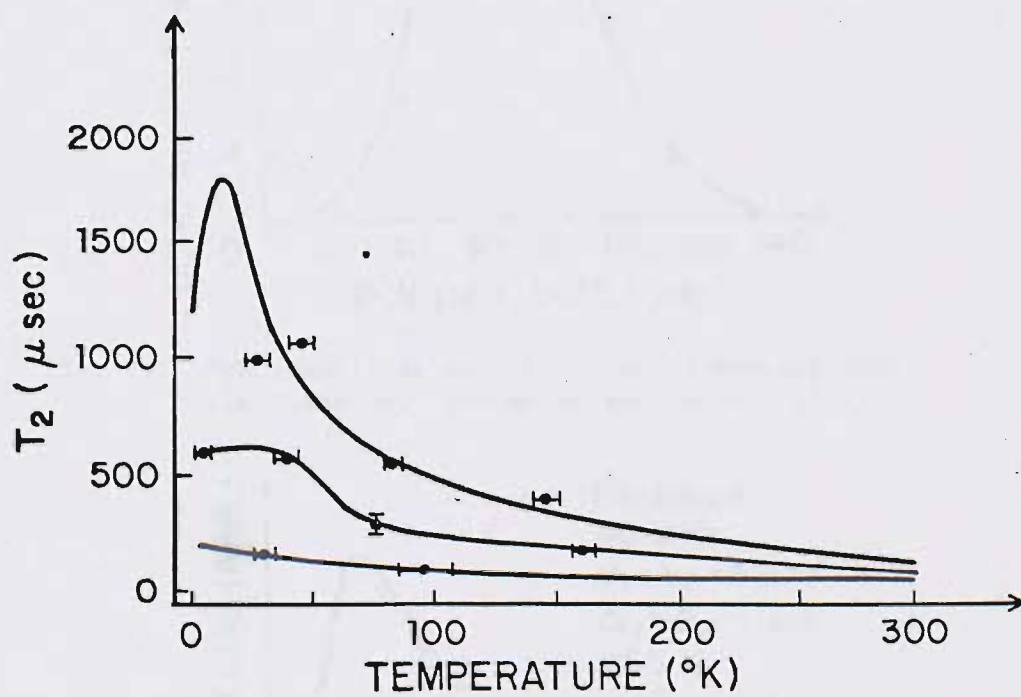


Fig. 7.1 Variation of the transverse relaxation time with temperature. (After Rubinstein et al. (47)).

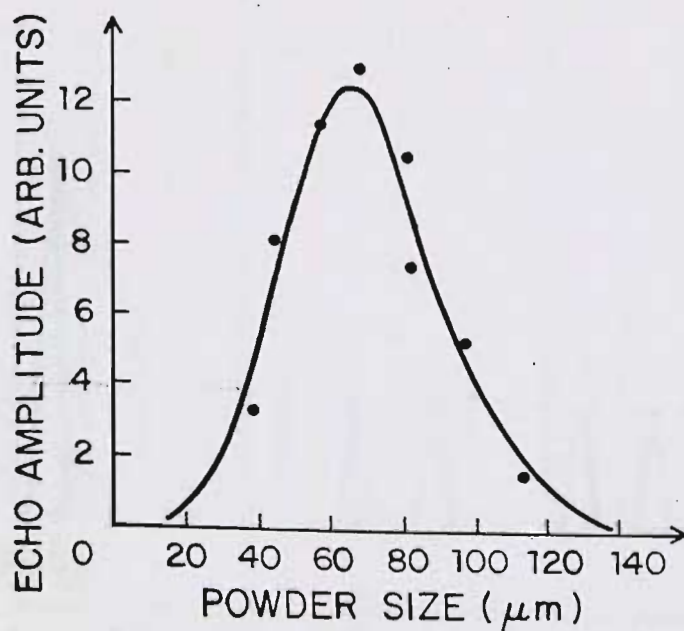


Fig. 7.2 Echo amplitude as a function of average particle diameter. (After Melcher et al. (51)).

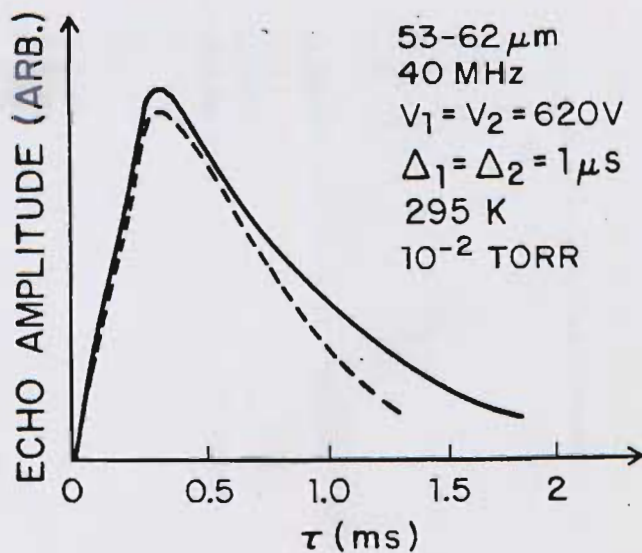


Fig. 7.3 Echo amplitude as a function of two-pulse separation (solid curve is experimental; dashed curve is from theory). (After Kajimura et al. (54)).

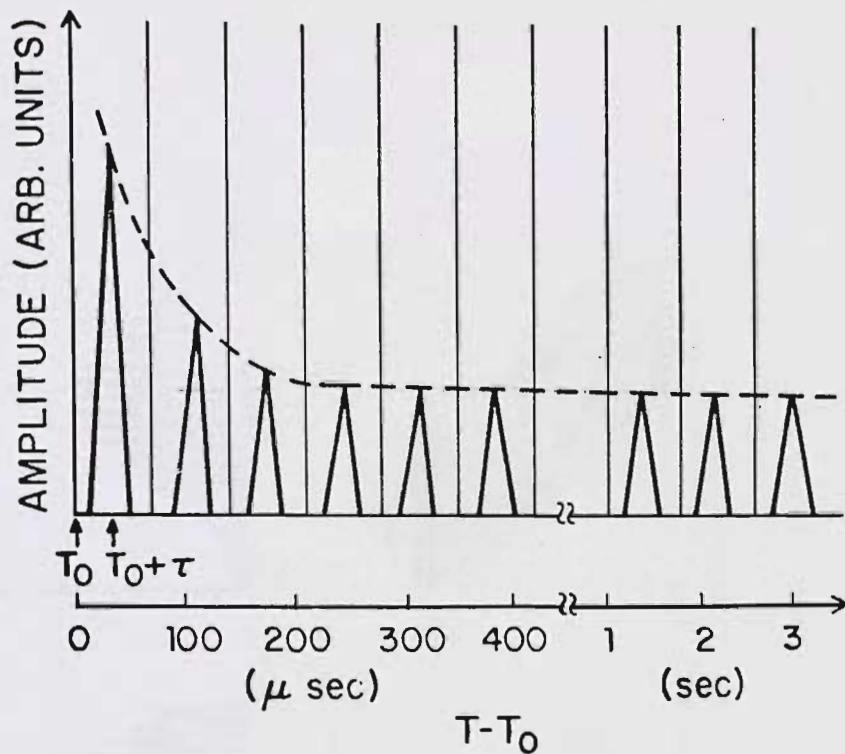


Fig. 7.4 Stimulated echo amplitude versus recall time (T) at constant two-pulse separation (τ). (After Popov et al. (61)).

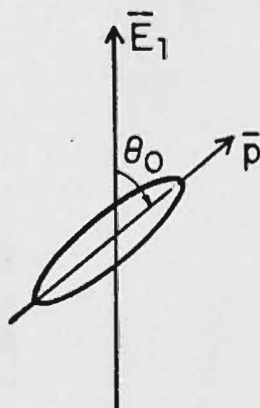


Fig. 7.5 Spatial orientation of electric field (\vec{E}) and dipole moment (\vec{p}).

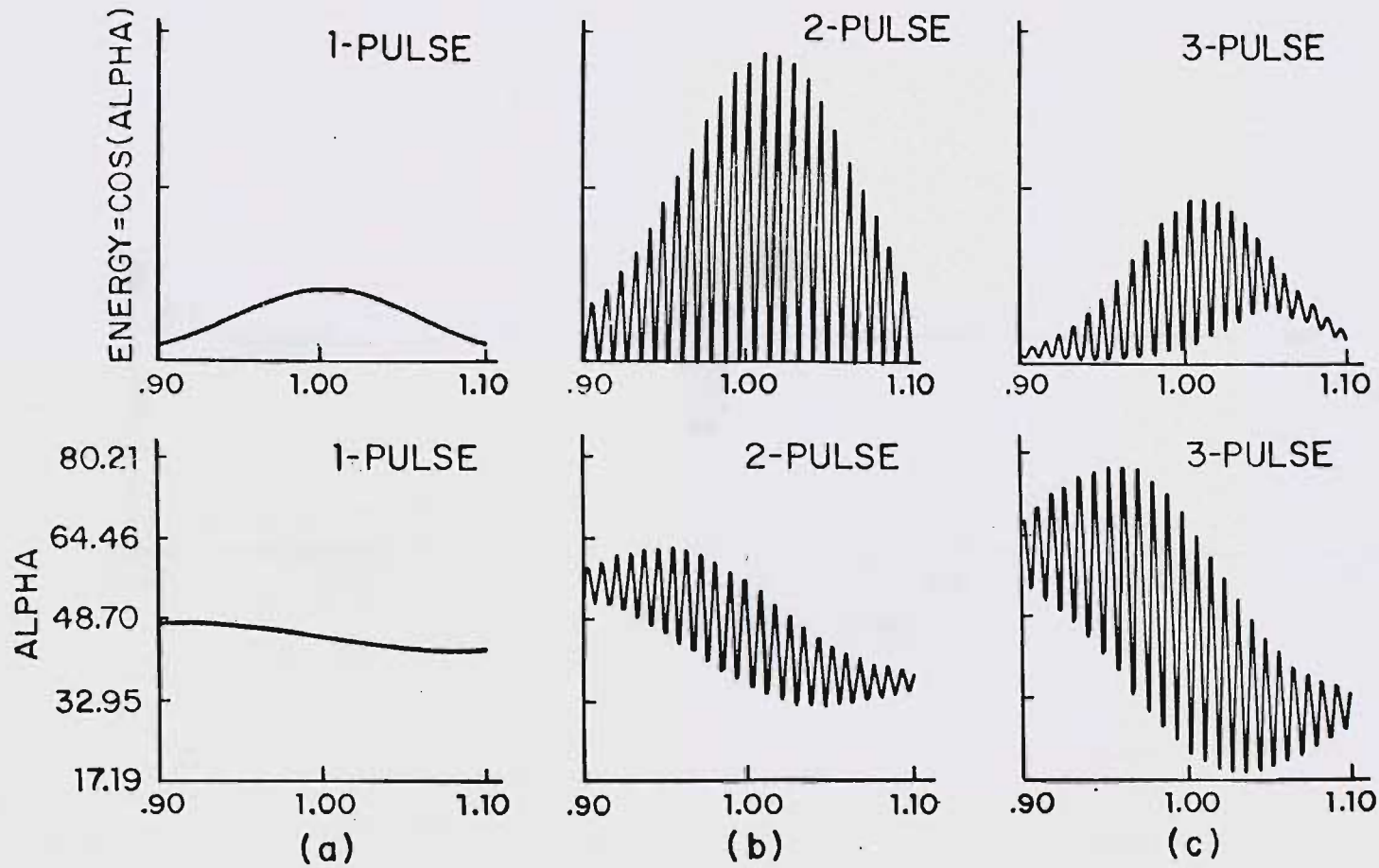


Fig. 7.6 Particle orientation and energy versus frequency (a) just after the first pulse, (b) after the second pulse, (c) after the third pulse. (After Wilms et al. (63)).

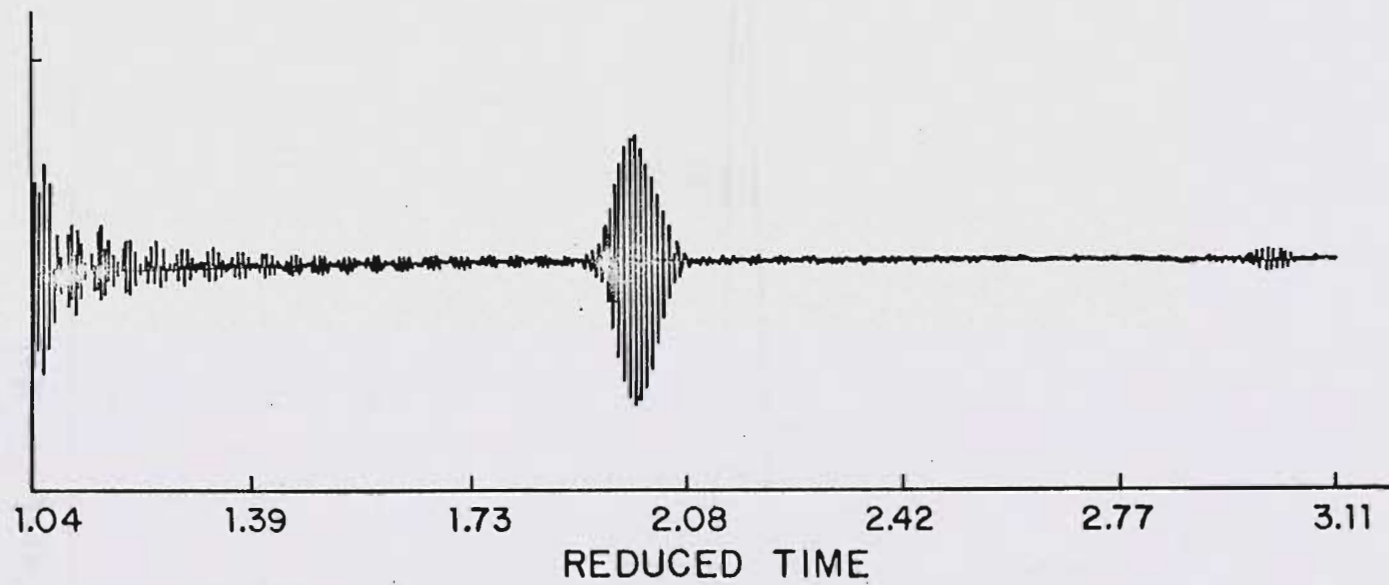


Fig. 7.7 The time development of $\Sigma q_1 \cos \alpha_1$ after the second pulse. (After Wilms et al. (63)).

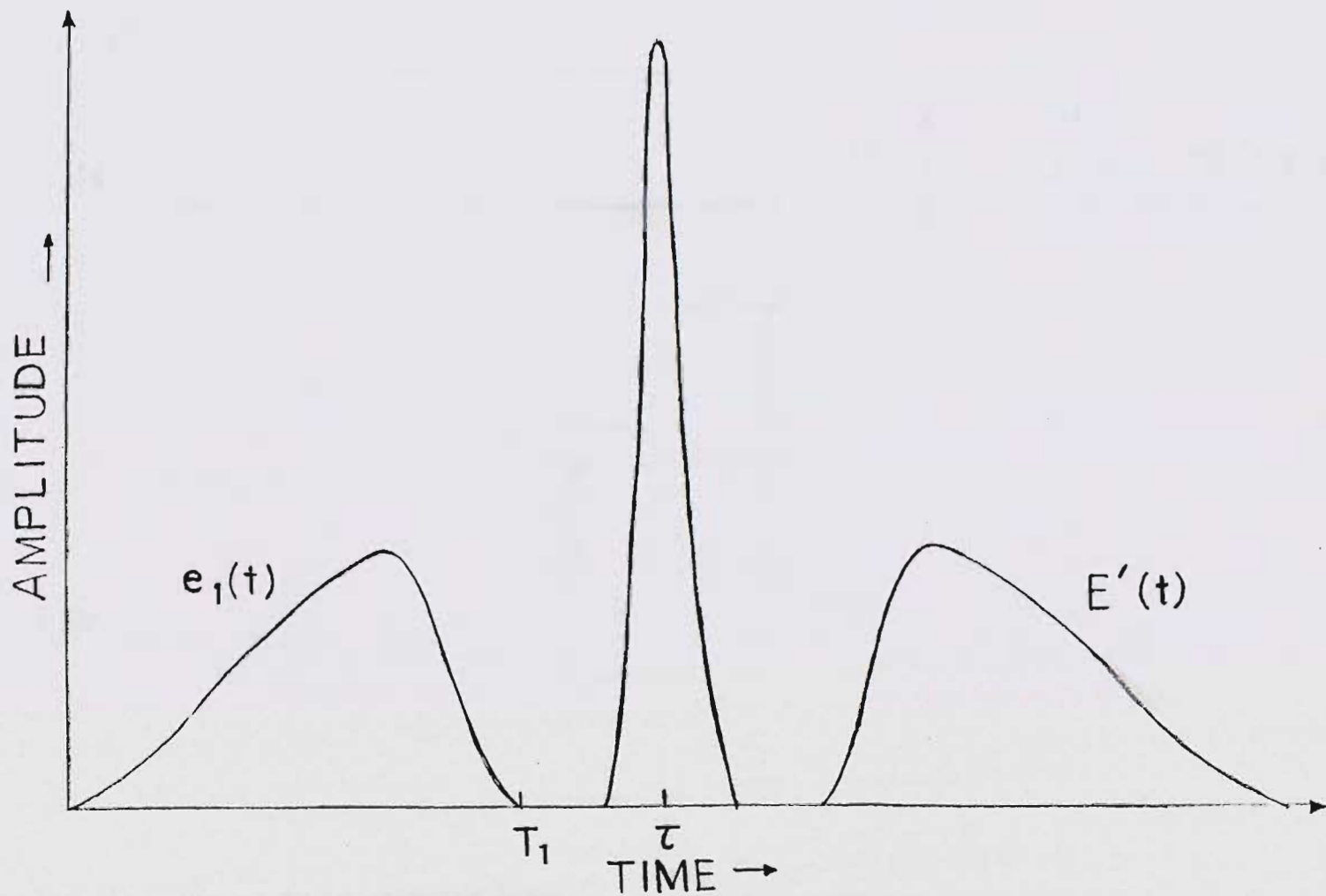


Fig. 8.1 Time-inverted signal recalled by delta function as a short range echo. (After Korpel (5)).

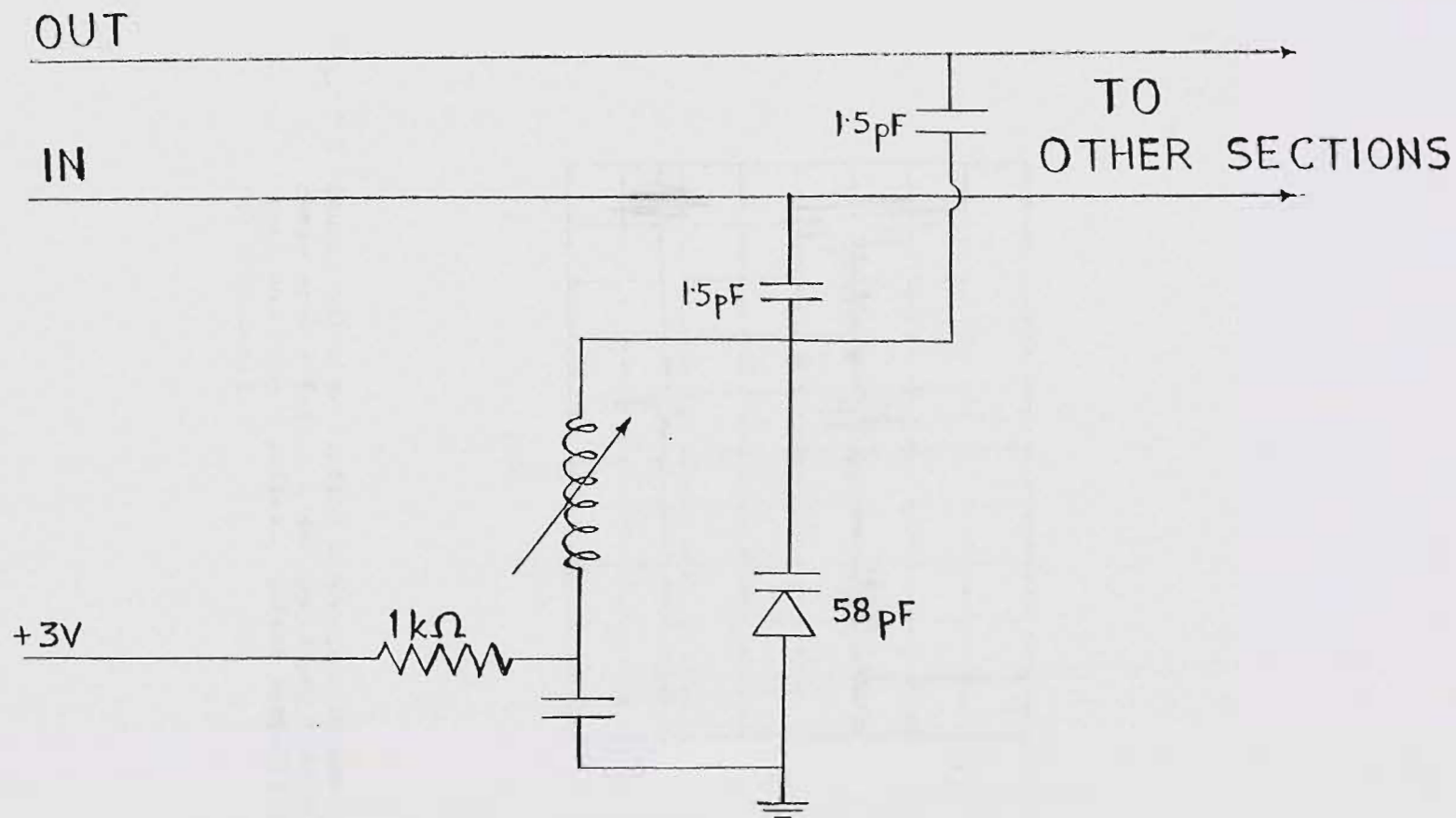
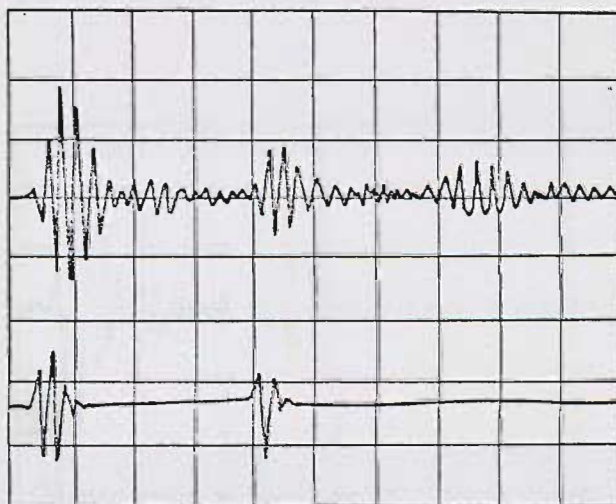
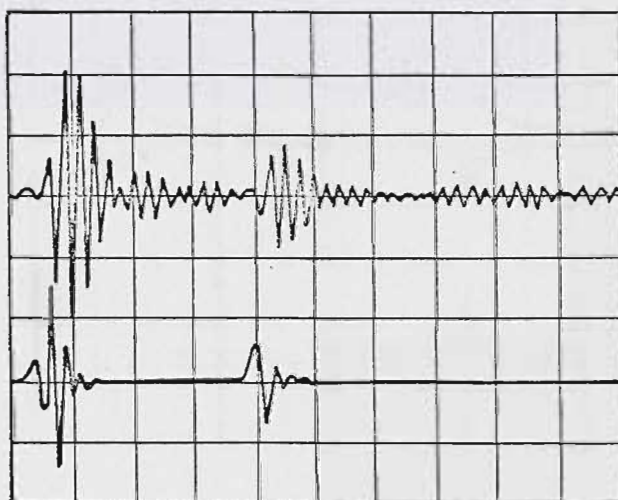


Fig. 8.2 One of 20 LC circuits modeling a general ensemble of nonlinear oscillators. (After Korpel (5)).



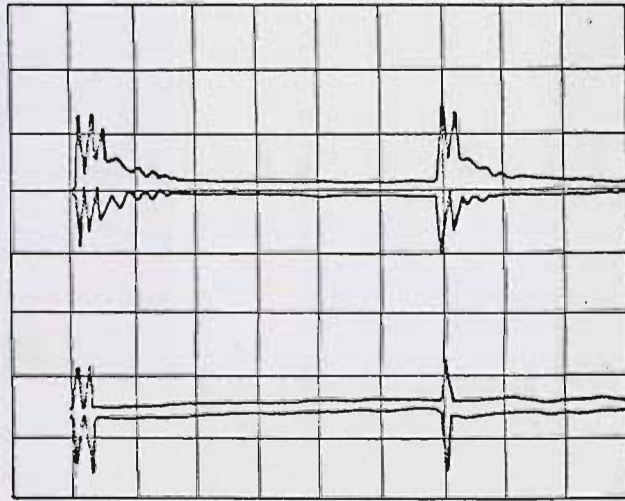
(a)

Fig. 8.3 Double pulse excitation demonstrating the short range echo effect. Lower and upper traces show input and output pulses. (After Korpel (5)).
(a) High-level.



(b)

Fig. 8.3 cont'd.
(b) Low-level.



(a)

Fig. 8.4 Long range echo experiment. Lower and upper traces show input and output pulses. (After Korpel (5)).
(a) Three pulses applied.



(b)

Fig. 8.4 cont'd.
(b) Two pulses applied.

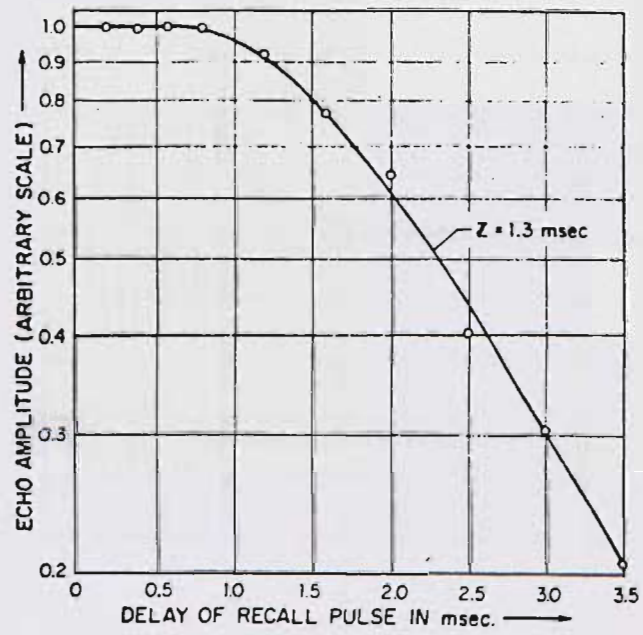
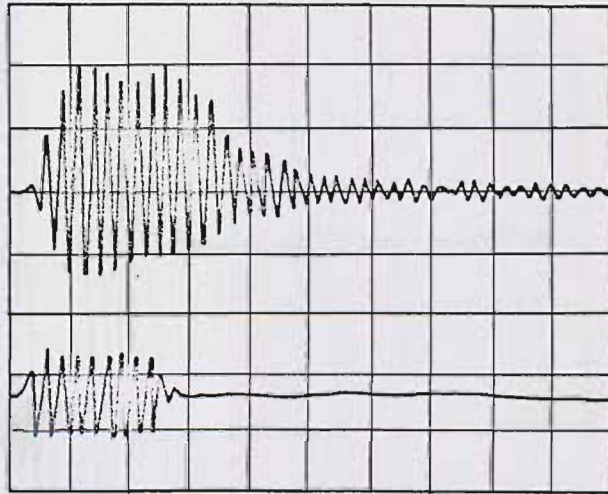
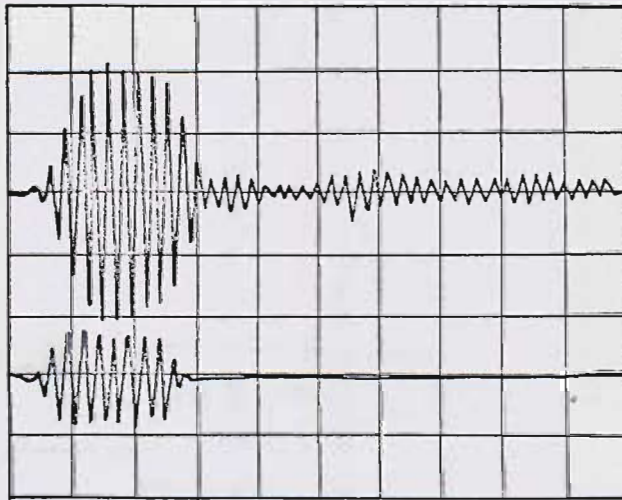


Fig 8.5 Long range echo amplitude versus recall time.
(After Korpel (5)).



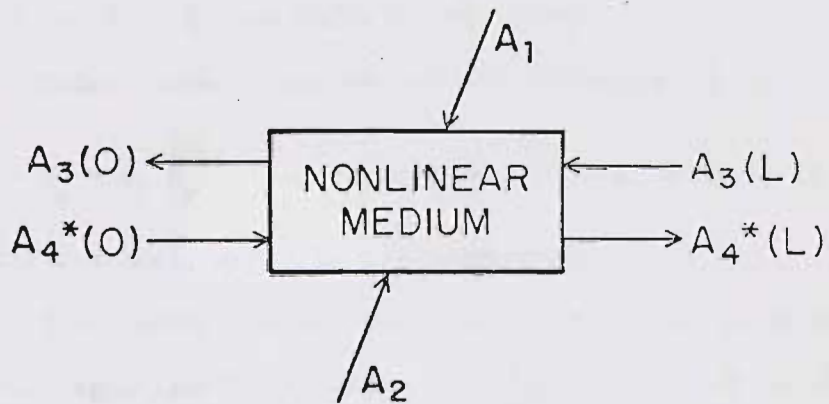
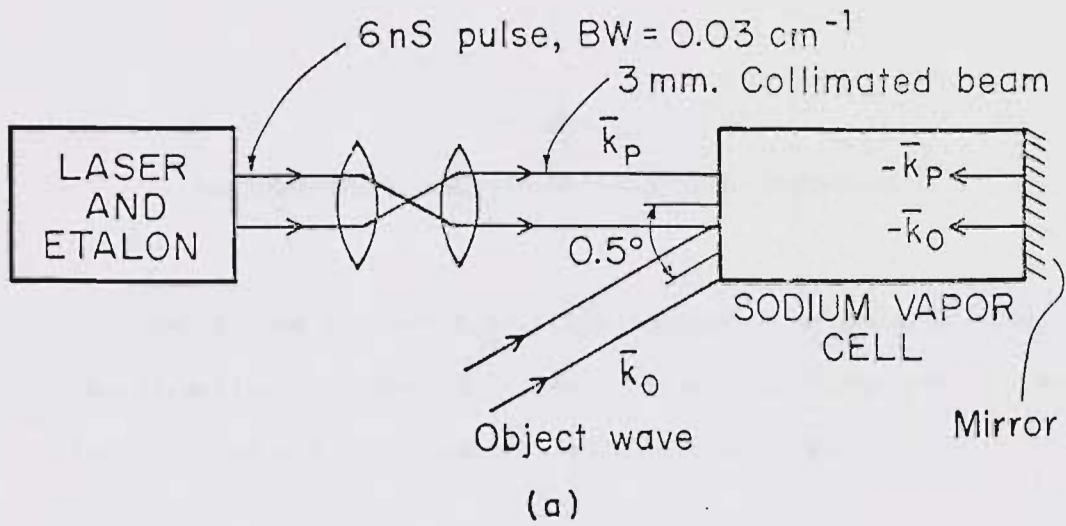
(a)

Fig. 8.6 Excitation with extended rectangular pulse.
(After Korpel (5)).
(a) High-level.



(b)

Fig. 8.6 cont'd.
(b) Low-level.



L = Effective width of interaction in medium

Fig. B.1 Optical phase conjugation (a) schematic arrangement, (b) vector representation.

APPENDIX A

MATHEMATICAL ANALYSIS OF SPIN-ECHO FORMATION

We proceed to investigate the physical processes involved in the formation of echoes in a spin system. We start with the Bloch equation for a local ensemble or cluster of spins:

$$\frac{d\bar{M}}{dt} = \gamma(\bar{M} \times \bar{H}). \quad (\text{A.1})$$

Case I: Spin System Under a Static Magnetic Field Alone.

Under thermal equilibrium, the components of magnetization are:

$$M_x = 0, M_y = 0 \text{ and } M_z = M_0 = \frac{CH_0}{T_0}, \text{ where } C \text{ is called the}$$

Curie constant, and T is the temperature in $^{\circ}\text{K}$.

Thus, under thermal equilibrium, the local ensemble acquires a net magnetization M_0 along the z -axis, along which the d.c. magnetic field \bar{H}_0 is applied. The average magnetizations M_x and M_y are both zero.

If, however, the system is not under thermal equilibrium, the general form of the equations describing the response is:

$$\frac{d\bar{M}_z}{dt} = \gamma(\bar{M} \times \bar{H})_z - \frac{\bar{M}_z - \bar{M}_0}{T_1}, \quad (\text{A.2})$$

$$\frac{d\bar{M}_y}{dt} = \gamma(\bar{M} \times \bar{H})_y - \frac{\bar{M}_y}{T_2}, \quad (\text{A.3})$$

$$\frac{d\bar{M}_x}{dt} = \gamma(\bar{M} \times \bar{H})_x - \frac{\bar{M}_x}{T_2} \quad (\text{A.4})$$

T_2 and T_1 represent the transverse and longitudinal relaxation times.

Under a static magnetic field $\bar{H} = H_0 \bar{a}_z$ alone, we may easily show, using eqn. (A.2) through (A.4), that:

$$M_z = M_0 + (M_{in} - M_0) \exp(-t/T_1) \quad (\text{A.5})$$

where M_{in} represents the initial value of M_z . Then M_z attains the equilibrium value M_0 after a time large compared to T_1 . Using the additional condition,

$$M_x^2 + M_y^2 + M_z^2 = M_0^2 \text{ for } t \ll T_2 \leq T_1, \text{ so that}$$

$$M_x^2 + M_y^2 = M_0^2 - M_{in}^2, \text{ we have the solutions for } M_y \text{ and } M_x \text{ as}$$

follows:

$$M_y = M_{yo} \exp(-t/T_2) \cos(\gamma H_0 t) \quad ,$$

$$M_x = M_{xo} \exp(-t/T_2) \sin(\gamma H_0 t) \quad ,$$

$$\text{where } M_{xo} = M_{yo} = (M_0^2 - M_{in}^2)^{1/2} \quad .$$

Thus, the net magnetization $\bar{M} = M_x \bar{a}_x + M_y \bar{a}_y + M_z \bar{a}_z$ can be described by a damped precession of the aggregate magnetic dipoles

about the z-axis with the rotating magnetization vector

$\bar{M}_{xy} = M_x \bar{a}_x + M_y \bar{a}_y$ in the xy-plane finally going to zero after a time large compared to T_2 .

The system under non thermal equilibrium, therefore, finally attains thermal equilibrium with all dipoles aligned parallel to the z-axis, or, more generally, with the dipoles precessing about the z-axis in a random fashion so as to keep $M_x = M_y = 0$ and $M_z = M_0$.

Case II: Spin System Subject to Static Magnetic Field and a Circularly Polarized R.F. Magnetic Field.

Suppose we immerse the spin system in a z-directed d.c. magnetic field \bar{H}_0 , and apply to it a circularly polarized r.f. magnetic field \bar{H} , rotating at an angular speed ω relative to the fixed coordinate system, in the xy plane.

This configuration is best analyzed by transforming the quantities relative to a rotating coordinate system, which we shall now demonstrate.

Suppose that we study the response of the system relative to a rotating frame of coordinates $x'y'z'$ which rotates with the r.f. field at angular speed ω with the z' axis coinciding with the z axis of the fixed frame. Thus the r.f. field becomes time invariant in the rotating frame. Let $\bar{H}_1 = H_m \bar{a}_x$, represent this field along the x' axis.

The modified Bloch equations in the rotating frame are:

$$\frac{d\bar{M}_z}{dt} = \gamma(\bar{M} \times \bar{H})_z - (\bar{\omega} \times \bar{M})_z - \frac{\bar{M}_z - \bar{M}_o}{T_1}, \quad (\text{A.6})$$

$$\frac{d\bar{M}_{y'}}{dt} = \gamma(\bar{M} \times \bar{H})_{y'} - (\bar{\omega} \times \bar{M})_{y'} - \frac{\bar{M}_{y'}}{T_2}, \quad (\text{A.7})$$

$$\frac{d\bar{M}_{x'}}{dt} = \gamma(\bar{M} \times \bar{H})_{x'} - (\bar{\omega} \times \bar{M})_{x'} - \frac{\bar{M}_{x'}}{T_2}. \quad (\text{A.8})$$

With $\bar{\omega} = -\omega_o \bar{a}_z$, where $\omega_o = \gamma H_o$, and using eqn. (A.6) through (A.8), we arrive at the following equation in M_z :

$$\frac{d^2 M_z}{dt^2} + \left(\frac{1}{T_1} + \frac{1}{T_2}\right) \frac{dM_z}{dt} + \left(\gamma^2 H_m^2 + \frac{1}{T_1 T_2}\right) M_z = \frac{M_o}{T_1 T_2}. \quad (\text{A.9})$$

The particular or steady state solution of the above is:

$$M_{zp} = \frac{M_o}{1 + T_1 T_2 \gamma^2 H_m^2}. \quad (\text{A.10})$$

The transient or complementary solution is found by setting the RHS to zero, and writing the equation in the form:

$$(D^2 + pD + q)M_z = 0, \text{ where}$$

$$D = \frac{d}{dt}, \quad p = \left(\frac{1}{T_1} + \frac{1}{T_2}\right), \quad q = \left(\gamma^2 H_m^2 + \frac{1}{T_1 T_2}\right).$$

Factoring the quadratic in D leads to:

$$D = -1/2\left(\frac{1}{T_1} + \frac{1}{T_2}\right) \pm 1/2\left[\left(\frac{1}{T_2} - \frac{1}{T_1}\right)^2 - (2\gamma H_m)^2\right]^{1/2}. \quad (\text{A.11})$$

Now suppose we have:

$$[\text{A}] \left[\frac{1}{T_2} - \frac{1}{T_1}\right] > 2\gamma H_m.$$

Then the quantity with the radical sign may be approximated as:

$$\sqrt{\quad} \approx \left(\frac{1}{T_2} - \frac{1}{T_1}\right) \left[1 - 1/2\left\{\frac{2\gamma H_m}{\frac{1}{T_2} - \frac{1}{T_1}}\right\}^2\right] = \left(\frac{1}{T_2} - \frac{1}{T_1}\right) - \frac{2\gamma^2 H_m^2}{\frac{1}{T_2} - \frac{1}{T_1}}. \quad (\text{A.12})$$

Using eqn. (A.12) and (A.11), and some useful simplifications,

the complementary solution for M_z may be written as:

$$M_{zc} = A_z \exp\left(-\frac{t}{T_1}\right) + B_z \exp\left(-\frac{t}{T_2}\right), \quad (\text{A.13})$$

where A_z and B_z are constants to be determined from the initial conditions.

The total solution for M_z is given by:

$$M_z = M_{zc} + M_{zp} = A_z \exp\left(-\frac{t}{T_1}\right) + B_z \exp\left(-\frac{t}{T_2}\right) + \frac{M_0}{1 + \gamma^2 H_m^2 T_1 T_2}. \quad (\text{A.14})$$

Now, the initial conditions at the instant the r.f. field is applied are:

$$M_z(0) = M_0, M_y, = M_x, = 0, \quad (\text{A.15})$$

provided that the r.f. field is applied long after the d.c. field is switched on, and,

$$\frac{dM_z}{dt} = -\gamma M_y H_m - \frac{M_z - M_0}{T_1} = 0, \text{ at } t = 0. \quad (\text{A.16})$$

Using (A.15) and (A.16) in (A.14), and solving for A_z and B_z , we finally obtain:

$$M_z = \frac{M_0}{T_1 - T_2} \left(\frac{\gamma^2 H_m^2 T_1 T_2}{1 + \gamma^2 H_m^2 T_1 T_2} \right) [T_1 \exp(-\frac{t}{T_1}) - T_2 \exp(-\frac{t}{T_2})] + \frac{M_0}{1 + \gamma^2 H_m^2 T_1 T_2}. \quad (\text{A.17})$$

The transient part of M_z in this case decays exponentially to zero, and M_z finally attains a steady state value. We shall discuss the implications of this solution later.

On the other hand, if we have:

$$[\text{B}] \quad 2\gamma H_m > \left(\frac{1}{T_1} - \frac{1}{T_2} \right).$$

Then the quantity with the radical sign approximates to:

$$\sqrt{\quad} = 2j\gamma H_m \left[1 - \frac{1}{2} \frac{\left\{ \frac{1}{T_2} - \frac{1}{T_1} \right\}^2}{(2\gamma H_m)^2} \right] = 2j\gamma H_m - j \left[\frac{\left(\frac{1}{T_2} - \frac{1}{T_1} \right)^2}{4\gamma H_m} \right]. \quad (\text{A.18})$$

Using eqn. (A.18) in (A.11), and assuming for simplicity that T_1 , $T_2 \rightarrow \infty$, we obtain the complementary solution for M_z as:

$$\begin{aligned} M_{zc} = & A_z \exp\left[-\frac{1}{2} \left(\frac{1}{T_1} + \frac{1}{T_2}\right)t\right] \exp(j\gamma H_m t) + \\ & + B_z \exp\left[-\frac{1}{2} \left(\frac{1}{T_1} + \frac{1}{T_2}\right)t\right] \exp(-j\gamma H_m t), \end{aligned} \quad (\text{A.19})$$

where the constants A_z and B_z are to be determined from the initial conditions.

The total solution for M_z is:

$$\begin{aligned} M_z = M_{zc} + M_{zp} = & \left\{ \exp\left[-\frac{1}{2} \left(\frac{1}{T_1} + \frac{1}{T_2}\right)t\right] \right\} \left[A_z \exp(j\gamma H_m t) + \right. \\ & \left. + B_z \exp(-j\gamma H_m t) \right] + \frac{M_o}{1 + \gamma^2 H_m^2 T_1 T_2}. \end{aligned} \quad (\text{A.20})$$

Using the initial conditions:

$$M_z(0) = M_o, \quad M_y(0) = M_x(0) = 0, \quad \text{and}$$

$$\frac{dM_z}{dt} = 0 \quad \text{at } t = 0,$$

we may show that:

$$A_z \approx B_z \approx \frac{\gamma_m^2 H_m^2 T_1 T_2}{2(1 + \gamma_m^2 H_m^2 T_1 T_2)} \quad (A.21)$$

Then we have for M_z :

$$\begin{aligned} M_z &= \frac{j\gamma_m^2 H_m^2 M_o T_1 T_2}{1 + \gamma_m^2 H_m^2 T_1 T_2} \{ \exp[-\frac{1}{2} (\frac{1}{T_1} + \frac{1}{T_2})t] \} \{ \frac{1}{2j} [\exp(j\gamma_m H_m t) + \\ &+ \exp(-j\gamma_m H_m t)] \} + \frac{M_o}{1 + \gamma_m^2 H_m^2 T_1 T_2} \\ &= \left[\frac{\gamma_m^2 H_m^2 M_o T_1 T_2}{1 + \gamma_m^2 H_m^2 T_1 T_2} \right] \exp[-\frac{1}{2} (\frac{1}{T_1} + \frac{1}{T_2})t] \cos(\gamma_m H_m t) + \frac{M_o}{1 + \gamma_m^2 H_m^2 T_1 T_2} \end{aligned} \quad (A.22)$$

The transient part of M_z in this case is a damped sinusoid (called a nutation) which decays exponentially to zero when M_z attains the steady state value.

Before we discuss the implications of this solution, we investigate the solutions for M_y , and M_x , in the rotating frame. The solution for M_x , is obtained directly as:

$$M_x' = M_{x0} \exp(-\frac{t}{T_2}), \quad (A.23)$$

where M_{x0} is a quantity to be determined by the boundary conditions.

For M_y , we solve the second order differential equation:

$$\frac{d^2 M_{y'}}{dt^2} + \left(\frac{1}{T_1} + \frac{1}{T_2}\right) \frac{dM_{y'}}{dt} + \left(\gamma_m^2 H_m^2 + \frac{1}{T_1 T_2}\right) M_{y'} = \frac{\gamma_m^H M_o}{T_1}. \quad (\text{A.24})$$

The steady state solution for $M_{y'}$, is:

$$M_{y'p} = \frac{\gamma_m^H M_o T_2}{1 + \gamma_m^2 H_m^2 T_1 T_2}. \quad (\text{A.25})$$

The transient solutions for $M_{y'}$, are similar to those for M_z , and are constructed so as to satisfy the boundary conditions. The complementary solution for $M_{y'}$, in the regime $\left(\frac{1}{T_2} - \frac{1}{T_1}\right) > 2\gamma_m^H$, is:

$$M_{y'c} = A_y \exp\left(-\frac{t}{T_1}\right) + B_y \exp\left(-\frac{t}{T_2}\right), \quad (\text{A.26})$$

where A_y and B_y are to be determined from the initial conditions.

The total solution for $M_{y'}$, is:

$$M_{y'} = A_y \exp\left(-\frac{t}{T_1}\right) + B_y \exp\left(-\frac{t}{T_2}\right) + \frac{\gamma_m^H T_2 M_o}{1 + \gamma_m^2 H_m^2 T_1 T_2}. \quad (\text{A.27})$$

Using the initial conditions:

$$M_{x'}(0) = 0,$$

$$M_{y'}(0) = 0, \text{ and,}$$

$\frac{dM_y}{dt} = \gamma M_o H_m$ at $t = 0$, we obtain, for the case $(\frac{1}{T_2} - \frac{1}{T_1}) > 2\gamma H_m$,

$$M_x' = 0, \quad (\text{A.28})$$

$$M_y' = A_y \exp\left(-\frac{t}{T_1}\right) + B_y \exp\left(-\frac{t}{T_2}\right) + \frac{\gamma H_m T_2 M_o}{1 + \gamma^2 H_m^2 T_1 T_2}, \quad (\text{A.29})$$

$$M_z = \frac{M_o}{T_1 - T_2} \left(\frac{\gamma^2 H_m^2 T_1 T_2}{1 + \gamma^2 H_m^2 T_1 T_2} \right) [T_1 \exp\left(-\frac{t}{T_1}\right) - T_2 \exp\left(-\frac{t}{T_2}\right)] + \frac{M_o}{1 + \gamma^2 H_m^2 T_1 T_2}. \quad (\text{A.30})$$

It is clearly evident from these solutions that the transient phase of the system under the rotating frame of reference consists of a steady exponential decay of M_z , and M_y' , which cannot describe any precessional motion in the rotating or fixed frame. The above situation, for two linearly (or circularly) polarized r.f. pulses, cannot lead to the formation of a spin echo in the usual sense. This will become clear from the interpretation of the other set of solutions in the rotating frame, which we present next. In the regime $2\gamma H_m > (\frac{1}{T_2} - \frac{1}{T_1})$, we obtain the following:

The total solution for M_y' is:

$$M_y = [\exp \{-\frac{1}{2} (\frac{1}{T_1} + \frac{1}{T_2}) t\}] [A_y \exp (j\gamma H_m t) + B_y \exp (-j\gamma H_m t)] + \frac{\gamma H_m T_2 M_o}{1 + \gamma^2 H_m^2 T_1 T_2}, \quad (\text{A.31})$$

where the constants A_y and B_y are to be determined from the initial conditions. Using the initial conditions:

$$M_x(0) = 0, \text{ (which leads to } M_x = 0),$$

$$M_y(0) = 0, \text{ and,}$$

$$\frac{dM_y}{dt} = \gamma H_m M_o \text{ at } t = 0, \text{ we obtain,}$$

$$A_y \approx -j \frac{M_o}{2} = \frac{M_o}{2j}, \quad (\text{A.32})$$

$$B_y \approx +j \frac{M_o}{2} = -\frac{M_o}{2j}. \quad (\text{A.33})$$

Then the total solution for M_y , becomes:

$$M_y = [\exp \{-\frac{1}{2} (\frac{1}{T_1} + \frac{1}{T_2}) t\}] [\frac{M_o}{2j} \exp (j\gamma H_m t) - \frac{M_o}{2j} \exp (-j\gamma H_m t)] + \frac{\gamma H_m T_2 M_o}{1 + \gamma^2 H_m^2 T_1 T_2}$$

$$= M_0 \sin(\gamma H_m t) \exp\left\{-\frac{1}{2}\left(\frac{1}{T_1} + \frac{1}{T_2}\right)t\right\} + \frac{\gamma H_m T_2 M_0}{1 + \gamma^2 H_m^2 T_1 T_2} .$$

(A.34)

The corresponding solution for M_z is:

$$M_z = M_0 \left[\frac{\gamma^2 H_m^2 T_1 T_2}{1 + \gamma^2 H_m^2 T_1 T_2} \right] \cos(\gamma H_m t) \exp\left\{-\frac{1}{2}\left(\frac{1}{T_1} + \frac{1}{T_2}\right)t\right\} +$$

$$+ \frac{M_0}{1 + \gamma^2 H_m^2 T_1 T_2}$$

$$\approx M_0 \cos(\gamma H_m t) \exp\left\{-\frac{1}{2}\left(\frac{1}{T_1} + \frac{1}{T_2}\right)t\right\} + \frac{M_0}{1 + \gamma^2 H_m^2 T_1 T_2} .$$

(A.35)

Now, the explanation of the spin-echo is highly simplified if we assume that T_1 is large enough to make the last terms in (A.34) and (A.35) small compared to the first terms in the time range $t \ll T_2 \leq T_1$. It may be noted here that if the last terms in (A.34) and (A.35) are not dropped, the resulting system would still describe the echo formation; the description would, however be more involved. We therefore have finally,

$$M_x' = 0, \tag{A.36}$$

$$M_y' \approx M_0 \sin(\gamma H_m t) \exp\left[-\frac{1}{2}\left(\frac{1}{T_1} + \frac{1}{T_2}\right)t\right], \tag{A.37}$$

$$M_z \approx M_0 \cos(\gamma H_m t) \exp\left[-\frac{1}{2}\left(\frac{1}{T_1} + \frac{1}{T_2}\right)t\right], \quad (\text{A.38})$$

for $t \ll T_2 \leq T_1$.

For long times M_y , and M_z acquire their steady state values as given by (A.25) and (A.10) respectively.

The solutions for M_z and M_y , in this case, in the transient regime, represent decaying sinusoids (nutations) at frequency $\omega = \gamma H_m$. The combination of these with M_x , results in a precession of the magnetic dipoles about the \bar{H}_1 field, i.e. the x' axis. It is this transient precession in the rotating frame that accounts for the echo effect in the spin system.

APPENDIX B

OPTICAL PHASE CONJUGATION BY DEGENERATE FOUR-WAVE MIXING

[DFWM]

The phenomenon of generating a time-reversed (or phase conjugated) wave in a nonlinear medium, by using three optical waves (degenerate in frequency) of appropriate propagation vectors, was first demonstrated by Yariv et al. [81] in 1977. The mathematical basis for such a process may be described as follows.

The interacting system consists of a nonlinear medium possessing a third order nonlinear optical susceptibility, $\chi_{NL}^{(3)}$. The excitation consists of two counter-propagating "pump" waves which interact with two counter-propagating, weak "object" waves, all the waves being at frequency " ω ". The resulting nonlinear interaction generates conjugate "image" waves that propagate opposite to the "object" waves. If one uses, in such a system, only one "object" wave instead of two, one obtains a single, phase-conjugated "image" wave, which is the required time-reversed wave.

A typical schematic diagram of the set up used to generate DFWM is shown in Fig. B.1. The nonlinear medium here is sodium vapor, with an atomic density of about $3 \times 10^{14} \text{ cm}^{-3}$. The vapor is enclosed in a cell, one end of which has a reflective coating. The forward pump wave is obtained from a laser; the backward pump

wave is generated through reflection. A fraction of the laser beam serves as the "object" wave (in the path of which, an object may be interposed), which is collinear to the pump to within 0.5° . The interaction length, L , defined elsewhere, is about 5 cm.

From Fig. B.1b, it is clear that the pump wave vectors (\bar{k}_1, \bar{k}_2) and the object and image wave vectors (\bar{k}_3, \bar{k}_4) must satisfy:

$$\bar{k}_1 + \bar{k}_2 = 0, \quad \bar{k}_3 + \bar{k}_4 = 0 \quad (\text{B.1})$$

Assuming the fields to be plane waves, we may write:

$$E_i(\bar{r}, t) = \frac{1}{2} A_i(\bar{r}_i) \exp[j(\omega t - \bar{k}_i \cdot \bar{r})] + \text{c.c.}, \quad (\text{B.2})$$

where r_i is measured along \bar{k}_i , and $i = 1, 2, 3, 4$. The fields, propagating through the nonlinear medium, satisfy the wave equation:

$$\nabla^2 \bar{E} = \mu_o \epsilon_o \frac{\partial^2 \bar{E}}{\partial z^2} + \mu_o \frac{\partial^2 \bar{p}}{\partial t^2}, \quad (\text{B.3})$$

where $\bar{p} = \epsilon_o \chi(E) \bar{E}$ is the polarization, and $\chi(E)$, the susceptibility, depends on absorption, dispersion, saturation and nonlinear mixing.

Using (B.3) and appropriate boundary conditions, it is possible to show that the object and image fields, E_o and E_i , are related by coupled differential equations, which solve to give:

$$E_o(L) = E_o(0) \sec \kappa L, \text{ and}, \quad (\text{B.4a})$$

$$E_i(0) = E_o^*(0) \tan \kappa L, \quad (\text{B.4b})$$

where $E_o(0)$, $E_o(L)$ are the object field amplitudes at the input and output faces of the medium, respectively, and $E_i(0)$ is the backward (or conjugated) image field amplitude at the input port. The coupling constant, κ , is given by:

$$\kappa = \frac{2\pi}{\lambda} n_2 |E_p|^2, \quad (\text{B.5})$$

where E_p is the pump amplitude, and n_2 is the nonlinear (Kerr) refractive index of the medium, given by:

$$n_2 = (\pi\mu^4 N) / h^3 (\Omega - \omega)^3, \quad (\text{B.6})$$

where μ is the dipole matrix element of transition, N the effective atomic density, Ω the transition frequency and ω is the optical frequency. The refractive index, n_2 , changes by an amount Δn (caused by a nonlinear Kerr effect that results in atomic level shifts in the medium), where Δn is quadratically related to the optical field amplitude, E , as $\Delta n = n_2 E^2$.

From (B.6) we see that, if we let $\Omega \rightarrow \omega$, the nonlinearity increases. It may be shown that for large nonlinearity, the image field may be amplified, and this can be accomplished at relatively low pump power.

The DFWM effect has been observed in, apart from gases, crystals of ruby [82], and some semiconductors [83]. In addition

to its inherent ability to correct phase aberrations in an object wave, the effect has been used in efficient spatial convolvers and correlators [84], and in narrow optical bandpass filters [85].

APPENDIX C
 GENERATION OF MULTIPLE TWO-PULSE ECHOES IN THE
 PRESENCE OF ANHARMONIC NONLINEARITY

If we have an r.f. pulse consisting of a carrier at ω_c , modulated by a narrow rectangular gate function "g(t)", of duration t_w , then the Fourier spectrum of the gate itself is given by:

$$G(\omega) = [g(t)] = \frac{\sin(\pi\omega/\omega_B)}{\omega},$$

where $2\omega_B = 2[\frac{2\pi}{t_w}]$ is the width of the main-lobe in the sinc function. Now if we have an excitation to a system of oscillators consisting of r.f. pulses at $t = 0$ and $t = \tau$, then we may write the excitations as follows:

$$\begin{aligned} f_1(t) &= A_1 g(t) \cos \omega_c t \\ &= \text{Re}[A_1 e^{j\omega_c t} \int_{-\infty}^{\infty} G(\omega) e^{j\omega t} d\omega]. \end{aligned} \quad (\text{C.1})$$

We may note in (C.1) that we have incorporated only the $+\omega_c$ components of the carrier spectrum, and, since g(t) is a real function, we require,

$$G(\omega) = G^*(-\omega). \quad (\text{C.2})$$

However, if we assume that the spectrum of $g(t)$ is bandlimited to $2\omega_B$, where $\omega_B \ll \omega_c$, then the effective frequency range in (C.1) falls entirely in the positive frequency plane. Thus, if now, through some frequency-dependent nonlinearity, the form of $G(\omega)$ is changed, the resulting inverse transform need not be a real time function any longer, since the final excitation function emerging from (C.1) would still be real.

Thus, assuming an oscillator spectrum that covers the entire bandwidth of the excitation, i.e. $H(\omega) = 1$, we may write the linear response of the system as:

$$\begin{aligned}
 R(t) &\propto f_1(t) + f_2(t-\tau) \\
 &= \text{Re}[A_1 e^{j\omega_c t} \int_{-\infty}^{\infty} G(\omega) e^{j\omega t} d\omega] + \text{Re}[A_2 e^{j\omega_c (t-\tau)} \int_{-\infty}^{\infty} \\
 &\quad G(\omega) e^{j\omega (t-\tau)} d\omega], \tag{C.3}
 \end{aligned}$$

where $f_2(t-\tau)$ is the r.f. pulse applied at $t = \tau$.

If now, from time $t \geq \tau^+$, the individual oscillators undergo an anharmonic frequency-shift, then the function $G(\omega)$ is modified to:

$$G'(\omega) = G(\omega) e^{j\Delta\omega(t-\tau)}. \tag{C.4}$$

In (C.4), we may note that depending on the form of the frequency-

shift $\Delta\omega$, $G'(\omega)$ may not satisfy the real-inverse transform property as in (C.2).

Thus, in general, the inverse-transform,

$$\int_{-\infty}^{\infty} G'(\omega) e^{j\omega t} d\omega, \text{ may be complex.}$$

We next assume that in (C.3), $G(\omega)$ is changed to $G'(\omega)$ as given by (C.4), and $A_2 \gg A_1$. Then the first term in (C.3) may be dropped in comparison to the second. Hence, the nonlinear response of the system becomes:

$$R_{NL}(t) \propto \text{Re}[A_2 e^{j\omega_c(t-\tau)} \int_{-\infty}^{\infty} G'(\omega) e^{j\omega(t-\tau)} d\omega]. \quad (\text{C.5})$$

We next assume that at $t = \tau$, the oscillators undergo an amplitude-dependent frequency-shift of the form:

$$\Delta\omega = -\alpha a^2, \quad (\text{C.6})$$

where a is the effective excitation amplitude seen at $t = \tau$. We may then write a^2 as follows:

$$a^2 = A_1^2 + A_2^2 + 2A_1A_2 \cos \omega\tau. \quad (\text{C.7})$$

Using (C.6), (C.7) and (C.4) in (C.5), we get:

$$R_{NL}(t) \propto \operatorname{Re}[A_2 e^{j\omega_c(t-\tau)} e^{-j\alpha(A_1^2 + A_2^2)(t-\tau)} \int_{-\infty}^{\infty} G(\omega) e^{j\omega(t-\tau)} \times \\ \times e^{-jb \cos \omega\tau} d\omega], \quad (C.8)$$

where $b = 2\alpha A_1 A_2 (t-\tau)$. We next use a familiar identity to write:

$$e^{-jb \cos \omega\tau} = \sum_{n=-\infty}^{\infty} J_n(b) \exp[jn(\frac{3\pi}{2} + \omega\tau)], \quad (C.9)$$

where $J_n(b)$ is the n th order Bessel function with argument "b".

Using (C.9) in (C.8), and remembering that "b" is independent of " ω ", we arrive at the following result:

$$R_{NL}(t) \propto \operatorname{Re}[A_2 e^{j\{\omega_c - \alpha(A_1^2 + A_2^2)\}(t-\tau)} \sum_{n=-\infty}^{\infty} J_n(b) e^{\frac{j3n\pi}{2}} \times \\ \times \int_{-\infty}^{\infty} G(\omega) e^{j\omega\{t+(n-1)\tau\}} d\omega]. \quad (C.10)$$

The integral in (C.10), which indeed satisfies the real inverse transform criterion, is easily solved as:

$$\int_{-\infty}^{\infty} G(\omega) e^{j\omega\{t+(n-1)\tau\}} d\omega = g\{t+(n-1)\tau\}. \quad (C.11)$$

Using (C.11) reduces (C.10) to:

$$R_{NL}(t) \propto \operatorname{Re}[A_2 e^{j\{\omega_c - \alpha(A_1^2 + A_2^2)\}(t-\tau)} \sum_{n=-\infty}^{\infty} J_n(b) e^{j\frac{3n\pi}{2}} \times \\ \times g\{t+(n-1)\tau\}] . \quad (\text{C.12})$$

In (C.12), we note that the terms involving $n = 0$ and higher represent "virtual" r.f. pulses that do not appear in the response for $t \geq \tau^+$. Thus, if we choose $n = -1, -2, \dots$, we find that (C.12) predicts "multiple" echoes, centered at $t = m\tau$, where $m = 2, 3, \dots$. These echoes are similar to the exciting r.f. pulses, except that the r.f. carrier associated with each is slightly different from " ω_c ", and has undergone a definite phase change.

If we put $n = -p$, where $p = 1, 2, \dots$, in (C.12) then $-p-1 = -m$, i.e. $m = p+1 = 2, 3, \dots$. Then the echo-term at $t = m\tau$ may be extracted from (C.12) as:

$$R_{m\tau}(t) \propto \operatorname{Re}[A_2 e^{j\{\omega_c - \alpha(A_1^2 + A_2^2)\}(t-\tau)} J_{-m+1}(b) e^{j\frac{3\pi}{2}(-m+1)} g(t-m\tau)] . \quad (\text{C.13})$$

Thus the echo-response at $t = 2\tau$ may be written as:

$$R_{2\tau}(t) \propto \operatorname{Re}[A_2 e^{j\{\omega_c - \alpha(A_1^2 + A_2^2)\}(t-\tau)} J_{-1}(b) e^{-j\frac{3\pi}{2}} g(t-2\tau)] . \quad (\text{C.14})$$

Since $J_{-1}(b) = -J_1(b)$, and $e^{-j3\pi/2} = +j$, (C.14) reduces to:

$$\begin{aligned}
 R_{2\tau}(t) &\propto \operatorname{Re}[-jA_2 e^{j\{\omega_c - \alpha(A_1^2 + A_2^2)\}(t-\tau)} J_1(b)g(t-2\tau)] \\
 &= A_2 J_1[2\alpha A_1 A_2(t-\tau)] \sin[\{\omega_c - \alpha(A_1^2 + A_2^2)\}(t-\tau)] g(t-2\tau) \\
 &= A_2 J_1[2\alpha A_1 A_2(t-\tau)] \cos[\{\omega_c - \alpha(A_1^2 + A_2^2)\}(t-\tau) - \frac{\pi}{2}] g(t-2\tau).
 \end{aligned} \tag{C.15}$$

It may be noted in (C.15) that the anharmonic nonlinearity has led to a shift in the carrier frequency in magnitude and phase. Furthermore, if the gate $g(t-2\tau)$ is sufficiently narrow about $t = 2\tau$, then we may replace $(t-\tau)$ in (C.15) by τ . We then obtain:

$$R_{2\tau}(t) \propto A_2 J_1[2\alpha A_1 A_2 \tau] \cos[\{\omega_c - \alpha(A_1^2 + A_2^2)\}(t-\tau) - \pi/2] g(t-2\tau). \tag{C.16}$$

Now if τ is small, and $2\alpha A_1 A_2 \tau \ll 1$, then we may write:

$$J_1(2\alpha A_1 A_2 \tau) \sim \alpha A_1 A_2 \tau. \tag{C.17}$$

Using (C.17) in (C.16), we obtain:

$$R_{2\tau}(t) \approx \alpha A_1 A_2^2 \tau \cos[\{\omega_c - \alpha(A_1^2 + A_2^2)\}(t-\tau) - \pi/2] g(t-2\tau). \tag{C.18}$$

Thus we see that for small values of τ , the two-pulse echo amplitude is linearly proportional to τ , which is indeed a familiar consequence of anharmonic nonlinearity as borne out by experiments.

REFERENCES

1. E.L. Hahn, "Spin echoes", Phys. Rev., vol. 80, no. 4, pp. 580-594, November 15, 1950.
2. E.L. Hahn, "Free nuclear induction", Physics Today, vol. 6, no. 11, pp. 4-9, November 1953.
3. U.Kh. Kopvillem, "Pulsed excitation of a system of weakly interacting particles", Sov. Phys. JETP, vol. 15, no. 5, pp. 924-931, November 1962.
4. R.W. Gould, "Echo phenomena", Phys. Lett., vol. 19, no. 6, pp. 477-478, December 1, 1965.
5. A. Korpel, "A simple description and demonstration of parametric echoes", J. Appl. Phys., vol. 49, no. 12, pp. 6125-6131, December 1978.
6. D.M. Bloom, P.F. Liao, and N.P. Economou, "Observation of amplified reflection by degenerate four-wave mixing in atomic sodium vapor", Optics Letters, vol. 2, no. 3, pp. 58-60, March 1978.
7. F. Bloch, "Nuclear induction", Phys. Rev., vol. 70, nos. 7 & 8, pp. 460-474, October 1 & 15, 1946.
8. C. Kittel, Introduction to Solid State Physics, John Wiley & Sons, Inc., New York 1976.
9. R.M. White, "Energy echoes", J. Appl. Phys., vol. 37, no. 4, pp. 1693-1696, March 15, 1966.
10. N.A. Kurnit, I.D. Abella, and S.R. Hartmann, "Observation of a photon echo", Phys. Rev. Lett., vol. 13, no. 9, pp. 567-568, November 9, 1969.
11. I.D. Abella, N.A. Kurnit, and S.R. Hartmann, "Photon echoes", Phys. Rev., vol. 141, no. 1, pp. 391-405, January 1966.
12. A. Yariv, Quantum Electronics, Wiley, New York, 1975.

13. P.A. Lindsay, Introduction to Quantum Electronics, Halsted Press, Wiley, New York, 1975.
14. R.P. Feynman, F. Vernon, and R.W. Hellwarth, "Geometrical representation of the Schrodinger equation for solving maser problems", J. Appl. Phys., vol. 28, no. 1, pp. 49-52, January 1957.
15. R.P. Feynman, The Feynman lectures on physics, Addison-Wesley, Palo Alto, 1964.
16. R.G. Brewer, "Coherent optical transients", Physics Today, vol. 30, no. 5, pp. 50-59, May 1977.
17. R.H. Dicke, "Coherence in spontaneous radiation processes", Phys. Rev., vol. 93, no. 1, pp. 99-110, January 1, 1954.
18. L.G. Rowan, E.L. Hahn, and W.B. Mims, "Electron spin-echo envelope modulation", Phys. Rev., vol. 137, pp. A61-A71, January 4, 1965.
19. C.K.N. Patel, and R.E. Sluster, "Photon echoes in gases", Phys. Rev. Lett., vol. 20, no. 20, pp. 1087-1091, May 13, 1968.
20. R.M. Hill, D.E. Kaplan, G.F. Herrmann, and S.K. Ichiki, "Emission microwave spectroscopy: OCS", Phys. Rev. Lett., vol. 18, no. 4, pp. 105-107, January 23, 1967.
21. J.L. Jenkins, and P.E. Wagner, "Microwave echoes in gaseous NH_3 ", Appl. Phys. Lett., vol. 13, no. 9, pp. 308-309, November 1, 1968.
22. D.E. Kaplan, R.M. Hill, and G.F. Herrmann, "Amplified ferri-magnetic echoes", Phys. Rev. Lett., vol. 20, no. 21, pp. 1156-1158, May 20, 1968.
23. D.E. Kaplan, R.M. Hill, and G.F. Herrmann, "Amplified ferri-magnetic echoes", J. Appl. Phys., vol. 40, no. 3, pp. 1164-1171, March 1, 1969.
24. W.B. Mims, "The detection of chirped radar signals by means of electron spin echoes", Proc. IEEE, vol. 51, no. 7, pp. 1127-1134, August 1963.
25. R.M. Hill, and D.E. Kaplan, "Cyclotron resonance echo", Phys. Rev. Lett., vol. 14, no. 26, pp. 1062-1063, June 28, 1965.
26. R.W. Gould, "Cyclotron echo phenomena", Am. J. Phys., vol. 37, no. 6, pp. 585-597, June 1969.

27. D.E. Kaplan, and R.M. Hill, "Observation of cyclotron echoes from a highly ionized plasma", Phys. Lett., vol. 22, no. 5, pp. 585-587, September 15, 1966.
28. R.W. Gould, T.M. O'Neil, and J.H. Malmberg, "Plasma wave echo", Phys. Rev. Lett., vol. 19, no. 5, pp. 219-222, July 31, 1967.
29. C.C. Johnson, Field and Wave Electrodynamics, McGraw Hill, New York, New York 1965.
30. L. Landau, "On the vibrations of the electronic plasma", J. Phys. USSR, vol. 10, no. 1, pp. 25-34, 1946.
31. D.R. Baker, N.R. Ahern, and A.Y. Wong, "Ion wave echoes", Phys. Rev. Lett., vol. 20, no. 7, pp. 318-321, February 12, 1968.
32. H. Ikezi, and N. Takahashi, "Observation of spatial ion-wave echoes", Phys. Rev. Lett., vol. 20, no. 4, pp. 140-142, January 22, 1968.
33. J.H. Malmberg, C.B. Wharton, R.W. Gould, and T.M. O'Neil, "Plasma wave echo experiment", Phys. Rev. Lett., vol. 20, no. 3, pp. 95-97, January 15, 1968.
34. I.B. Goldberg, E. Ehrenfreund, and M. Weger, "Fluxoid echoes", Phys. Rev. Lett., vol. 20, no. 11, pp. 539-540, March 11, 1968.
35. H. Alloul, and C. Froideaux, "New echo phenomena in superconductors and in normal metals", Phys. Rev. Lett., vol. 20, no. 22, pp. 1235-1236, May 27, 1968.
36. U.Kh. Kopvillem, B.P. Smolyakov, and R.Z. Sharipov, "Polarization echo in ferroelectric single crystal KH_2PO_4 ", JETP Lett., vol. 13, no. 10, pp. 398-400, May 20, 1971.
37. A.R. Kessel, I.A. Safin, and A.M. Gold'dman, "Macroscopic analog of the spin-echo effect in polycrystalline ferroelectrics", Sov. Phys. - Solid State, vol. 12, no. 10, pp. 2488-2489, April 1971.
38. S.N. Popov, and N.N. Krainik, "An anomalous echo in ferroelectric SbSI ", Sov. Phys. - Solid State, vol. 12, no. 10, pp. 2440-2444, April 1971.
39. J. Joffrin, and A. Levelut, "Boson echoes: A new tool to study phonon interactions", Phys. Rev. Lett., vol. 29, no. 19, pp. 1325-1327, November 6, 1972.

40. N.S. Shiren, R.L. Melcher, D.K. Garrod, and T.G. Kazyaka, "Echo phenomena in piezoelectric crystals", *Phys. Rev. Lett.*, vol. 31, no. 13, pp. 819-821, September 24, 1973.
41. R.L. Melcher, and N.S. Shiren, "New class of polarization echoes", *Phys. Rev. Lett.*, vol. 34, no. 12, pp. 731-733, March 24, 1975.
42. Ya. Ya. Asadullin, V.M. Berezov, V.D. Korepanov, and V.S. Romanov, "Anomalous relaxation of stimulated echo in piezoelectric crystals", *JETP Lett.*, vol. 22, no. 5, pp. 132-133, September 5, 1975.
43. H.M. Gerard, in *Acoustic Surface Waves*, ed. A.A. Oliner Springer Verlag, New York, 1978.
44. E.A. Ash, *ibid.*
45. N.N. Krainik, S.N. Popov, and G.A. Smolenskii, "Phonon (electroacoustic) echo in crystals", *Sov. Phys. Acoustics*, vol. 22, no. 1, pp. 83-84, Jan.-Feb., 1976.
46. S. Kupca, and C.W. Searle, "Magnetomechanically excited echoes in ferrites", *J. Appl. Phys.*, vol. 46, no. 10, pp. 4612-4613, October 1975.
47. M. Rubinstein, and G.H. Stauss, "Magnetoacoustic excitation of radiofrequency resonances and echoes in magnetic materials", *J. Appl. Phys.*, vol. 39, no. 1, pp. 81-88, January 1968.
48. Z.A. Pacult, P.C. Reidi, and D.P. Tunstal, "Radio frequency echoes in metallic powders", *J. Phys. F*, vol. 3, no. 10, pp. 1843-1952, October 1973.
49. R.L. Melcher, and N.S. Shiren, "Polarization echoes and long time storage in piezoelectric powders", *Phys. Rev. Lett.*, vol. 36, no. 15, pp. 888-891, April 12, 1976.
50. N.N. Krainik, V.V. Lemanov, S.N. Popov, and G.A. Smolenskii, "Phonon echo in crystalline powders", *Sov. Phys. - Solid State*, vol. 17, no. 8, pp. 1635-1636, August 1975.
51. R.L. Melcher, and N.S. Shiren, "Echo storage in piezoelectric powders", 1975 Ultrasonics Symposium Proceedings, IEEE Cat. #75, CHO 994-4SU, pp. 672-673.
52. P.I. Kuindersma, S. Huizenga, J. Kommandeur, and G.A. Sawatzky, "Echo phenomena in simple oscillators", *Phys. Rev. B*, vol. 13, no. 2, pp. 496-499, January 15, 1976.

53. A.R. Kessel', S.A. Zel'dovich, and I.L. Gurevich, "Theory of the electroacoustic echo in piezoelectric powders", *Sov. Phys.-Solid State*, vol. 18, no. 3, pp. 473-476, March 1976.
54. K. Kajimura, K. Fossheim, T.G. Kazyaka, R.L. Melcher, and N.S. Shiren, "Dynamic polarization echoes in powders", *Phys. Rev. Lett.*, vol. 37, no. 17, pp. 1151-1154, October 25, 1976.
55. K. Fossheim, K. Kajimura, T.G. Kazyaka, R.L. Melcher, and N.S. Shiren, "Dynamic polarization echoes in piezoelectric powders", *Phys. Rev. B*, vol. 17, no. 3, pp. 964-997, February 1, 1978.
56. S. Stokka, and K. Fossheim, "Dynamic polarization echoes in KDP powder", *J. Phys. C: Solid State Phys.*, vol. 11, no. 19, pp. 3949-3959, October 14, 1978.
57. H.P. Kunkel, S. Kupca, and C.W. Searle, "The nonlinear mechanism leading to polarization echoes in some powdered materials", *Appl. Phys. Lett.*, vol. 33, no. 4, pp. 364-366, August 15, 1978.
58. I.L. Gurevich, S.A. Zel'dovich, and A.R. Kessel', "Electroacoustic echo at doubled frequency", *Sov. Phys. Solid State*, vol. 19, no. 5, pp. 896, May 1977.
59. U. Kh. Kopvillem, and S.V. Prants, "Formation of polarization echo and polarization avalanche signals in nonpiezoelectric dielectrics", *Sov. Phys. JETP*, vol. 49, no. 3, pp. 525-529, March 1979.
60. U. Kh. Kopvillem, and S.V. Prants, "Possibility of polarization echoes and avalanches in nonpiezoelectric materials", *J. Phys. C Solid State Phys.*, vol. 12, no. 10, pp. 1927-1935, May 28, 1979.
61. S.N. Popov, N.N. Krainik, and G.A. Smolenskii, "Three pulse phonon (electroacoustic) echo with large relaxation time", *JETP Lett.*, vol. 21, no. 9, pp. 253-254, May 5, 1975.
62. S.N. Popov, N.N. Krainik, and G.A. Smolenskii, "Three pulse electroacoustic echo under conditions of acoustic resonance", *Sov. Phys. JETP*, vol. 42, no. 3, pp. 494-496, September 1975.
63. K. Wilms, and G. Vertogen, "A theoretical description of polarization echoes and long memory times in piezoelectric powders", *Solid State Comm.*, vol. 20, no. 12, pp. 1165-1167, 1976.
64. T. Kimura, K. Onuki, and S. Yoshikawa, "Repetitive readout effect of a polarization echo", *J. Appl. Phys.*, vol. 50, no. 4, pp. 2991-2992, April 1979.

65. V.M. Berezov, Ya. Ya. Asadullin, V.D. Korepanov, and V.S. Romanov, "Anomalous relaxation of polarization echo in piezoelectric crystals", Sov. Phys. JETP, vol. 42, no. 5, pp. 851-854, November 1975.
66. J.W. Goodman, Introduction to Fourier optics, Mc-Graw Hill, New York, 1968.
67. Ya. Ya. Asadullin, Z. Sh. Idiatullin, and F.M. Samigullin, "Polarization echo in a powder and surface properties of a piezoelectric", Sov. Tech. Phys. Lett., vol. 3, no. 4, pp. 121-122, April 1977.
68. V.M. Berezov, and V.S. Romanov, "Role of the dislocation mechanism in the polarization-echo phenomenon", JETP Lett., vol. 25, no. 3, pp. 151-152, February 5, 1977.
69. D. Cheeke, and A.A. Lakhani, "Orientation dependence of the memory echo in piezoelectric powders", Solid State Comm., vol. 25, no. 5, pp. 289-291, 1978.
70. A. Billman, Ch. Frenois, G. Guillot, and A. Levelut, "Stimulated phonon echoes in resonant powders", J. de Physique, vol. 39, no. 21, pp. L407-L410, November 1978.
71. H. Etinger, A. Lakhani, and D. Cheeke, "Aspect theoriques des echoes de polarization pour une poudre piezoelectrique", Can. J. Phys., vol. 56, no. 7, pp. 865-871, July 1978.
72. Ya. Ya. Asadullin, "On the origin of memory in echo phenomena in ferroelectric powders", Ferroelectrics, vol. 20, no. 3 & 4, pp. 241-243, 1978.
73. A.R. Kessel, "On the mechanism of the long time phase memory in piezoelectric powders", Ferroelectrics, vol. 22, no. 1 & 2, pp. 759-761, 1978.
74. G.A. Sawatzky, and S. Huizinga, "Information storage in piezoelectric powders", App. Phys. Lett., vol. 28, no. 9, pp. 476-478, May 1976.
75. H.M. Smith, Principles of Holography, Wiley, New York, 1969.
76. V.P. Smolyakov, and E.P. Khaimovich, "Polarization echo and induction signals excited by pulses of various durations", Sov. Phys. JETP, vol. 49, no. 4, pp. 661-664, April 1979.
77. C.H. Page, "Instantaneous power spectra", J. Appl. Phys., vol. 23, no. 1, pp. 103-106, January 1952.

78. H.C. Longuet-Higgins, "Holographic model of temporal recall", Nature, vol. 217, p. 104, January 6, 1968.
79. D. Gabor, "Holographic model of temporal recall", Nature, vol. 217, p. 584, February 10, 1968.
80. D. Gabor, "Improved holographic model of temporal recall", Nature, vol. 217, pp. 1288-1289, March 30, 1968.
81. A. Yariv, and D.M. Pepper, "Amplified reflection, phase conjugation, and oscillation in degenerate four-wave mixing", Optics Letters, vol. 1, no. 1, pp. 16-18, July 1977.
82. Liao, and Bloom, "Continuous-wave backward-wave generation by degenerate four-wave mixing in ruby", Optics Letters, vol. 3, no. 1, pp. 4-6, July 1978.
83. R.K. Jain, M.B. Klein, and R.C. Lind, "High-efficiency degenerate four-wave mixing of 1.06- μm radiation in silicon", Optics Letters, vol. 4, no. 10, pp. 328-330, October 1979.
84. D.M. Pepper, J. AuYeung, D. Fekete, and A. Yariv, "Spatial convolution and correlation of optical field via degenerate four-wave mixing", Optics Letters, vol. 3, no. 1, pp. 7-9, July 1978.
85. D.M. Pepper, and R.L. Abrams, "Narrow optical bandpass filter via nearly degenerate four-wave mixing", Optics Letters, vol. 3, no. 6, pp. 212-214, December 1978.